On the Role of AEBP2 in Thymus Development and Function



Wei Wu

Lady Margaret Hall

University of Oxford

Supervisor : Prof. Georg Holländer

Thesis submitted for the degree of

Doctor of Philosophy

Trinity 2019

Acknowledgements

I would like to express my sincere gratitude to my supervisor, Professor Georg Holländer, for the continuous support and guidance of my DPhil project. I am truly grateful for his patience, inspiration and encouragement through the last four years. Many thanks also go to Professor Rob Klose for the support he has provided on epigenetics studies in my project and Professor Neil Brockdorff and his lab for providing the AEBP2 constitutively KO mouse model for my research.

Besides my supervisors, I also would like to thank many people who have contributed enormously for my project over the last for years. Among them, Tiago Luis helped me with the thymus transplant experiment; Kevin Rue-Albrecht and Adam Handel helped me with the bioinformatic analyses of the RNA sequencing data; Hannah Chen, Annina Grädel, Bergithe Oftedal, Emma Haberman, Mary Deadman, Stefano Maio, Ioanna Rota, Stanley Cheuk in our lab assisted me with experiments; Thomas Barthlott from our lab in Basel provided technical supports for my project; Mary Deadman and Fatima Dhalla helped me proofread my thesis drafts. I also thank Hector Barbosa, Kathrin Jansen and all other past and present lab members of the Developmental Immunology Group for their moral support and stimulating discussions, and the BMS staff who have spent great amount of time taking care of my mouse colonies.

Many thanks to Xin Xu and Hoileong Lee, my sincere friends from my college LMH, for being supportive and listening me out whenever I need them. A special thanks goes to Yiran Meng and Meng Xia for their support in scientific discussions and technical issues in my project. I also would like to thank Qian Cheng for his helps and company in the last two years in Oxford, and Yiyan Zheng, Tina Wei, Jiahe Yang, Chen Zhao, Xiaopeng Fu, Guanlin Wang, Rong Li and many other Chinese friends in the WIMM for making me feel less homesick abroad.

I dedicate this thesis to my parents who have always been supportive about all my decisions since I come abroad 9 years ago. I would not have come this far without your love.

Abstract

The ability to distinguish between “Self” and “Non-Self” constitutes the most important functional feature of the immune system. It is primarily instructed for T cells by thymic epithelial cells (TECs) and is made possible by the TEC’s unique capacity to transcribe at the population level nearly all protein coding genes. This expertise, known as promiscuous gene expression (PGE), is in part dependent on the presence of the transcriptional facilitator, Autoimmune Regulator (AIRE) in a subpopulation of medullary TEC (mTEC).
H3K27me3 is an important posttranslational modification that epigenetically silences gene expression. A notable exception to this restrictive role of H3K27me3 appears to be the marking of loci that are promiscuously expressed in mTEC to generate a molecular library of self-antigens required for effectively central T cell tolerance induction. H3K27me3 marks are placed by the Polycomb Repressive Complex 2 (PRC2) which includes AEBP2, a well conserved zinc finger protein understood to serve as a targeting protein for the complex.

To assess the role of AEBP2 in TEC biology in general and PGE in AIRE+ medullar TEC in particular, mice with a loss of *Aebp2* expression in all TEC was analyzed. The absence of AEBP2 in mTECs compromised PGE and resulted in a preferentially decrease of tissue restricted antigen (TRAs) expression dependent on AIRE. A lack of AEBP2 in cortical TECs (cTECs) affected multiple tissue development signaling pathways which may be responsible for the change in cTEC/mTEC ratio at embryonic stage.
A lack of AEBP2 in thymocytes affected the early thymocyte development and caused an increased negative selection in both cortex and medulla as well as the post-selection maturation of CD4+ and CD8+ thymocytes. During the investigation of *Aebp2* deficient thymocytes via haematopoietic cell transplantation, a robust growth advantage in all haematopoietic lineages was observed. Transcriptome analysis showed an up-regulation of Aurora Kinase A (*Aurka)* in Aebp2-/- HSCs which may lead to the enhanced proliferation.
Taken together, the expression of AEBP2 is essential for the expression of a comprehensive repertoire of self-antigens as well as the development of haematopoietic progenitor cells including thymocytes.

List of Abbreviations

AEBP2. . . . . AE Binding Protein 2 (AEBP2)

AIRE . . . . . Autoimmune Regulator

APC . . . . . Antigen Presenting Cells

BSA . . . . . Bovine Serum Albumin

ChIP . . . . . .Chromatin Immunoprecipitation

CMJ . . . . . Corticomedullary Junction

CSF . . . . . Colony-stimulating factor

cTEC . . . . . Cortical Thymic Epithelial Cells

DC . . . . . Dendritic Cells

DN . . . . . Double Negative

DNA . . . . . Deoxyribonucleic Acid

DP . . . . . Double Positive

E # . . . . . Embryonic Day #

EED . . . . . Embryonic Ectoderm Development

EpCAM . . . . . Epithelial cell adhesion molecule

EPO . . . . . erythropoietin

ETP . . . . . Early Thymic Progenitor

EZH2 . . . . . Enhancer of Zeste Homolog 2

FL. . . . . Fetal Liver

FBS. . . . . Fetal Bovine Serum

gMFI . . . . . Geometric Mean Fluorescence Intensity

H3K# . . . . . Lysine at position # of histone 3

HSC. . . . . .Haematopoietic Stem Cell

iNKT cell . . . . Invariant Natural Killer T Cell

JARID2 . . . . . Jumonji And AT-Rich Interaction Domain Containing 2

K # . . . . . Cytokeratin #

KO . . . . . Knockout

MHC . . . . . Major Histocompatibility Complex

MPP. . . . . .Multipotent Progenitor

mRNA . . . . . Messenger Ribonucleic Acid

mTEC . . . . . .Medullary Thymic Epithelial Cells

PCR . . . . . Polymerase Chain Reaction

pMHC . . . . . Peptide Major Histocompatibility Complex

PGE . . . . . Promiscuous Gene Expression

PRC2 . . . . . Polycomb Repressive Complex 2

PTM . . . . . .Post-Translational Modification

qPCR . . . . . Quantitative real-time PCR

RAG . . . . . .Recombination Activating Gene

RNA . . . . . .Ribonucleic Acid

S1PR1 . . . . . Sphingosine-1 Phosphate Receptor-1

SP . . . . . .Single Positive

SUZ12 . . . . . Suppressor of Zeste 12

TCR . . . . . T-Cell Receptor

TEC . . . . . Thymic Epithelial Cells

TPR . . . . . Tetratricopeptide Repeats

TPO. . . . . Thrombopoietin

TRA . . . . . Tissue-Restricted Antigen

Treg cell . . . . Regulatory T cell

TSS . . . . . Transcriptional Start Site

UEA . . . . . Ulex europaeus agglutinin

WT . . . . . .Wild Type

Table of Contents

Acknowledgements ..... *i*

Abstract ..... *ii*

List of Abbreviations ..... *iii*

Chapter 1. Introduction *1*

1.1 Haematopoiesis **1**

1.1.1 HSC 1

1.1.2 Heterogeneity of HSC and multipotent progenitors 1

1.1.3 Mechanisms informing cell-fate decision 3

1.1.4 Developmental changes in HSCs' capacity for renewal and differentiation 4

1.1.5 The control of HSC function 6

1.2 The Adaptive immune system: A short primer **7**

1.2.1 Functional characteristics of the adaptive immune system 8

1.2.2 Lymphoid organs 9

1.2.3 T Lymphocytes 10

1. 3 Thymus **16**

1.3.1 TEC development 17

1.3.2 The basic principles of T cell development 20

1.3.3 Thymocyte migration mediated by chemotactic signals within thymic environment 23

1.4 Epigenetics **24**

1.4.1 A concise overview of epigenetics 24

1.4.2. PRC2-Epigenetics 25

1.5 Aim of the project **29**

Chapter 2. Methods and Materials *31*

2.1 Mouse work **31**

2.2 Mouse models **31**

2.2.1 *Aebp2* conventional KO mouse model 31

2.2.2 Mouse gDNA preparation for genotyping PCR 31

2.2.3 Genotyping protocol 32

2.3 Microbiology **33**

2.3.1 Preparation of DH5α competent cells 33

2.3.2 Sub-cloning of *Aebp2* plasmids 34

2.3.3 Transformation 38

2.4 Biochemical and molecular biological assays **39**

2.4.1 Cell culture 39

2.4.2 Cultured cell transfection 39

2.4.3 Protein extracts, immunological analysis, and antibodies 39

2.4.4 Immunoprecipitation (IP) and Co-IP 39

2.4.5 Western blot (WB) 40

2.4.6 Cytospin 41

2.4.7 Immunofluorescence (IF) 41

2.4.8 quantitative Real Time (RT)-PCR 42

2.5 Flow cytometry staining **44**

2.6 Transplantation assays 45
2.6.1 Fetal thymus transplant under the kidney capsule 45
2.6.2 Fetal liver transplant 46
2.6.3 Adult BM HSC transplant 46

2.7 Organ preparation and cell isolation 47
2.7.1 TEC isolation 47
2.7.2 T cell isolation 48

2.8 Bulk RNA sequencing 49
2.8.1 TEC RNA sequencing 49
2.8.2 HSC RNA sequencing 50

2.9 Statistics 50

2.10 Standard reagents and antibodies: 50

Chapter 3. In vitro profiling of Aebp2 60

3.1 Aebp2 is expressed in both TEC and lymphoid compartments 60

3.2 AEBP2 physically interacts in mTEC with the PRC2 core component EZH2 62

3.3 AEBP2 association with EZH2 is independent of exons 1-3 63

3.4 A potential Nuclear localization signal (NLS) in AEBP2 65

3.5 Discussion 68

Chapter 4. Mice constitutively deficient in AEBP2 exhibit defects in thymic development 70

4.1 Change in thymocyte maturation in the absence of AEBP2 expression 70
4.1.1 Constitutive AEBP deficiency causes a reduction in total thymic cellularity 70
4.1.2 A disturbed DN thymocyte development 71
4.1.3 Fewer DP cells were found in *Aebp2*-deficient E18.5 thymi 73

4.2 Increased mTEC frequency in the absence of AEBP2 expression 74

4.3 Transplantation of Aebp2-deficient fetal thymus tissue 77
4.3.1 Absence of *Aebp2* within the TEC compartment had a minor effect on total cellularity 78
4.3.2 Thymocyte frequencies during development were normal in *Aebp2*$^{-/-}$ thymi 78
4.3.3 *Aebp2*$^{-/-}$ TECs provided a normal environment for thymocyte positive selection 82
4.3.4 *Aebp2*$^{-/-}$ TECs were able to undergo negative selection of thymocytes 88

4.4 Changes in gene expression profiles in *Aebp2*-deficient E18.5 TEC 90
4.4.1 Both embryonic and somatic isoforms of *Aebp2* were depleted from E18.5 *Aebp2*$^{-/-}$ TECs ... 91
4.4.2 Mutually independent transcription of *Aebp2* and *Aire* 91
4.4.3 AEBP2 is associated with PGE in mTECs 93
4.4.4 H3K27me3 marks AEBP2 induced TRGs 96
4.4.5 The role of AEBP2 in TEC development 98

4.5 Discussion 101

Chapter 5. Loss of AEBP2 affects haematopoiesis and thymocyte development 106

5.1 The phenotype of E18.5 *Aebp2*$^{-/-}$ thymocytes is cell-intrinsic 106
5.1.1 A reduction of CD45.2+ donor thymocyte number was observed 106
5.1.2 Thymocyte development in the absence of AEBP2 107

5.2 Engraftment of *Aebp2*$^{-/-}$ early thymic progenitors 110

5.3 Both CD4 and CD8 thymocytes had an accelerated maturation when AEBP2 was absent 111
5.3.1 Altered positive selection for *Aebp2*$^{-/-}$ thymocytes 111
5.3.2 Both CD4 and CD8 thymocytes had an accelerated maturation 113

5.4 Absence of AEBP2 expression in T cells correlates with enhanced thymocyte negative selection 118

5.5 Egress of *Aebp2*-/- mature thymocytes mediated by $S1P_1$ expression 120

5.6 Peripheral T cell compartment in the absence of AEBP2 122
5.6.1 An increase of *Aebp2*$^{-/-}$ $\alpha\beta$T cells in the LN 123
5.6.2 A reduction of the peripheral Treg population in the absence of AEBP2 127

5.7 Competitive advantage in *Aebp2*$^{-/-}$ haematopoietic cells. 129
5.7.1 Competitive advantage was observed in *Aebp2*$^{-/-}$ thymocytes 129
5.7.2 Competitive advantage commenced in haematopoietic stem and progenitor cells (HSPCs) 131
5.7.3 Competitive advantage in the absence of AEBP2 affected myeloid progenitor cells in the adult bone marrow 134
5.7.4 Competitive advantage in the absence of AEBP2 affected haematopoietic cells in the periphery 137
5.7.5 Competitive advantage of long-term HSCs in the absence of AEBP2 140
5.7.6 Myeloid progenitor cells showed growth advantage after serial transplantation 143
5.7.7 *Aebp2*$^{-/-}$ fetal HSCs are more proliferative compared to the wild type HSCs 145
5.7.8 The engraftment advantage of *Aebp2*$^{-/-}$ HSCs may be caused by an early activation of the Aurora Kinase A (Aurka) 147

5.8 Discussion 148

Chapter 6. Conclusions and Future works 153

6.1 The role of AEBP2 in TEC development and function 153
6.1.1 Conclusions 153
6.1.2 Future works 154

6.2 The role of AEBP2 in haematopoiesis and thymocyte development 155
6.2.1 Conclusions 155
6.2.2 Future works 157

Reference 158

Appendix 172

Chapter 1. Introduction

1.1 Haematopoiesis

1.1.1 HSC

The haematopoietic stem cell (HSC) gives rise to all subsets of blood cells, which are largely divided into lymphoid and myeloid cells, a process termed haematopoiesis (1). Lymphoid cells include T lymphocytes, B lymphocytes, and natural killer (NK) cells, whereas myeloid cells consist of erythrocytes, megakaryocytes, monocytes, macrophages, eosinophils, neutrophils, basophils and platelets. Besides its ability to differentiate into these different blood cell types, a feature representing HSC's multipotency, a key characteristic of HSCs is their ability for self-renewal. Both of these essential properties of HSC have been proven by the use of bone marrow transplantation experiments (2).

1.1.2 Heterogeneity of HSC and multipotent progenitors

Between self-renewing HSCs and cells that are committed to a specific blood cell lineage, are several stages of progenitor cells that each display a limited self-renewal capacity and restricted developmental potency as they can give rise to only one or more distinct blood lineages. Nowadays it is, however, well appreciated that HSC represent a heterogeneous populations in terms of the competence for self-renewal and differentiation (1). Based on the former, HSC are divided into long-term, intermediate, and short-term subsets of HSC. HSCs that engraft initially in a mouse and, when re-grafted into a second recipient, sustain haematopoiesis for more than 16 weeks are considered cells with a long-term repopulation capacity (i.e. long-term HSCs) (3,4). In contrast, HSCs that only repopulate

the first transplant recipient in a transient fashion are regarded to be either short-term or intermediate HSCs depending on the time during which they can rise to haematopoietic progeny and thus are able for self-renewal (5). Using single-cell transplantation assays, several research groups have also identified HSCs that preferentially give rise to specific blood cell lineages (6–8). Surprisingly, this competence and hence functional heterogeneity is not simply a stochastic feature of HSCs since this feature is stably maintained in the course of serial transplantations (6,9–11). More recent findings suggest that the complexity of HSC differentiation is controlled by a network of multiple regulators which will be introduced in the following section. Moreover, it is also worthy to note that lineage-biased HSCs harbour the potential to differentiate also into other lineages in vitro than what the in vivo behaviour displays probably due to the heterogeneity of HSC population (6,12).

A cell type termed multipotent progenitors (MPPs) is also capable of giving rise to all blood lineages but these cells have a distinctly lower self-renewal competency in mouse (4). Moreover, based on their preferential differentiation route, they are broadly divided into MPP2, MPP3 and MPP4 subsets, with MPP2 and MPP3 being biased to myeloid cells and MPP4 partial towards a lymphoid cell fate. The MPP3 population also has the capability to differentiate into lymphoid lineages (13,14) (Figure 1.1).

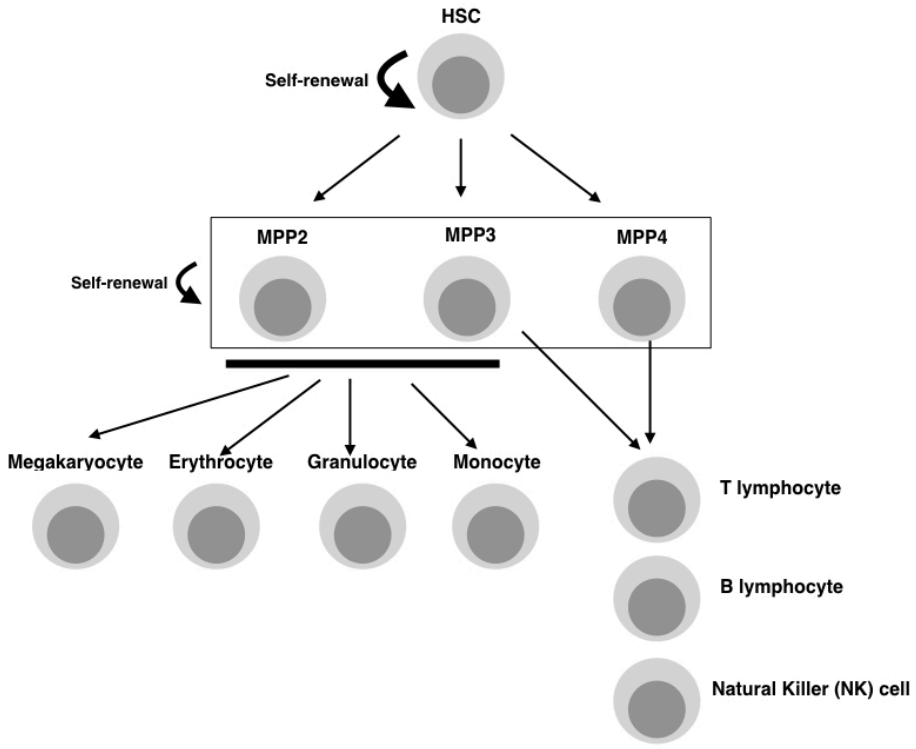

Figure 1.1: A scheme view of haematopoiesis

HSCs give rise to MPP2-4 which can further differentiate into different cell lineages. Only HSCs possess self-renewal and multi-potent abilities whereas MPPs are considered to have limited or no self-renewal ability. MPP2 and MPP3 are distinct MPP populations that preferentially differentiate to myeloid cells. MPP4 on the other hand is biased towards lymphoid lineage. MPP3 is also able to generate lymphoid cells.

1.1.3 Mechanisms informing cell-fate decision

The generation of mature blood cells from haematopoietic stem and progenitor cells (HSPCs) is a tightly controlled program. Both cell-intrinsic transcriptional and epigenetic regulators on one hand (i.e. transcription factors GATA1 and PU.1, etc) (10,15–18) and extrinsic environmental factors, such as haematopoietic cytokines (i.e. erythropoietin (EPO), colony-stimulating factor (CSF), etc), on the other hand (19–21) play important roles. With the development of new technologies such as single-cell transplantation and

colony-forming assays, new differentiation routes have been identified that contributed to our present understanding of a highly complex haematopoietic differentiation system as determined by in vitro experiments. It must however be stressed, that this developmental potential is not necessarily what happens in vivo as one needs to bear in mind that in vivo steady state conditions may dictate a different cell behaviour.

1.1.4 Developmental changes in HSCs' capacity for renewal and differentiation

The first detectable haematopoietic cells during embryogenesis are nucleated erythrocytes and macrophages. They are first identified in the yolk sac between embryonic day 7-7.5 in the mouse (22) and about day 18 of gestation in humans (23). Some multipotent progenitor cells with limited repopulating ability start to appear soon after the first detection of the haematopoietic cells (24,25). The first cells comparable to HSCs emerge in the aorta-gonado-mesonephros (AGM) region at embryonic day 10.5 (26–28) and in week 5 to 6 of gestation in humans (25,29). Later, HSCs can also be found in other tissues including placenta and fetal liver (30,31). The fetal liver constitutes after the transient AGM the next major haematopoietic organ; there HSCs expand significantly in number (26,32). By embryonic day 17, mouse HSCs move to the bone marrow for their typical residence throughout the rest of the animal's lifetime (33). During mouse embryonic development, although to a less degree compared to fetal liver, haematopoiesis can occur in the spleen (33). In adult mouse, HSCs can also be found in the spleen and lungs (34,35). The role of these extramedullary niches and whether the HSCs produce specific subsets of haematopoietic cells need to be addressed in further details.

There are developmental and functional differences between fetal and adult HSCs (36–38) which brings up the question of whether adult HSCs are actually derived from fetal

HSCs. Employing cell tracing studies with fluorescently labelled fetal HSCs, the transplantation of such cells into irradiated adult recipients demonstrated that engrafted fetal HSCs give rise to a significant number of both fetal and adult haematopoietic cells (39,40). Also, in single cell transplantation experiments, a single fetal HSC was shown to be able to generate the full range of haematopoietic cells in adult recipients (41). Taken together, experimental evidence indicates that, a big proportion of, if not all, adult HSCs arise from their fetal counterparts.

Studies have also shown that fetal liver HSCs differ from adult bone marrow HSCs in terms of their self-renewal and differentiation abilities (38,42–44). Indeed, fetal HSCs show a higher proliferative activity when compared to adult HSCs which are usually in a quiescent state (42,45,46).

Fetal and adult HSCs also differ significantly in terms of their individual lineage outputs. For example, fetal liver HSCs produce twice as many granulocytes and monocytes compared to the adult BM HSCs in a transplantation setting (47). Interestingly, this functional feature ascribed to fetal HSCs is retained for as long as 3 weeks after birth when HSCs adopt a lineage output behaviour that is now functionally indistinguishable from that of adult HSCs. The molecular mechanisms accounting for this functional shift could be cell-intrinsic maturational processes that require time to be fully operational and do not coincide with the transition from in utero development to post-natal life. Whatever the underlying mechanisms may be, further experimental work will be needed to uncover them.

Fetal and adult HSCs also have different lineage decisions within both myeloid and lymphoid subsets. The population of B cells can be divided into the two separate subtypes of B-1 and B-2 cells. Previous research has shown that although both fetal and adult HSCs

can give rise to B-2 cells, B-1 cells are exclusively derived from fetal HSC as elegantly demonstrated by transplantation experiments probing the developmental potential of fetal liver cells and adult bone marrow derived HSC (48). Meanwhile, T cells commit early in their differentiation to one of two distinct fates, namely cells with a αβ or γδ T cell antigen receptor (TCR). This dichotomy occurs at a specific intrathymic developmental stage referred to as double negative (DN) 2 (49). The development and selection of T cells bearing a αβ TCR are well characterized and will be further explained below (1.3.2). In contrast, the maturation of γδT cells is less well characterized (49). These cells egress from the thymus where they are generated to the periphery where dependent on the anatomical site, they may express the cell surface markers CD24, CD25, CD27, CD44 and/or CD122. Previous studies found that some populations of γδT cells (marked by their TCR heterodimers, Vγ3 Vδ1 and Vγ4 Vδ1) can only be produced by fetal HSCs whereas adult HSCs produce γδT cells bearing TCRs with a different use of individual receptor chains Vγ2 and Vγ5 (50,51). In addition, invariant NK T cells are also produced in the thymus. In summary, HSCs display different functional properties that correlate with distinct developmental stages.

1.1.5 The control of HSC function

The developmental potential and function differs between fetal and adult HSC, as discussed above, despite the fact that the former gives rise to the latter. This difference in biology begs the question what controls this behaviour and whether these influences are either intrinsic, extrinsic or both. Transcriptomic analyses have provided insight into the molecular mechanisms that control HSC function (52–54). For example, the gene *Lin28b,* which encodes a protein of the same name that binds micro RNA species of the Let-7

family, was found to be expressed at a higher level in fetal liver HSCs when compared to adult HSC resident in the bone marrow. Overexpression of *Lin28b* (or its homologue *Lin28a*) in adult HSCs up-regulated *Hmga2*, a gene encoding the High Mobility Group AT-Hook 2 protein involved in DNA damage/telomere stress induced senescence and chromatin regulation/acetylation, via inhibiting several Let-7 family members. Overexpression of either *Lin28b* or *Hmga2* in adult HSCs increases consequently the self-renewal ability of these cells to a level comparable to that of fetal liver HSCs. Thus the *Lin28b–let-7–Hmga2* axis is important for the regulation of essential HSC properties and its activity correlates with mouse development as Lin28 decreases in many tissues parallel to foetal progression to birth. Importantly, more recent evidence would indicate that *let-7* plays a vital role also in regulating multipotent progenitors placed downstream of HSC as well as terminally differentiated blood cells (55).

1.2 The Adaptive immune system: A short primer

The immune system constitutes a collection of molecules, cells and processes within our body that has the essential capacity to protect against a broad range of threats, including microbial pathogens and malignantly transformed cells, and thus maintaining the body's tissue integrity. Two essential effector arms have been identified that mediate this defence, the innate immune system and the adaptive immune system. The former represents a nonspecific defence mechanism that come into play immediately or within hours of an antigen exposure and involves an array of different humoral factors and cells which lack antigen-specific receptors that mediate the defence response. In contrast, the adaptive immune system is characterized by the ability to employ antigen specific receptors which typically come into play when the first line of defence by the innate immune system fails.

These antigen receptors require that their utility has been tested and selected for the needs of a given individual as functionally they should be selected to be able to effectively distinguish between potentially life-threatening "Non-Self" and vital "Self". This vital function is genetically determined and physically instructed during the effector' cells ontogeny. Consequently, antigen-recognizing effector cells of the adaptive immune system must ideally be responsive to foreign antigens but tolerant to molecules that constitute natural components of an individual's organism. This competence to distinguish between "Non-Self" and "Self" is an acquired competence that results from a highly selective process that has evolved during evolution, and that results in an essential functionality that is characterized in a given individual by a responsiveness to all possible antigens with the notable exception of self-antigens against which the immune system should be tolerant to avoid autoimmunity (56).

The adaptive immune system has two separate, yet complementary and interacting effector mechanisms, referred to as humoral and cell-mediated immunity, respectively. Humoral immunity is mediated by macromolecules in extracellular fluids, such as antibodies which are secreted by B cells typically under the control of T cells. On the other hand, cell-mediated immunity is accomplished by activation of antigen-specific T lymphocytes which can either induce cell death of target cells via the release of enzymes or cytokines or alternatively provide help to orchestrate the humoral immune response.

1.2.1 Functional characteristics of the adaptive immune system

The main determining key feature of the adaptive immunity that distinguishes it from innate immunity is the ability of this system to create an immunological memory, namely the capacity to "remember" antigens that have previously been in contact with an

individual immune system. This memory allows for a more effective and rapid immune response to the same antigen on subsequent encounters, even if these occur many years later. The adaptive immune system can therefore provide a highly specific and long-lasting protection against pathogens whereby there is seemingly no limitation of the number of different antigens that can be detect by this defence system. A successful vaccination builds on the phenomenon of immunological memory where a controlled exposure to an immunogenic yet not pathogenic antigen eventually elicits an immunological memory. This response is beneficial should the vaccinated individual be exposed to pathogens that express an antigen for which an immunological memory has been generated as a result of vaccination.

1.2.2 Lymphoid organs

Lymphoid tissue are structured aggregates of different cell types but mostly lymphoid cells that adopt distinct structural characteristics according to local anatomical requirements. The most highly organised lymphoid tissues can be divided into two categories based on their easily identifiable architectures and functions: primary and secondary lymphoid organs (57). Primary lymphoid organs, such as the bone marrow and the thymus, provide specialized stromal niches for the commitment to and clonal expansion of B and T lymphocytes. Precursors that can give eventually rise to mature T lymphocyte are produced in the bone marrow and migrate to the thymus for further differentiation and maturation. After being licensed to be fully functional effector cells via a rigorous series of selection and maturational steps, these immunologically competent naïve lymphocytes migrate to and eventually seed secondary lymphoid organs, where they are ready to respond to potentially pathogenic foreign antigens, presented by

antigen-presenting cells. Secondary lymphoid tissues (secondary lymphoid organs, SLO) in mammals include lymph nodes and spleen, skin-associated lymphoid tissues (SALT), and the mucosa-associated lymphoid tissues (MALT) present in the bronchi of the respiratory tract (BALT), the nasopharynx (NASLT) and the gut (GALT).

1.2.3 T Lymphocytes

Lymphocytes are specialized effector cells of the adaptive immune system that have differentiated from HSCs via well-defined intermediate developmental stages (1). Based on molecular, developmental and functional differences, lymphocytes are categorized in vertebrates into the two distinct populations of T and B lymphocytes, with the former being generated in the thymus and the latter emerging in the bone marrow (58). After the seeding of haematopoietic precursors to the thymus, their interaction with the thymic stromal microenvironment allows for an interaction of the cells' NOTCH1 receptor with its corresponding ligand, delta-like 4 (DLL4), expressed on thymic epithelial cells, the major cellular component of the thymus stroma. This interaction transduces signals that lock these precursors cells irreversibly into a T cell fate (59,60). On the other hand, B cells develop in the bone marrow dependent on a number of transcription factors, such as PAX5 and E2A (58).

In order to recognize a virtually unlimited range of antigens, the population of lymphocytes generates an extremely large variety of distinct antigen receptors, termed T cell receptors (TCR) and B cell receptors (BCR), respectively. The diversity of these heterodimeric receptors is determined by the recombination of variable (V), diversity (D), and joining (J) gene segments mediated by a complex molecular machinery including the products of the recombination-activation genes (RAG) 1 and RAG2, a process termed

V(D)J recombination (61). The individual chains of these antigen receptors contain a highly variable part, referred to as complementarity-determining region (CDR), which is the main sequence in contact with the antigen and hence most crucial for the antigen recognition diversity of TCR and BCR (62).

The TCR is a transmembrane structure that is composed of either an α and β chain or, a γ and δ chain linked by disulphide bonds. Due to these structural features, T lymphocytes are broadly divided into αβ and γδ T cells (63). Although both lineages develop in the thymus, the majority of T cells are αβ T cells. Mature αβ T cells are phenotypically categorised into cells that express either CD4 or CD8 on their surface which correlates with distinct functional capacities.

1.2.3.1 T cell activation

Newly generated, antigenically inexperienced and thus termed naive CD4 and CD8 T cells exit the thymus and home to SLO such as the spleen, lymph nodes. They are characterized by the surface expression of the adhesion marker L-selectin (CD62L) which, together with the chemokine receptor CCR7 cooperatively controls the extravasation via high endothelial venules to lymph nodes, thus acting as homing receptors (64).

T cells require signalling through their TCR to be activated. Associated with the outward facing TCR heterodimer is a family of invariant CD3 molecules composed of the transmembrane CD3δ, CD3ε, and CD3γ molecules associate in a defined stoichiometry with the TCR ζ chain placed on the inner aspect of the cytoplasmic membrane (65). This unit is responsible for the transmission of signals emanating from the correct stimulation of the TCR. The activation of this signalling complex results in the phosphorylation of

downstream intracellular molecules that collectively elicit a T cell response according to the cells functional capacity.

TCR activation is usually restricted to the binding of the receptor chains to a complex composed of an antigenic peptide presented by major histocompatibility complex (MHC) molecules on the surface of antigen-presenting cells whereby this interaction (designated TCR::pMHC) needs to be not only specific but also of sufficient affinity. To secure the latter, additional molecular interactions are in place that stabilise the binding. Most important in this regard are the glycoproteins CD4 or CD8 which serve as co-receptors to the TCR binding to invariant sequences of MHC class II and class I molecules (see below), respectively. For T cells to be responsive to their cognate antigen, that antigen must be correctly processed and bound the MHC molecule. For this purpose, a sophisticated intracellular machinery of enzymes and transporter molecules control the digestion and delivery of foreign and mutated Self proteins (i.e. “antigens”) to specific cellular compartments where their short peptides are placed into the antigen-binding groove of MHC molecules and eventually displayed on the cell surface for recognition by the TCR. This process is termed antigen presentation and is crucial for T cell activation and hence is central to the adaptive immune response.

As already mentioned, there two types of MHC molecules, designated MHC class I and class II (66). MHC Class I is recognised by T cells that express the co-receptor CD8 and characteristically but not exclusively effect a cytotoxic function (hence known as cytotoxic T cells, CTLs). MHC Class I molecules are expressed on most nucleated mammalian cells. Infected cells presenting a foreign peptide bound to MHC Class I on their cell surface are prone to be recognised by CTLs and will trigger a response that may result in their killing.

MHC Class II molecules interact with CD4 and this interaction stabilises the TCR::pMHC interaction between T cells and antigen-presenting cells. Cells expressing CD4 include helper T cells of different functional kinds and regulatory T cells. The expression of MHC Class II molecules is under physiological conditions restricted to a selected number of cells capable of taking up, processing and presenting antigens, hence termed antigen presenting cells (APCs). This particular cell function is provided by B cells, dendritic cells, macrophages and thymic epithelial cells (TEC). The latter constitute a unique type of MHC II expressing APC as they present self-antigens to the maturing T cells so that these cells can probe the utility of their TCR specificity. The TCR::pMHC interactions in this context therefore do not serve the purpose to trigger an immune response against foreign antigens but rather display a vast repertoire of peptides derived from self-antigens to educate T cells to become non-responsive to these "harmless" antigens. These processes are described in more detail in the following chapter 1.3.

1.2.3.2 T cell differentiation

T cells with a CD4 phenotype constitute a heterogeneous population composed of several, functionally distinct subsets of effector cells that differ in their cytokine production, their range of intracellular transcription factors, display of chemokine receptors and many other molecular features (67). In the 1980s, immunologists recognised a relatively simple system of basically two distinct types of CD4-positive T cells, T helper (Th) type (Th1) and Th2 cells, each being functionally and phenotypically distinct (68). Since these early days of molecular immunology, additional subpopulations have been detected and characterized which resulted in a growing number of phenotypically and molecularly distinct categories of CD4 T cells. These newly identified CD4 T cell subpopulations

include Th17 cells (69), regulatory T cells (Treg; a population originally known as suppressor T cell), Th9, Th22, Tfh, ThGM (70). There is a significant plasticity in the identity of these distinct subpopulations with transformations between the different types of CD4 T cells which may also share the expression of specific cytokines. For instance, Th17 cells are able to adopt a Th1 cell phenotype (71,72) and IL-10 which was initially recognized as a Th2-specific cytokine can also be expressed by Th1, Th17 and Tregs (73). To date, it is still unclear whether the transformation between different T helper cell subsets is bi-directional or limited to uni-directionality. The major CD4 T cell subsets introduced are listed below.

Subsets	Function	Major Cytokines produced
T helper (Th) 1	Against intracellular bacteria and viruses	IFN-gamma
Th2	Against large extracellular pathogens	IL-4
Th9	Against parasitic helminth infections	IL-9
Th22	Against microbial pathogens in skin tissues	IL-22
Follicular helper T (Tfh)	Regulation and development of antigen-specific B cell immunity	IL-21
Granulocyte macrophage-colony-stimulating factor (GM-CSF) secreting (ThGM)	Secreting GM-CSF to stimulate immune responses	GM-CSF
Th17	Against specific fungi and extracellular bacteria and regulate autoimmunity	IL-17
Regulatory T (Treg)	Suppressing the development of autoimmunity	IL-10, TGF-beta

The diversity of T helper cell subsets is important for the adaptive immune system to recognize a wide range of pathogens and orchestrate a rapid yet bespoke and antigen-type focused immune response. With immunological senescence and a starkly reduced

generation of naïve T cells, secondary to thymus involution it is critical that the individual T cell subsets are maintained in the periphery whilst keeping their functionality, not least to preserve the competence of an antigen-specific immune defence at an acceptable economic cost.

1.2.3.3 T cell memory

T cells, as mentioned, play important roles in both humoral and cell-mediated immunity. However, once the primary response against pathogens is achieved, there will inevitably be the need to contract the number of effector cells involved in that response whilst maintaining the capacity to respond upon re-exposure to the same antigen with a faster and more effective immune response. This functional demand is met by the generation of memory T cells. Compared to their naïve counterpart, these cells are prone to respond earlier with fewer cognate antigens in the course of an immune response. Moreover, memory T cells display an increased proliferation potential which aids the clearance of the antigenic challenge. Unlike naïve T cells, which mainly stay in the SLO, memory T cells can patrol tissues other than lymphoid tissues which constitutes an important, additional prerequisite for a fast response to pathogens.

For both CD4 and CD8 lineages, there are two subtypes of memory cells, central memory (T_{CM}) and effector memory (T_{EM}) T cells. In the mouse, the population of T_{CM} is commonly characterized by the high expression of adhesion markers CD62L and CD44, another glycoprotein on the cell surface that serves a function in cell–cell interactions, cell adhesion and migration. In contrast, T_{EM} express CD62L only at low levels. These two memory T cell populations also differ in their proliferative behaviour: T_{CM} possess a high proliferative potential following antigen re-encounter, whereas T_{EM}, display a

limited proliferation but have a rapid release of their effector function such as the secretion of preformed granzyme B and IFN-γ. The high expression of CD62L on T_{CM} mediates an efficient capacity to home to the SLO, where they have an increased probability to encounter foreign antigens circulating through this tissue by immigrating APC such as dendritic cells. Conversely, the physiological lack of CD62L expression by T_{EM} allows their trafficking through all peripheral tissues including nonlymphoid tissues. Hence the T_{EM} serves as a "fleet of quick response agents" in peripheral (i.e. non-lymphoid) tissues where reinfection has occurred (74). Taken together, T_{EM} and T_{CM} cells eliminate a previously encountered pathogen in an experienced and cooperative way whereby the former rapidly controls infection on site meanwhile the latter generates a population of effector cells to eliminate the pathogenic threat.

1. 3 Thymus

The thymus is a primary lymphoid organs which provides the sole unique microenvironment required for the development of functionally competent and self-tolerant T cells. Histologically, the thymus comprises two lobes which can be sub-divided into a central medullary region and a peripheral cortical region. Cortical and medullary thymic epithelial cells (cTECs and mTECs) are the major stromal cells in both cortex and medulla and indispensable for the regular development and selection of developing T cell, also termed thymocytes (75). The development of thymocytes is subject to a yet incompletely defined series of molecular cues of key developmental signals provided sequentially by cTEC and then mTEC. These cues can be provided either as soluble or as membrane bound signals thus highlighting the need of a close functional and physical interaction between thymocytes and TEC, a phenomenon known as thymic cross-talk and

fundamental to the function of the thymus to orchestrate T cell development and maturation (76–78).

1.3.1 TEC development

TEC, the most abundant component of the thymic stroma, originate at day 10.5 of mouse gestation (E10.5) from the endodermal lining of the ventral aspect of third pharyngeal pouch (3rd pp)(79). During the earliest TEC development stages, known as patterning, a group of transcription factors, including Hoxa3, Pax1/9, Eya1, Six1/4, and Tbx1, instruct the endodermal epithelia to adopt a cell fate that eventually gives rise to TEC (80–84). Early thymic organogenesis is initially physically coupled to the development of the parathyroid glands as these also stem from the 3rd pp, albeit from its dorsal aspect. The development of the thymus and the parathyroid glands are, however, controlled by the transcription factors FOXN1 and GCM2, respectively (85–87). Multiple signalling pathways well studied in the context of different organ formations are also essential for the formation of the thymus in general and early TEC development in particular, including the signals elicited by ligands such as bone morphogenetic protein (BMP) (88,89), Wingless/Integrated (Wnt) (90,91), Hedgehog (Hh) (92), and fibroblast growth factor 7/10 (93). Importantly, many of these pathways require FOXN1, which subsequently influences the development and differentiation of TEC subpopulations.

TECs can be phenotypically and functionally divided into two phenotypically, morphologically and anatomically distinct populations, namely the aforementioned cTECs and mTECs. Indeed, in late embryonic development and post-natal life, the surface marker Ly51 and reactivity to the ulex europaeus agglutinin I (UEA-1) lectin are

used to distinguish between cTEC and mTECs, respectively. A common TEC progenitor has been identified for both cTEC and mTEC subpopulations in early developmental stages in mice (94–96). Although originating from the same progenitor cell, these two distinct TEC populations do not develop at the same time and at the same location during thymus organogenesis. cTEC can be identified by their expression of the TEC-specific proteasome component β5t (97,98) as early as E11.5 whereas mTEC characterized by the expression of claudin-3, -4 and SSEA1 only emerge at E13.5 in mouse embryo (99). Indeed, a few recent studies found that TEC expressing typical cTECs markers (CD205, β5t) can give rise to both cTECs and mTECs (97,100–102) suggesting that these cells are bi-potent with regards to their ability to contribute to both TEC lineages. Based on these findings, a serial progression model of embryonic TEC development has been established in which a common TEC progenitor transits via phenotypically cTEC-like stage to the mTEC lineage (94). Following commitment to a mTEC fate, epithelia at early developmental stages during this lineage trajectory progressively lose their expression of cTEC markers (e.g. β5t, Ly51) and gain the expression of mTEC-specific molecular features. Although bipotent TEC progenitors have also been found in the postnatal thymus (103), it has been to date difficult to dissect and characterize the differentiation of this population due to their similarities to cTEC. The molecular mechanisms regulating cTEC development remain largely undefined. In contrast, mTEC maturation is somewhat better defined as it has been observed that these cells are reliant for their differentiation on the activation signals provide by the activation of the NF-κB signalling pathway, prominently triggered by ligands of the TNF receptor family members such as RANK, CD40, and LTβR (104–106). Postnatal mTECs are categorized into distinct maturational stages according to their expression of CD80, MHC class II and the Autoimmune

Regulator (AIRE) (107). mTEC lineage-committed progenitors give rise to immature $CD80^{lo}$AIRE-$MHCII^{lo}$ mTEC (108). This population referred to as $mTEC^{lo}$ subsequently progresses to a highly proliferative mature mTEC populations characterized by a $CD80^{hi}$ AIRE- $MHCII^{hi}$ phenotype (designated $mTEC^{hi}$) which then can express AIRE to become a second mature mTEC populations (i.e. AIRE+CD80+$MHCII^{hi}$ mTEC). The expression of the transcriptional facilitator AIRE allows $mTEC^{hi}$ to transcribe an additional 4000 genes encoding peripheral tissue restricted antigens (TRA) (109). This array provides a molecular mirror of "Self" and is required to establish immunological T cell tolerance as their peptides represent an individual's own tissues and are used to probe the reactivity of newly generated T cells. This process of expressing TRA in a tissue-agnostic fashion is known as promiscuous gene expression (PGE, see below) (107,109).

mTECs generate in an instructive fashion a repertoire of T cells that are tolerant to TRA and therefore 'Self', whilst able to remain responsive to an seemingly unrestricted number of foreign antigens. The precise molecular mechanisms for PGE are still largely undefined. Some insight has, however, been gained by dissecting AIRE's role and mode of operation in mature $mTEC^{hi}$, which at the population level semi-stochastically expresses more than 18,000 protein coding genes thus accounts for the transcription of about 85% of the entire protein coding genome (109,110), a cellular phenomenon observed nowhere else in the body. Importantly, AIRE does not directly bind to DNA necessitating a functional and even possibly physical association with other molecular partners that mediated the recognition and interaction with nucleic acids and/or chromatin structures (111,112). AIRE-regulated genes are typically associated with an enrichment in tri-methylation (me3) of lysine (K) 27 within the flexible N-terminus tail of histone 3 (H3K27me3) (109). Essential for normal development and cell identity, this post-

translational modification (PTM) is commonly associated with genes that are transcriptionally inactive and indicative of densely packed heterochromatin (113). Polycomb Repressive Complex 2 (PRC2) is the sole complex responsible for catalysing the addition of this histone PTM.

1.3.2 The basic principles of T cell development

Blood-borne T cell precursors home to the thymus through blood vessels located at the cortical-medullary junction (CMJ) (114). Once placed within the microenvironment of the thymus, these cells are subject to a sequential series of cell stages to finally acquire the phenotype and functional capacity of mature T cells tolerant to "Self". The earliest stages of intrathymic T cell differentiation are marked by an absence in the cell surface expression of the TCR, CD4 and CD8, why these are commonly referred to as CD4-CD8- double negative (DN). Using the expression of two additional surface markers, CD25 and CD44, DN thymocytes can be further characterized into four progressively emerging sub-stages along the uniform developmental trajectory of thymocytes that eventually give rise to αβTCR-positive cells: the DN1 stage is characterised by a CD44+CD25- phenotype; DN2 is typified by CD44+CD25+; DN3 is identified as CD44-CD25+; and DN4 have a CD44-CD25- pattern (115). Immature early thymocytes at the DN1 and DN2 stages can still adopt either αβ or γδ T cell lineage fate whereas DN3 thymocytes have fully committed to an αβ T cell fate (116). At this stage, thymocytes begin to express, initially only intracytoplasmically, a TCRβ chain following the successful and in-frame mediated somatic V(D)J rearrangement and the expression of an invariant pre-α TCR which does not require any DNA recombination (117,118). The resultant heterodimeric structure is referred to as the pre-TCR and its successful cell surface expression provides a first

quality control in the development of thymocytes, designated β–selection. Thymocytes at this maturational stage are hence examined whether they express a correctly rearranged TCR β-chain able to signal (119–121). In the event that the requirements for passing this checkpoint are not met, for example consequent to the absence of an in-frame recombination of the TCRβ chain or due to a lack of key regulators (e.g. *RAG1*, *RAG2* expression), thymocytes fail to progress beyond the DN3 stage and eventually will undergo programmed cell death. However, having successfully completed TCR β selection, the cells will reach the DN4 stage where the undergo several rounds of proliferation and begin (in the mouse) to rearrange and eventually express the α chain to replace the pre-α chain. Following the receipt of a successful TCR signal, DN4 eventually express CD4 and CD8. The sequence by which these two co-receptors are expressed is genetically determined though in most mouse strains CD8 is expressed first giving rise to a transient population of immature single positive (SP, i.e. CD4-CD8) thymocytes. Eventually thymocytes express both CD4 and CD8 and are referred to as double positive (DP). This phenotype constitutes the largest lymphoid population within the thymus (116). With the expression of a complete αβTCR on the cell surface, DP thymocytes commence their education which aims to select T cells with antigen receptor specificity that is useful for an individual yet still able to recognise a seemingly unrestricted range of foreign antigens. This education consists of distinct selection steps that sequentially involve initially cTECs and later also mTECs. As previously mentioned, both TEC types serve as APC and express for this purpose both MHC class I and II molecules on their surface to which peptides derived from promiscuously expressed TRA are bound. The affinity of the TCR expressed during early developmental stages to pMHC on TECs determines the fate of DP thymocytes: cells with insufficiently high affinity will not receive survival

signals required for their further differentiation and thus undergo apoptosis. This first selection is referred to as thymocyte positive selection, takes place in the cortex and determines the effectiveness of the TCR to recognise a pMHC. Thymocytes that are competent to transmit essential intracellular signals counteract the inherent induction of programmed cell death and hence escape the phenomenon known as death by neglect (116,122).

Thymocytes positively selected are subsequently subjected to a series of further selection steps. These aim to delete T cells that recognising Self-derived peptides presented by MHC molecules via a TCR with a sufficiently high affinity that these cells harbour the potential to elicit an autoimmune (i.e. self-destructive) response once they have egressed to the periphery. This elimination is referred to as thymocyte negative selection. Only thymocytes that express a TCR of intermediate affinity for their cognate pMHC receive the correct signal strength and consequently are kept alive as they are allowed to differentiate into mature SP CD4 or SP CD8 positive thymocytes (123). Recent studies have convincingly shown that thymocyte negative selection occurs both in the cortex as well as in the medulla involving both TEC and hematopoietic APC such as dendritic cells and B cells. It is of note that only 3-5% of DP cells survive selection and migrate from the cortex to the medulla (124,125).

The commitment to either the CD4 or CD8 T cell lineage correlates with the MHC specificity of the cell's TCR restriction but remains still incompletely defined. In the last two decades, the key transcription factors ThPOK and Runx3 have been identified to play a critical role in the process of how access to these two separate CD4 and CD8 T cell lineages is controlled (126,127). There are also a few other transcription factors and epigenetic regulation involved in the CD4/CD8 commitment (128).

SP thymocytes having passed the scrutiny of negative selection (129–131) undergo a post-selectional maturation before they exit the medulla of the thymus and migrate to peripheral lymphoid tissues as antigen un-experienced, naïve T cells. This egress from the thymus constitutes an active process mediated by G-protein-coupled receptors (132) where the up-regulation of the sphingosine-1-phosphate receptor 1 (S1P1) plays an important role (133,134). The concentration gradient of the receptor's specific ligand, S1P, drives this directed movement for a higher concentration exists of this chemoattractant in serum than in most other tissues (135). In addition, CCL9-mediated CCR7 signalling has also been inferred in the process of thymocyte emigration (136). However, this signalling axis appears only to be operational for newly generated thymocytes in the neonatal thymus. Such a restriction would therefore also suggest a developmental switch between two different modes of controlling thymocyte emigration which are determined by ontogeny.

1.3.3 Thymocyte migration mediated by chemotactic signals within the thymic environment

Thymocytes are subject to a complex intrathymic migratory behaviour which secures, inter alia, that the individual selection steps can occur in distinct anatomical sites within the thymus where special niches are provided. This migration is a highly ordered process that involves several cytokines, chemokines and their respective receptors (75). After entering the thymus via the CMJ, early lymphoid precursors move directly to the subcapsular region of the thymic cortex (137), dependent on their expression of chemokine receptors such as CXCR4, CCR7, and CCR9 (130–132). The developmental processes of β-selection positive and wave 1 negative selection occur in the cortex

whereas the subsequent defining stages of negative selection (wave 2) and post-selectional maturation take place in the medulla (138). Access of DP thymocytes to the medulla requires the expression of CCR7 which recognises the chemokines CCL19 and CCL21 produced by mTECs (139). Although both the migration of early precursors from the CMJ to the depth of the cortex and the migration of DP cells from cortex to medulla require CCR7-mediated signals, the specific mechanism that distinguish between these different paths are still incompletely defined.

1.4 Epigenetics

1.4.1 A concise overview of epigenetics

Epigenetics is the study of heritable control and regulation in gene expression and function that is independent of changes to the DNA sequence. Accumulating evidence in recent years indicates that organogenesis and development is under epigenetic control to achieve spatio-temporal changes in gene expression as the genetic information does not change before and after cellular differentiation.

Haematopoiesis and thymic development, as introduced above, are highly dynamic developmental processes which require strict transcriptional control. Indeed, epigenetic modification, especially DNA and histone modification, is widely studied in these developmental procedures (140,141). H3K27me3 is one of the most important histone modifications that regulate gene expression. The following section will introduce the enzymatic complex depositing this histone mark.

1.4.2. PRC2-Epigenetics

1.4.2.1 Polycomb group proteins

In insects, segmentation during development is spatio-temporally regulated by the precise expression of Hox genes, which encode a set of transcription factors required for correct embryogenesis to occur (142). Previous studies using *Drosophila melanogaster* have detailed this process of tissue patterning and identified upstream regulatory factors controlling Hox gene expression. During early embryogenesis, Hox genes are silenced via their cis-regulatory elements by direct binding of Gap proteins, such as Hunchback (Hb), Krüppel (Kr) and Knirps (Kni) (143,144). However, during later developmental stages, Gap genes cease to be transcribed and consequently polycomb group (PcG) molecules gain a vital role in maintaining the repressive state of Hox genes (145–147). Unlike many of the Gap proteins which serve as transcription factors, most PcG proteins are unable to bind directly to DNA but bind to regions of chromatin called polycomb response elements (PREs) to maintain the transcriptional repression of Hox genes (148,149).

1.4.2.2 PRC1 and PRC2

Given their development importance, PcG proteins are highly conserved between species ranging from Drosophila to vertebrates. In mammals, PcG proteins are recruited to CpG islands where they effect the transcriptional silencing of genes (150). PcG proteins form two major multimeric enzymatic complexes, designated polycomb repressive complex 1 (PRC1) and PRC2, with each displaying functionally distinct catalytic activities. PRC1 mediates mono-ubiquitylation of lysine 119 on histone H2A (H2AK119ub1) via its catalytic subunit, the E3 ligase RING1A or RING1B; whereas PRC2 catalyzes mono-,

di-, and tri-methylation lysines at position 27 on the tail of H3 histones resulting in a feature defined as H3K27me1, H3K27me2 and H3K27me3 (151). Both complexes are often found to target the same genomic loci leading to effective gene repression. Conventionally, canonical PRC1 recognize PRC2-mediated H3K27me3 chromatin marks via their CBX subunit, which in turn enforces a repressive chromatin state (152). This finding suggests a sequential process in maintaining gene repression from PRC1 to PRC2. However, some other studies show that PRC1-mediated ubiquitylation promotes PRC2 recruitment demonstrating an alternative method of cross-talk between PRC1 and PRC2, which are both necessary for maintaining gene repression (153,154).

1.4.2.3 H3K27 methylation

In mammals, PRC2 is the only known histone methyltransferase (HMT) that catalyzes in an escalating fashion the post-translational modifications of H3K27 leading from an unmethylated lysine to mono-, di-, and eventually tri-methylated residue (151). In mouse embryonic stem cells (mESCs) and human haematopoietic stem cells (hHSCs), H3K27me1 is associated with actively transcribed genes (155), and in some situations, this modification of H3 is still detected despite a functional PRC2, indicating that the deposition of H3K27me1 may not be regulated by PRC2 alone (156,157). Studies in mESCs have shown that approximately 50% of the histone H3 is di-methylated whereas H3K27me1 and H3K27me3 show a similar rate (15%) suggesting an intermediary role of H3K27me2 in gene silencing (158). H3K27me3 is a stable mark for gene repression and also serves as a docking site for canonical PRC1 recognition and subsequent contribution to chromatin compaction (159). Notably, in some situations, i.e. embryonic stem cells, a transcriptionally permissive histone modification (H3K4me3) can co-exist

with H3K27me3 in a bivalent state (160,161). Genes marked with such a bivalent mark can either be swiftly transcriptionally activated or silenced as by contextual demand which is highly relevant during development and cell fate decisions.

1.4.2.4 PRC2 core components

PRC2 is composed of four core subunits, Suppressor Of Zeste 12 (SUZ12), Embryonic ectoderm development (EED), Enhancer Of Zeste 1/2 (EZH1/2) and pRB-associated protein 46/48 (RBAP46/48) (159). EZH1/2 acts as a methyltransferase and contains a SET domain which transfers a methyl group from the cofactor S-adenosyl-L-methionine (SAM) to Lysine at position 27 in the tail of histone H3. The mammalian homologues EZH1 and EZH2 are interchangeable subunits and form similar PRC2 complexes with different targeting mechanisms and eventually distinct functional consequences. EZH1 targets only a subset of genes that are influenced by EZH2 and affects only to a lesser extent the global H3K27me2/3 level (162). Both resolution of the crystal structures and biochemical studies have indicated that the catalytic SET domain of EZH2 is only accessible within the core complex contains both EED and SUZ12 (152,163). EED interacts with H3K27me3 via its aromatic cage which in turn leads to the allosteric activation of the methyltransferase element of PRC2 (164). Depletion of EED disrupts the propagation of H3K27 methylation marks to neighbouring unmodified histone H3, and hence disrupts embryonic development and haematopoietic homeostasis (163). SUZ12 plays a key role in PRC2 binding to the nucleosome with the help of RBAP46/48 via its Vrn2-Emf2-Fis2-Su(z)12 (VEFS) domain in the C-terminus (165). Recent biochemical and structural studies have furthermore shown an allosteric inhibition of PRC2 which is mediated by the interaction of the SUZ12 VEFS domain with the active

nucleosome marks, H3K4me3 and H3K36me2/3. This mechanism indicates that PRC2 may mediate a crosstalk between active and repressive histone methylation marks (166,167).

1.4.2.5 PRC2 accessory factors

In addition to the four core components, the PRC2 complex also interact in a tissue specific manner with several other molecules that fine-tune its function as cofactors such as the Adipocyte Enhancer-Binding Protein 2 (AEBP2), Jumonji AT rich interactive domain 2 (JARID2) and Polycomb-like (PCL) proteins (168–170).

AEBP2 is a zinc finger protein that was originally identified as a transcriptional repressor that binds to a regulatory sequence (AE-1) of an adipose fatty acid-binding protein. AEBP2 is ubiquitously expressed in mouse tissues and its structure reveals three Gli-Krüppel (Cys2-His2)-type zinc finger domains. The first and third zinc finger motifs of AEBP2 show the potential for DNA binding whereas the middle domain is important for transcriptional repression (171). In *Drosophila*, a protein homologous to the mammalian AEBP2, called JING, plays important roles in the development of the central neural system (172,173). Given that AEBP2 has the structural potential to bind to DNA and is an integral component of PRC2 found in mESC (169), and although AEBP2 lends itself as an excellent candidate to target PRC2 to specific regions of mammalian chromatin, its capacity to bind DNA in the context of PRC2 is unresolved. Recent structural studies have shown that by interacting with the N terminus of SUZ12, the SET domain of EZH2 and the C-terminus of RBAP46/48, AEBP2 is expected to stabilize the core PRC2 complex (167,174,175). Biochemical studies intended to dissecting AEBP2 into several functional domains demonstrated that its C terminal domains are responsible for PRC2

to bind to nucleosomes and the stimulation of the complex' HMTase activity (174,176). Taken together, AEBP2 serves an important role as a scaffold protein and an enhancer of PRC2's catalytic function.

1.4.2.6 PRC2 and PGE

Genes encoding tissue-restricted antigens that are targets of AIRE-regulated PGE are preferentially associated in mTEC^{hi} with repressive H3K27me3 marks (109). As PRC2 is the sole complex responsible for catalysing H3K27me3 modification in these cells, a role for AEBP2 is inferred in the molecular machinery that allows PGE to occur and effective thymocyte negative selection to occur.

1.5 Aim of the project

Recent research from our lab has shown that AIRE regulated gene loci are typically characterized by a significant reduction in the tri-methylation of lysine 4 of histone 3 (H3K4me3) but an enrichment of tri-methylation of lysine 27 (H3K27me3). This latter post-translational modification is catalysed by PRC2.

AEBP2 is a co-factor of PRC2 and may facilitate the targeting of PRC2 to specific gene loci where the complex exerts transcriptional repression.

The first aim of my doctoral project aims therefore to define the molecular role of AEBP2 in the development and function of thymic epithelia, with a special focus on the competence of AEBP2-deficient cells to affect PGE.

T cell precursors originating from the bone marrow, access the thymus via the vasculature and enter into its microenvironment at the cortico-medullary junction. During their

commitment to a T cell fate and the subsequent differentiation to phenotypically and functionally mature naïve effector and regulatory T cells, thymocytes migrate through the entire depth of the cortex to reach the subcortical region from where they migrate back to the cortico-medullary junction and eventually to the medulla. PRC2-mediated H3H27me3 modification has been shown to play a vital role in the development process. *The second aim of my project* seeks to investigate the role of AEBP2 within the context of PRC2 in thymocyte development.

Chapter 2. Methods and Materials

2.1 Mouse work

All animal work was done in fully compliance with UK Home Office regulations. Mice colonies were maintained in John Radcliffe Hospital biomedical science facilities in the University of Oxford unless otherwise stated. All mice used for experiments in this project were eventually culled by Schedule 1 methods. Procedures conducted on the mice strictly followed the project license in the lab.

2.2 Mouse models

2.2.1 *Aebp2* conventional KO mouse model

This mouse model was kindly provided by Professor Neil Brockdorff from Department of Biochemistry, the University of Oxford (169). By inserting a splice acceptor cassette in front of exon 2, only the first exon of *Aebp2* is transcribed which translates a 217 amino acids (aa) peptide (Figure 2.1).

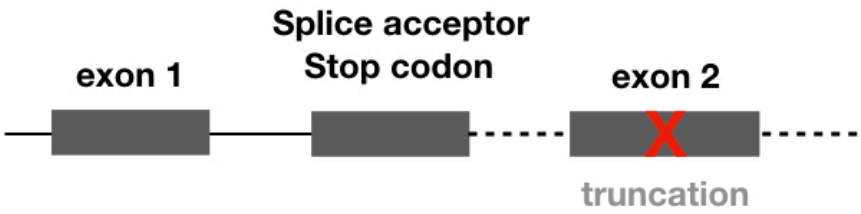

Figure 2.1 Diagram of *Aebp2* conventional KO mouse model

Insertion of splice acceptor and stop codon causes the truncation of exon 2 and the following exons.

2.2.2 Mouse gDNA preparation for genotyping PCR

I harvested the ear notch from mice that are older than 10 days or embryonic tissue.

Proteinase PK was added to the lysis buffer (recipe listed in the reagent part of the chapter) at a concentration of 0.1 mg /ml. I then add samples to 0.6ml Lysis buffer plus PK and incubate the samples at 55 ºC overnight (or a few hours are enough). The samples were centrifuged at max speed (16.2-21.1g [13-14.8K rpm] for 15min at RT with the micro centrifuge, and the supernatant were transferred to new tubes and 600**µ**l of Isopropanol was added into the tube to precipitate the released DNA. The samples were mixed well by inverting the tube and centrifuged at max speed for 15min at RT. I then carefully pour off the supernatant and wash the pellet with 600**µ**l 70% EtOH to remove salt which could interfere with PCR reaction later on. The tubes were centrifuged again at max speed for 15min at RT and the supernatant were poured off carefully. The pellets were air dried and then resuspended in around 50 **µ**l of TE depending on size of the tissue. I then denatured the proteinase PK within the DNA samples at 60 ºC for from 2 hours to overnight and then stored the DNA samples at + 4ºC for a period of up to a month or at – 20ºC for a long term storage. I normally use 3µl for PCR for AEBP2 genotyping.

2.2.3 Genotyping protocol

Genotyping with SequalPrep PCR kit (Invitrogen) for one reaction	
Template gDNA	3µl
10x buffer (dNTP included)	2µl
DMSO	0.4µl
10x Enhancer A	2µl

10uM Casor 2F & 2R mix	2µl
polymerase	0.36µl
Nuclease-free water	10.24µl
Total volume	20µl

94 °C	2mins	
94 °C	10s	X30 cycles
57.8 °C	30s	
68 °C	3mins	
72 °C		

2.3 Microbiology

2.3.1 Preparation of DH5α competent cells

DH5α cells frozen in glycerol were taken out onto an LB agar (from Fisher Scientific) plate (without antibiotics) and grown the plate overnight at 37 °C. Sterile 100 mM $CaCl_2$ and 100 mM MgCl2 solutions were prepared and chilled overnight at 4 °C. Next day, I inoculate one single colony from the LB agar plate into 20 ml sterile liquid LB (Fisher Scientific) and incubate them on a shaker at 37 °C overnight. On day 3, I inoculate 200 ml LB media with the 20 ml starter culture and incubate at 37 °C on a shaker. I then carefully measure the optical density (OD) by spectrophotometer (VWR) until it reaches approximately 0.4 and immediately chill the media on ice for 10 mins. From this step

onwards, all pipettes, tubes and solutions used need to be pre-chilled to 4 °C. The cells were spun down for 10 mins at 3000 rpm (1950g) at 4 °C in the bench top centrifuge and resuspended in 10 ml 100 mM MgCl2. The cells were kept on ice for 10 mins and the pelleting step were repeated. I then resuspend the cells with 20 ml 100 mM $CaCl_2$ solution and keep them on ice for 20 mins. The cells were stored at -80 °C in a final concentration of 15% glycerol (1 ml cells + 0.25 ml 80% glycerol) for later transformation.

2.3.2 Sub-cloning of *Aebp2* plasmids

C-terminal Flag AEBP2 exons 1-3 expressing plasmid

The pCMV plasmid containing full length *Aebp2* isoform 1 (adult isoform) was purchased from OriGene company (Figure 2.2). There is a Flag tag fused to the C terminus of *Aebp2*. Exons 1-3 of *Aebp2* were amplified by PCR from this plasmid with primer sets (F-BamHI-Aebp2 and R-XhoI-Aebp2 exon3). BamHI–Aebp2 exons 1-3–XhoI were then inserted back into the original plasmid replacing full length *Aebp2* by multiple cloning sites (MCSs) BamHI and XhoI (Figure 2.3).

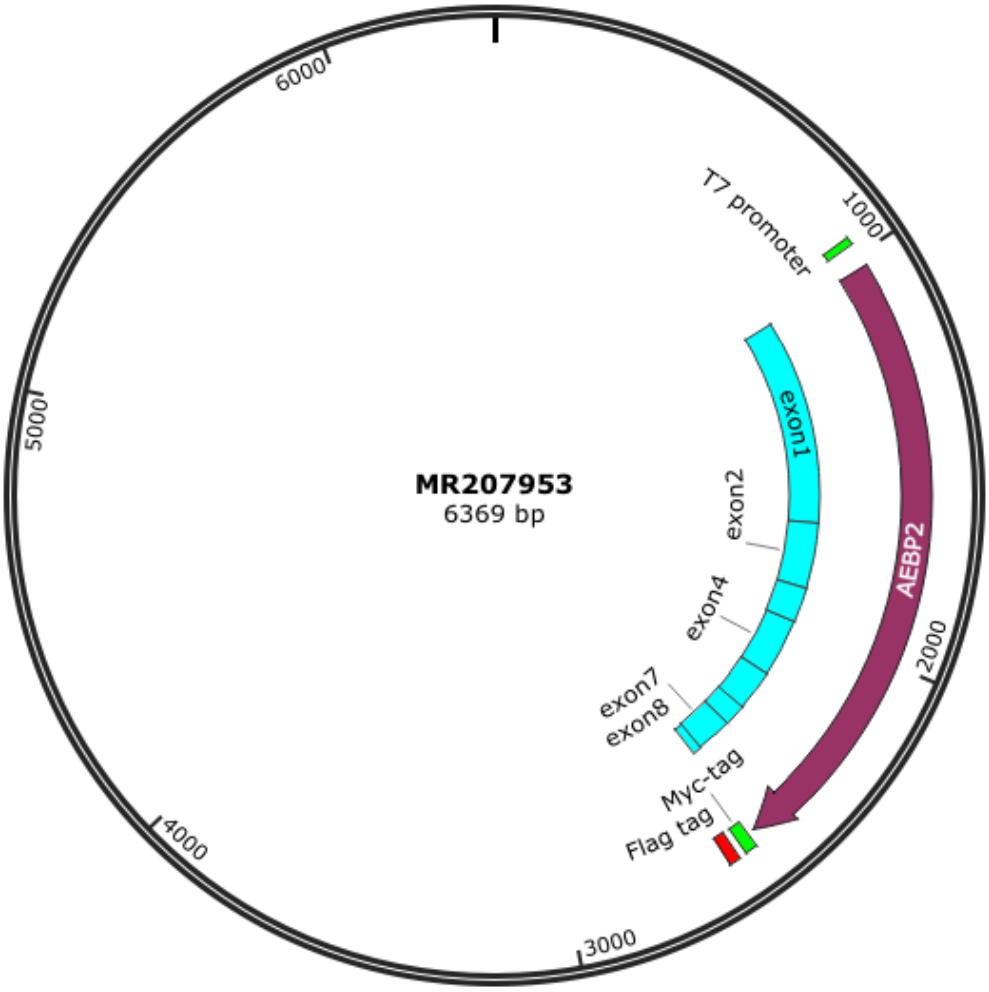

Figure 2.2: Map of C-terminal Flag tagged full length AEBP2 plasmid

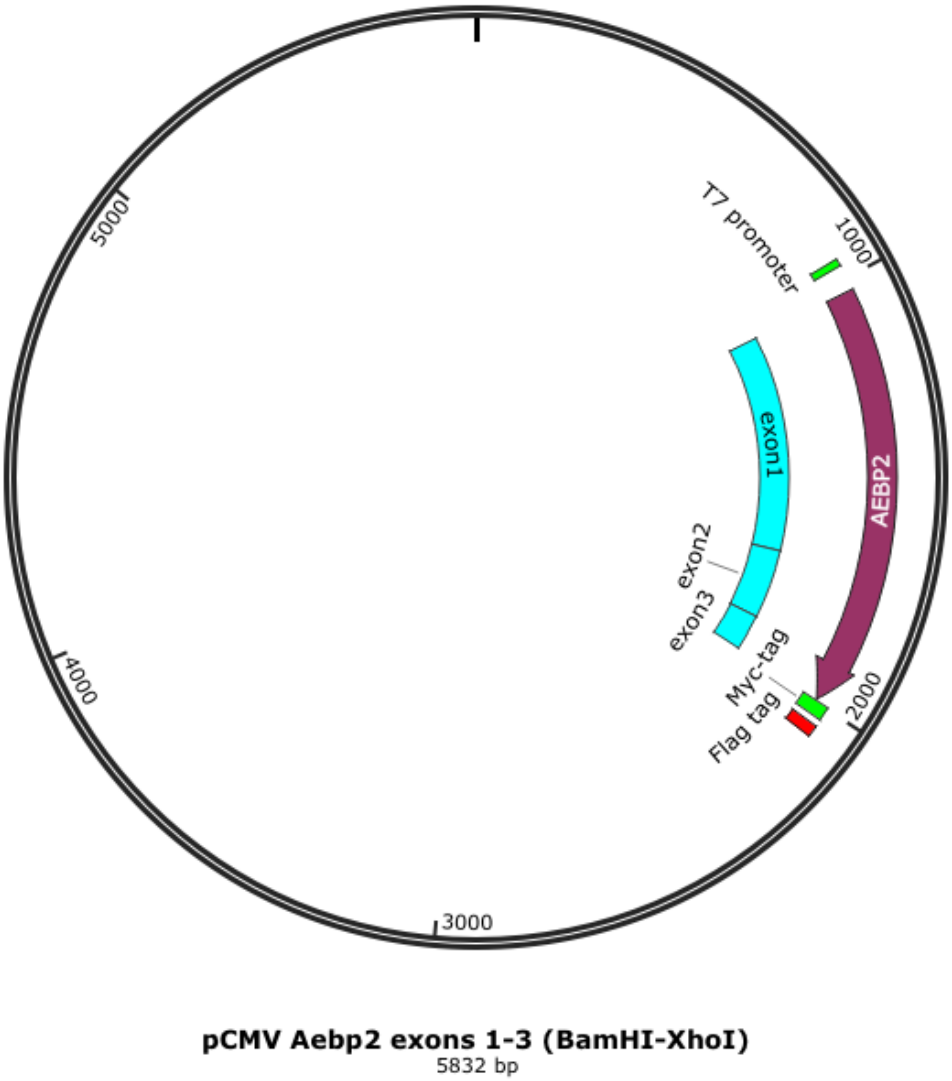

Figure 2.3: Map of C-terminal Flag tagged AEBP2 exons 1-3 plasmid

N-terminal Flag AEBP2 exons 1-3 expressing plasmid

The pLion plasmid is an empty vector that has a Flag tag on the N-terminus of the MCS. It is kindly given by a colleague in the Weatherall Institute of Molecular Medicine (WIMM) to generate the plasmid containing either full length or exons 1-3 of AEBP2 with N-terminal Flag. *Aebp2* exons 1-3 were cloned by PCR from pCMV full length *Aebp2* plasmid introduced above using primer sets (F-EcoRI-Aebp2 and R-XbaI-Aebp2 exon3) and inserted into pLion plasmid by MCSs EcoRI and XbaI (Figure 2.4).

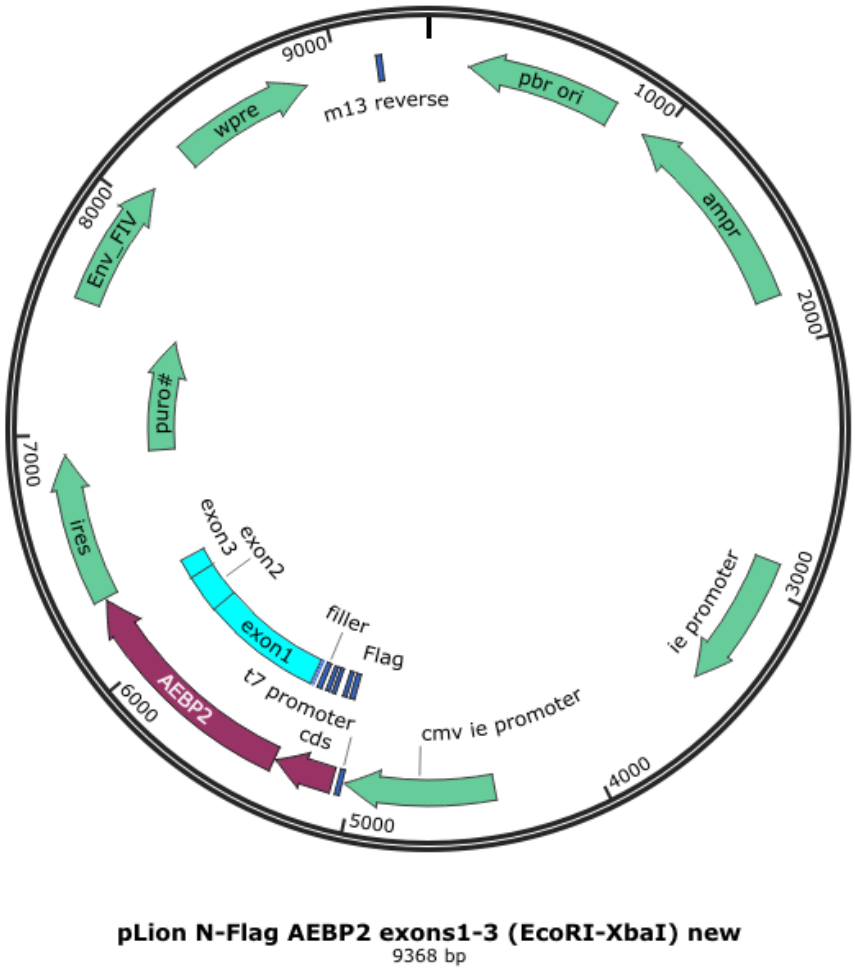

Figure 2.4: Map of N-terminal Flag tagged AEBP2 exons 1-3 plasmid

N-terminal Flag full AEBP2 expressing plasmid

Full length *Aebp2* were cloned from pCMV *Aebp2* plasmid introduced above by primer sets (F-EcoRI-Aebp2 and R-XbaI-Aebp2 full length). It is then inserted into the pLion plasmid by MCSs EcoRI and XbaI (Figure 2.5).

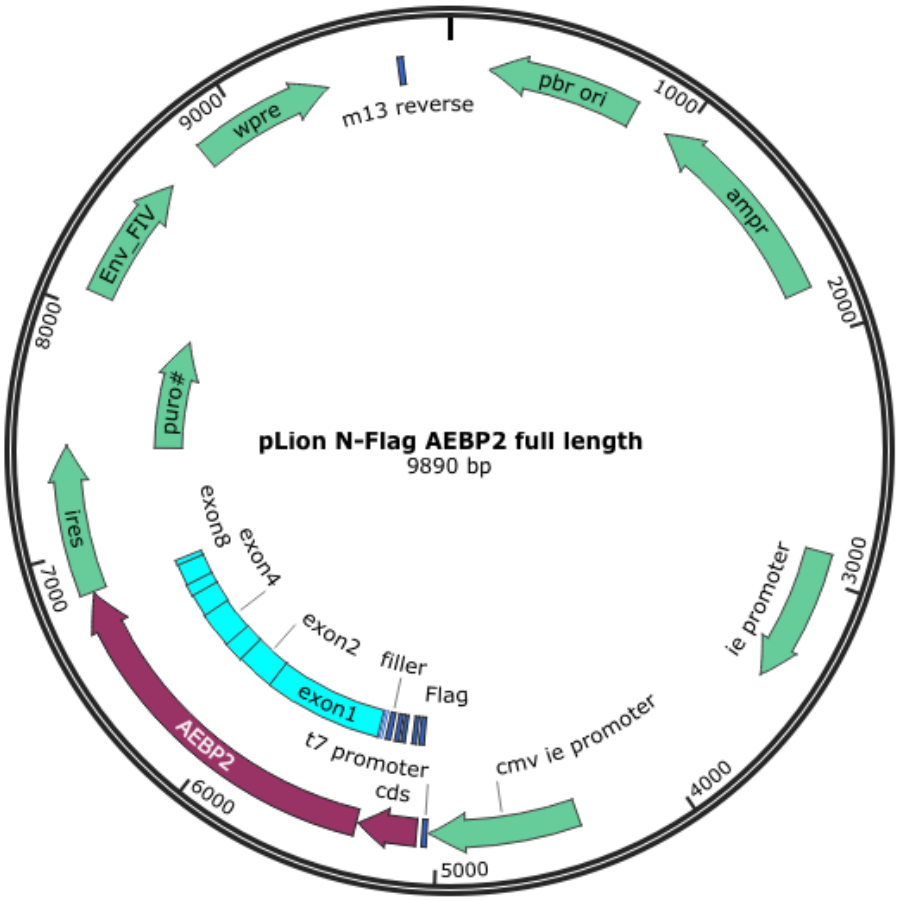

Figure 2.5: Map of N-terminal Flag tagged AEBP2 full length plasmid

2.3.3 Transformation

The plasmid DNA was added into DH5α cells and gently mix them by pipetting. The cells were kept on ice for 20 mins and then heat shocked by incubating at 42 °C for 2 mins and chilled back on ice immediately for 2 mins. If the plasmid is with Ampicillin resistance, the cells were placed immediately on the plate supplemented with Ampicillin and incubated overnight at 37 ºC. If it's with Kanamycin resistance, 1ml 2x LB was added into the cells and incubated at 37 ºC for 30 mins. Afterwards, the cells were placed on the Kanamycin plate and incubated overnight at 37 ºC.

2.4 Biochemical and molecular biological assays

2.4.1 Cell culture

HEK293T and Hela cell lines were cultured in Dulbecco's modified Eagle's medium, supplemented with 10% fetal calf serum, 100 IU/ml penicillin, 100 μg/ml streptomycin. Mouse mTEC 1c6 cell lines were cultured in IMDM (containing Glutamax and HEPES), supplemented with 10% fetal calf serum, 100 IU/ml penicillin, 100 μg/ml streptomycin.

2.4.2 Cultured cell transfection

Transfection of recombinant plasmids into cultured cell lines was conducted with FuGENE HD reagent (Promega). The amount of plasmid DNA required for the assay was calculated based on the online database after inputting correct cell type and cell number. Mix the DNA with indicated amount of optiMEM and FuGENE HD reagent sequentially. Incubate 5-10 mins in room temperature and add the required volume to the cells gently.

2.4.3 Protein extracts, immunological analysis, and antibodies

Cells were lysed in an ice-cold buffer (20mM Tris-HCl (pH7.5), 0.1% NP-40, 1mM DTT, 4mM ATP, 5mM MgCl2, 1mM Phenylmethylsulfonyl fluoride (PMSF)) and incubated 15min on ice. Centrifuge the cell extract at 450g for 20min at 4°C and transfer the supernatant to a clean 1.7ml eppendorf tube for later assays, such as co-immunoprecipitation (Co-IP) and Western blot (WB).

2.4.4 Immunoprecipitation (IP) and Co-IP

Protein extracts were incubated with antibodies recognizing the particular protein, and magnetic protein A or G beads (Thermo Scientific) that can capture the Fc region of

antibodies for 1 hour or overnight in the cold room under rotation. Afterwards, the beads were captured with a magnetic rack and washed gently for three times with wash buffer (50 mM Tris-HCl pH 7.5, 150 mM NaCl, 10% (w/v) glycerol, supplemented with 0.05% Triton X-100 before use). I then completely removed the wash buffer after last wash and resuspended the beads with cell lysis buffer. The precipitated proteins captured by the beads were denatured by adding sample buffer (250 mM Tris-HCl [pH 6.8], 10% [w/v] SDS, 35% [v/v] glycerol, 0.05% BPB, add 0.7 M (final concentration=5%) 2-mercaptoethanol (14.3M) right before use) and incubated for 5 mins at 95 °C. Note: Protein A and G have different affinities for IgG from different species. Choose carefully between them depending on the host species for antibody generation.

2.4.5 Western blot (WB)

Protein samples either directly from cell lysate or after IP/Co-IP assays need to be denatured with sample buffer by incubation for 5 mins at 95 °C. The samples were then added into the precast protein electrophoresis gel (BioRad) for separation (Carefully choose the gel percentage depending on the protein sizes for good separation). Separated proteins were then transferred onto polyvinylidene difluoride (PVDF) membrane for fixation and incubated with the indicated primary antibodies after blocking the membrane to decrease the nonspecific background. Fluorescent or Horseradish Peroxidase (HRP)-conjugated secondary antibodies (LiCOR) were then used to recognize the primary antibody. Fluorescent secondary antibodies were directly detected by LiCOR scanner whereas HRP-conjugated ones were incubated with enhanced chemiluminescence (ECL) reagent (ThermoFisher) and then detected by FUSION FX scanner.

2.4.6 Cytospin

The cells were isolated and resuspended at 10,000 cells in 100µl of ice cold PBS. The cells were kept on ice while preparing the cytospin holder. A labelled slide was loaded into a Cytospin holder with Shandon Filter card and funnel. I then pre-wet the filter by loading 100µl PBS through the funnel and centrifuging at 1100rpm for 2 mins in the Cytospin centrifuge. Next I loaded the cells into the funnel and centrifuge at 1100rpm for 3 mins in the Cytospin centrifuge. The slides were placed onto a slide holder and allowed to air dry for a few minutes. I then delineated cell spot with a PanPen and placed the slides into -20 ºC Acetone and incubated them for 10mins to permeabilize and fix the cells. The slides were then ready for immunofluorescent staining.

N.B. An alternative way to permeabilize and fix the cells is using 0.1% Triton X-100 in PBS for 15 min on ice.

2.4.7 Immunofluorescence (IF)

The slides were washed 2 times with RT PBS for 5 mins and blocked with 200µl appropriate serum (1XPBS + 5% goat serum (0.75ml goat serum +14.25ml PBS)) for 30-60mins at RT. I then flicked off the blocking solution and added the primary antibody diluted with the blocking solution at the appropriate dilution and incubate for 60 mins at 37 °C. Next I washed the slides 3 times with PBS and incubated the slides with the fluorescent secondary antibody for 60 mins at 37 °C in the dark. I then washed off the secondary antibody with PBS three times and let the slides dry in the dark. Prolong Gold antifade mounting reagent (premixed with DAPI) was used to mount the slides and cover with cover slides. The slides were sealed with nail polish and the slides were ready for imaging via fluorescent microscopes. The slides can be stored at 4 ºC keeping from light.

N.B. Treat a spot in the identical fashion by only incubating it with the secondary antibody for without the primary antibody to control for the secondary antibody non-specific binding.

2.4.8 quantitative Real Time (RT)-PCR

2.4.8.1 total RNA extraction and cDNA synthesis

I Prepared at least 15,000 cells for the extraction of total RNA for qRT-PCR. The total RNA was extracted with RNeasy plus micro kit (Qiagen) following the manufacturer's recommendations. Afterwards, cDNA was synthesized using SensiFAST cDNA kit (Bioline) with 13 µl total RNA from the previous step as follows,

Total RNA	13µl
5X TransAmp Buffer	4µl
sterile nuclease-free water (Ambion)	3µl
Total volume	20µl

The reaction solutions were mixed gently and incubated with the thermocycler using following program for one cycle.

25 °C 10mins

42 °C 15mins

85 °C 5mins

2.4.8.2 qRT-PCR using SensiMix from BioLine (QT605)

The mastermix solutions were prepared as follows. 0.1ml 96-well plate was prepared and each sample and no template control (NTC) were run in triplicate (Include NTC for each primer pair). 9µl mastermix was mixed with 1 µl cDNA or water (for NTC) per well. The plate was covered with optical sealing film and spun down for 10 seconds and subsequently run in AB StepOne Plus Real-Time PCR System.

	1x	**Final**
Water	3.6µl	
2x SensiMix Sybr	5µl	1x
F primer (10µM)	0.2µl	0.2µM
R primer (10µM)	0.2µl	0.2µM
Total	**9µl**	

qRT-PCR program was set up by choosing 96-wells, quantitation comparative Ct (ΔΔCt), Sybr green reagents, and including melt curve, standard 2hr run. The plate was set up by selecting template type and primer sets, reference sample and endogenous control.

Choose the reaction volume as 10µl, and follow the program below:

95°C 10mins

40x 95°C 15secs

Ta 15secs (Ta = Tm or Tm-3°C)

72°C 15secs

Melt curve (default)

95°C 15secs

60°C 1min

95°C 15secs

After the run was finished, NTCs were checked to make sure they are clear in amplification plots (use melt curve to help), and correct Ct values were set using both log and linear view followed by analysing the data. The data can be exported as excel files for quantitative analysis.

(Optional) qPCR products can be run on agarose gel to confirm whether the amplification was specific and no primer dimers were formed, especially when using a primer pair for the first time.

N.B. Do not write on plate as marker can interfere with fluorescence absorbance.

2.5 Flow cytometry staining

I isolated the tissue and prepared the single cell suspension using ice cold FACS buffer. Cell number was counted by CASY cell counter and correct number was distributed into the round-bottom polypropylene FACS tubes. 2 ml FACS buffer was added into the tube and the cells were spun down at 450 g at 4 ^{o}C for 5 mins. The supernatant was discarded and the cells were stained with the antibody master mixes at 4 ^{o}C for 20 mins. The cells were washed afterwards by adding 2 ml FACS buffer and centrifuged at 450 g at 4 ^{o}C for

5 mins. After decanting the supernatant, the cells were resuspended. The cells were ready for flow cytometry analysis or the next round of antibody staining.

2.6 Transplantation assays

2.6.1 Fetal thymus transplant under the kidney capsule

Aebp2^{tm1a} heterozygous mice were time mated to obtain embryos at E18.5. The thymi were harvested from these embryos and grown as fetal thymic organ culture (FTOC) for 1 day while the tail tissues were taken for genotyping. The next day, recipient B6.SJL.CD45.1 male mice between 11-12 weeks of age were anaesthetised by subcutaneously administering equal parts 1 mg/ml Domitor (Vetoquinol) and 100 mg/ml Ketamidor (Chanelle) prepared by animal weight, followed by an equal volume of the analgesic Buprecare (Animalcare) at 0.3 mg/ml. When the recipient mice were fully anaesthetised, two whole WT or *Aebp2*$^{-/-}$ embryonic thymic lobes were transplanted under the renal capsule of the left kidney of recipient mice using aseptic surgery. After the transplantation, mice were administered 5 mg/ml of the anaesthetic reversal drug Antisedan (Vetoquinol) in a dose volume equal to the amount of Dormitor given and 500 µl PBS (Gibco) to prevent dehydration. Mice were monitored until reflexes had returned fully, then daily for 8 days and twice weekly thereafter. Recipient mice were culled for flow cytometry analyses 6 weeks post-transplantation.

The surgery was kindly performed by Tiago Luis (University of Oxford). Vicryl Rapide (Johnson & Johnson) dissolvable sutures were used.

2.6.2 Fetal liver transplant

Aebp2^{tm1a} heterozygous mice were time mated to obtain embryos at E15.5. When performing transplantation experiment with a competitor system, timed mating of B6.SJL.CD45.1 crossing with our in-house CD45.2 strain was used to obtain CD45.1/2 FL cells at E15.5. Fetal livers were dissected from these embryos and pipetted through 18 gauges needles with 2 ml syringes to achieve a single cell suspension. Cells were spun down at 300g and stored with 10% DMSO in FBS in LN for later use. On the day of fetal liver transplantation experiment, FL cells were thawed and washed with pre-warmed 1X dPBS with 0.02% BSA. After being spun down and resuspended in 1-2 ml 1X dPBS with 0.02% BSA, the cell numbers were counted and mixed with CD45.1/2 competitor cells to get 4 million total FL cells (2 million Aebp2 ^{tm1a} + 2 million CD45.1/2 cells) per 50 µl 1X dPBS with 0.02% BSA. The cells were kept on ice before injection. Recipient B6.SJL.CD45.1 male mice at 6-7 weeks old were lethally irradiated at a dose of 1050 rad (split into 550rad + 500 rad with at least 4 hours in between) to achieve the depletion of haematopoietic cells and thymocytes. Recipient mice were injected intravenously with the prepared fetal liver cell suspensions. The injected mice were then monitored twice daily for 16 days and three times per week thereafter. For short-term FL transplantation, recipient mice were culled 6 weeks post-transplantation for analyses.

2.6.3 Adult BM HSC transplant

For the long-term serial transplant experiment, there were two steps of transplantation. A primary transplant was performed as for the FL transplant as introduced above. 16 weeks post-transplantation, 1000 CD45.2+ BM HSCs from experimental groups were FACS sorted from the primary recipients and mixed with same number of CD45.1/2 competitor

adult BM HSCs from CD45.1/2 wild type mice. 200,000 unfractionated total BM cells from 6 week-old B6.SJL.CD45.1 mice (as protector cells) were added as well and i.v. injected into lethally irradiated B6.SJL.CD45.1 secondary recipient mice. 16 weeks post-transplantation, the mice were culled for analyses.

2.7 Organ preparation and cell isolation

2.7.1 TEC isolation

Thymi were isolated and cleaned to get rid of the residual fat and connective tissue. They then undergo a serial steps of enzymatic digestion by incubating with liberase buffer at 37 ^{o}C. For thymi from adult mice, 2 ml of liberase buffer was added to each sample and gently pipetted to disrupt the sample with tips that were cut beforehand. Incubate the solution at 37 ^{o}C for 10 mins and then collect the supernatant. Repeat the step 2 more times using 1 ml of fresh liberase buffer each time. For the embryonic thymi, use 500 - 1000 µl liberase buffer in total for digestion per sample. The supernatant samples were collected with a 50 ml Falcon tube (Corning) containing 40 ml cold FACS buffer on ice and then centrifuged at 435 g (1500 rpm) to achieve a single cell suspension.

Adult TECs usually need to be enriched before any following assays. They were incubated with anti-CD45 beads (Miltenyi Biotec) at a concentration of 100 X 10^6 cells per 1 ml for 15 mins at 4 ^{o}C according to the manufacturer's instruction. Afterwards, the cells were washed with FACS buffer and filtered through a 30 µm filter (Millipore). The cells were then resuspended at a concentration of 100 million per 1 ml FACS buffer and loaded onto the AutoMACS separator (Miltenyi Biotec) for the depletion of CD45+ cells. Choose the "depletes" program and rinse between each sample for that purpose.

2.7.2 T cell isolation

The thymi, spleen and LN were gently squashed with frosted glass slides (Thermo Scientific) that were pre-wet with FACS buffer. For analysis using splenocytes, after releasing the cells from the spleen, the red blood cells (RBCs) were lysed with RBC buffer by mixing with cell samples at 1 : 4 ratio and incubate the mix on ice for 5 mins. Cells were then washed with cold FACS buffer and filtered through a 70 μm filter (Millipore) and subsequently resuspended with FACS buffer to achieve a single cell suspension.

N.B. For the assays using T cells from spleens, the Fc receptor of myeloid, B cells and some other cell types need to be blocked to prevent artificially false positive staining of primary antibodies.

2.7.3 Haematopoietic cell isolation from BM

Haematopoietic stem and progenitor cells (HSPCs) were harvested by crushing the femurs and tibiae using a mortar and pestle with FACS buffer. Usually the crushing takes two rounds until the bones turn white. The cell suspensions were collected through a 70 μm filter (Millipore) directly into a 50 ml Falcon tube and washed with FACS buffer. The cells need to undergo RBC lysis before the following staining steps applied. The cells need to be blocked for Fc receptor same as spleen samples before following staining.

2.8 Bulk RNA sequencing

2.8.1 TEC RNA sequencing

1500 cTECs (EpCAM+ Ly51+) and 1500 mTECs (EpCAM+ UEA1+) from wild type and *Aebp2*$^{-/-}$ E18.5 embryos were FACS sorted directly into RLT plus buffer from RNeasy plus kit (Qiagen) followed by total RNA extraction with the kit. Paired-end (2 x 75 bp) sequencing was performed using the Illumina HiSeq 4000 machine running Smart-seq2 chemistry (Wellcome Trust Centre for Human Genetics, University of Oxford). QC metrics were generated by the FastQC package and all samples passed QC. All 12 RNA-seq libraries were sequenced on a single lane. Raw reads were mapped to the *Mus musculus* (mm10) reference genome using HISAT2. HISAT was run in a 2-pass approach with options "--score-min L,0.0,-0.2" and known splice sites for the first pass, and novel splice sites detected across all samples for the second pass. Gene-level count data was obtained using featureCounts program (http://bioinf.wehi.edu.au/featureCounts/). Separately, raw reads were also processed using Salmon to quantify transcript abundance. Salmon was run with options "--gcBias". Ensembl transcript and gene annotations (release 91) were obtained using the biomaRt package and used to aggregate Salmon TPM transcript abundance at the gene-level. Differential expression was performed using the DESeq2 package.

One of the *Aebp2*$^{-/-}$ embryos was found to be male whereas the other two *Aebp2*$^{-/-}$ and three WT embryos were female. Therefore the male gender outlier was excluded from all the analyses presented in the thesis.

2.8.2 HSC RNA sequencing

500 HSCs (Lin-Sca1+Kit+Flt3-CD150+CD48-) from wild type and *Aebp2*$^{-/-}$ E15.5 fetal liver were FACS sorted directly into RLT plus buffer from RNeasy plus kit (Qiagen) followed by total RNA extraction with the kit.. Paired-end (2 x 75 bp) sequencing was performed using the Illumina HiSeq 4000 machine running Smart-seq2 chemistry (Wellcome Trust Centre for Human Genetics, University of Oxford). Data were QC'ed using FastQC, trimmed using Trimmomatic, aligned using STAR, reads assigned to genes using HTSeq and differential analysis performed using edgeR (with trimmed M of means normalisation and general linear modelling - significance was reported if the false discovery rate (estimated by Benjamini Hochberg) was less than 0.05.

2.9 Statistics

Statistical analysis was conducted with Prism (Graph Pad). Experimental data is depicted as mean ± standard deviation (SD). Statistical significance was determined using two-tailed, unpaired Student's t-tests. Significance is represented as * $p < 0.05$; ** $p < 0.01$; *** $p < 0.001$; *** $p < 0.0001$

2.10 Standard reagents and antibodies:

Buffer/Media	Ingredients	Final Concentration
FACS buffer	Phosphate-Buffered Saline (PBS)	1X
	Fetal Calf Serum (FCS)	2%
MACS buffer	PBS	1X

	Bovine Serum Albumin (BSA)	0.2%
Liberase digestion buffer	PBS	1X
	Liberase	2.5mg/ml
	Dnase	10mg/ml
Agarose gel loading dye	Glycerol	30%
	Bromophenol Blue	4mg/ml
	Xylene Cyanol FF	4mg/ml
Mouse tissue lysis buffer	Tris HCl pH8.5	100mM
	Ethylenediaminetetra-acetic acid (EDTA)	5mM
	Sodium Dodecyl Sulfate (SDS)	0.20%
	Sodium Chloride (NaCl)	200mM
	Proteinase K	0.20%
Cell lysis buffer for Western blotting (WB)	Tris HCl pH8.0	25mM
	NaCl	50mM
	NP-40	1%
	DTT	1mM
	Prtease inhibitor	1tablet in 10ml

	PMSF	0.2mM
Runing buffer for WB (1X)	Tris Base	3.03g in 1L
	Glycine	14.4g in 1L
	SDS	1g in 1L
Transfer buffer for WB (1X)	Tris Base	3.03g in 1L
	Glycine	14.4g in 1L
	Methanol	20% in 1L
TBS-T buffer (wash buffer) for WB	Tris HCl pH7.5	50mM
	NaCl	150mM
	Tween-20	0.10%
Block buffer for WB	BSA	3-5% in 1X TBS-T buffer
Red Blood Cell (RBC) lysis buffer	Ammonium chloride (NH4Cl)	8.26mg/ml
	Sodium Bicarbonate (NaHCO3)	1.19mg/ml
	EDTA	0.1mM
Tris-EDTA (TE) buffer	Tris HCl pH7.5	10mM
	EDTA	1mM
Fetal liver harvest buffer	PBS	1X
	BSA	0.20%

Flow cytometry Antibody list

Antibody	**Clone**	**Isotype**	**Fluorochrome**	**Source**
Aire	5H12	Rat IgG2c, κ	Alexa Fluor 488	eBioscience
B220	RA3-6B2	Rat IgG2a, κ	PE	BioLegend
CCR7	4B12	Rat LOU/M IgG2a	BV421, BV605, PE	BD Biosciences
CD117	2B8	Rat IgG2b, κ	PE Cy5	BioLegend
CD11b	M1/70	Rat IgG2b, κ	Biotin	BioLegend
CD11c	N418	Armenian Hamster IgG	Biotin	BioLegend
CD19	1D3	Rat IgG2a, κ	Biotin	eBioscience
CD205	205yekta	Rat IgG2a, κ	PE efluor610	BioLegend
CD24	M1/69	Rat IgG2b, κ	APC, FITC	BioLegend
CD25	PC61.5	Rat IgG1, l	BV605, efluor450	eBioscience
CD28	37.51	Syrian Hamster IgG	-	BioLegend
CD31	390	Rat IgG2a, κ	Biotin	BioLegend
CD3ε	145-2C11	Armenian Hamster IgG	-	BioLegend
CD3ε	17A2	Rat IgG2b, κ	-	BioLegend
CD3ε	145-2C11	Armenian Hamster IgG	PerCP Cy5.5	eBioscience

CD4	RM4-5	Rat IgG2a, κ	APC Cy7, PE Texas Red	BioLegend
CD44	IM7	Rat IgG2b, κ	PE Cy7, PE efluor610	eBioscience
CD45	30-F11	Rat IgG2b, κ	Alexa Fluor 700	BioLegend
CD45.1	A20	Mouse IgG2a, κ	BV510	BioLegend
CD45.2	104	Mouse IgG2a, κ	BV510	BioLegend
CD49b	DX5	Rat IgM, κ	Biotin	BioLegend
CD5	53-7.3	Rat IgG2a, κ	PE Cy5,PerCP Cy5.5	BioLegend
CD62L	MEL-14	Rat IgG2a, κ	PE Cy7	BioLegend
CD69	H1.2F3	Armenian Hamster IgG	PE Cy5, PE Cy7	BioLegend
CD80	16-10A1	Armenian Hamster IgG	PE Cy5	BioLegend
CD86	GL-1	Rat IgG2a, κ	PE Cy7	BioLegend
CD8a	53-6.7	Rat IgG2a, κ	Alexa Fluor 700	BioLegend
Epcam	G8.8	Rat IgG2a, κ	PerCP Cy5.5	BioLegend
F4/80	BM8	Rat IgG2a, κ	Biotin	BioLegend
Fc Block (Mouse)	2.4G2	Rat IgG2b, κ	-	BD Biosciences
FoxP3	FJK-16s	Rat IgG2a, κ	PE efluor610	eBioscience
Gr-1	RB6-8C5	Rat IgG2b, κ	Biotin	BioLegend

Helios	22F6	Armenian Hamster IgG	BV421	BioLegend
I-A/I-E	M5/114.15.2	Rat IgG2b, κ	FITC, BV421	BioLegend
Ly51	6C3	Rat IgG2a, κ	PE	BioLegend
MHC-I	28-14-8	Mouse IgG2a, κ	PE	eBioscience
NK1.1	PK136	Mouse IgG2a, κ	Biotin	BioLegend
PD-1	29F.1A12	Rat IgG2a, κ	APC	BioLegend
Qa-2	695H1-9-9	Mouse IgG2a, κ	Biotin	BioLegend
Streptavidin	-	-	APC, APC Cy7, BV605, PerCP Cy5.5, PE Cy5	BioLegend
TCRβ	H57-597	Rat IgG2b, κ	APC Cy7, FITC, PE	eBioscience
TCRγδ	GL3	Armenian Hamster IgG	Biotin	eBioscience
Ter119	TER-119	Rat IgG2b, κ	Biotin	BioLegend
ckit	2B8	Rat / IgG2b, κ	APCe780	eBioscience
CD150	TC15-12F12.2	Rat IgG2a, λ	PECy7	BioLegend
CD48	HM48-1	Armenian Hamster IgG	APC	BioLegend
CD150	TC15-12F12.2	Rat IgG2a, λ	APC	BioLegend

CD41	eBioMWReg30 (MWReg30)	Rat / IgG1, κ	PECy7	eBioscience
FcgR	93	Rat / IgG2a, λ	PerCPe710	eBioscience
CD105	MJ7/18 (RUO)	Rat IgG2a, κ	BV421	BD Biosciences

WB antibody list

Antibody	**Clone**	**Isotype**	**Source**
EZH2	D2C9	Rabbit IgG	Cell Signaling
AEBP2		Rabbit IgG	Generated by a collaborator

IF antibody list

Antibody	**Clone**	**Isotype**	**Source**
Flag	M2	Mouse IgG1	Sigma

Cytokines for HSC in vitro culture

Cytokine	**Final concentration**	**Source**
Recombinant Murine IL-3	5 ng/ml	PEPROTECH

Recombinant Murine SCF	2 ng/ml	PEPROTECH
Recombinant Human Flt3-ligand	5 ng/ml	PEPROTECH
Recombinant Human TPO	5 ng/ml	PEPROTECH
Recombinant Mouse G-CSF	10 ng/ml	STEMCELL
Recombinant Mouse GM-CSF	10 ng/ml	STEMCELL

Primers:

Primer name	**Upper case**
F-EcoRI-Aebp2	CCAAGAATTCTGCCGCCGCGCTCGCCGA
R-XbaI-Aebp2 exon3	TCTAGATTACTTGAAAGGCTTGTCTCCACTGTG
R-XbaI-Aebp2 full length	CCTCTAGATTACCTCTTCAACCTCTTCTGCGGC
F-BamHI-Aebp2	CCCGGATCCGGTACCGAGGAGATC
R-XhoI-Aebp2 exon3	GGCTCGAGCTTGAAAGGCTTGTCTCCACTG
mAebp2-a1 (Forward)	CGGCCAGCGCTACACCCCAAGAACT
mAebp2-a2 (Forward)	GGGGAGCCGCTGAGCCGCATGGACT
mAebp2-b (Reverse)	GAAGCATGCCTGGCACTGGTC
casor_2F	ATAAAAATGTGAGGAGCCAGATGTG
casor_2R	TGGCTTCTTAGGGACTTGCT
cKO For_WW	CGTACAATTGGATATCGAGCTCG
WW_01	CGCCTTCTATGAAAGGTTGG
WW2_RV	CGCATCGCCTTCTATCGC
WW3_Fr	ACGAAGTTATAAACAACGCGTG
WW4_Fw	CTTGCTGTTCCTGTTAGACC
WW5_Rv	GCTTGTTCATTCCAGCTTTAG
WW6_Fw	TGCTATACGAAGTTATGCATGC
WW7_Fw	GTCAGGTCTCATTACAGATGG
WW8_Rv	CCCTCACACACTGCACTC

WW9_Fw	CTTTGGATCCACTGATCAGC
WW10_Rv	CTTGGTTCCCAAAAGGCTTTC
Loxp Fwd	GGGGATGGCTACAGAATAT
Loxp Rv1	TCCAGCTTTAGAAGGAGATTC
Loxp Rv2	ACGCGTTGTTTATAACTTCG
E2A Fwd	CAGATGGTGGCCTGGATACT
E2A Rv	CATCCCTGCTGTAGCTGTCA
Bcl11b Fwd	GGGCGATGCCAGAATAGAT
Bcl11b Rv	GGTAGCCTCCACATGGTCAG
Runx1 Fwd	CTCGGCAGAACTGAGAAATG
Runx1 Rv	GGTGATGGTCAGAGTGA
Runx3 Fwd	GGTTCAACGACCTTCGATTC
Runx3 Rv	GGTCCATCCACAGTGACCTT
ThPOK Fwd	ACCCAACGGCTGAAAGGA
ThPOK Rv	GCTGCTGTGGTCTGGGAAT

Chapter 3. In vitro profiling of *Aebp2*

PRC2-mediated methylation of H3K27 (mainly H3K27me3) plays a vital role in maintaining the repression of many regulator genes in mouse ES cells (177). Nowadays, it is widely appreciated that this histone modification tightly associates with lineage-specific gene repression which is crucial in the context of organogenesis and tissue development (159). The development of the thymus (for both TEC and thymocyte compartments) is a multi-step process that includes cell commitment, proliferation, and maturation (138,178). Indeed, T cell development in the thymus has attracted interest as an informative step-wise model to study the function and molecular basis of PRC2 in gene regulation (179–183). Due to its importance in tissue development, a loss of PRC2 function consequent to a deletion of the core component *Ezh2* results in a block in early development (179). These defects are usually accompanied by limited cell number and lower differentiation degree of the cells, which makes extensive functional studies very difficult. In order to study the molecular mechanism of PRC2 in thymus development and function, I choose to investigate the role of AEBP2, one of the co-factors associated with PRC2. AEBP2 stabilizes the PRC2 and enhances the HMTase activity of the complex (174,176). Yet, deletion of AEBP2 does not disrupt PRC2's enzymatic activity completely which allows us to study the role of AEBP2 in the context of PRC2 across all developmental stages.

3.1 Aebp2 is expressed in both TEC and lymphoid compartments

AEBP2 is evolutionarily well conserved and had originally been identified as a transcriptional repressor (171). Structurally, AEBP2 contains four major domains; i.e. acid, neutral, zinc finger, and basic domain (168). The zinc finger and basic domains have

the highest level of sequence conservation across all animal species, whereas the acid and neutral domains are lineage-specific. In mammals, the zinc finger and basic domains interact with PRC2 core components (167,184). Mouse genomic analysis revealed that *Aebp2* transcription involves two splicing alternatives at the 5' end, that produce two dominant RNA isoforms (185). The major difference between these two isoforms is that one does not contain the exon1, which encodes the N-terminal acid and neutral domains. qRT-PCR analyses of several mouse tissues (brain, testis, heart, and 14 day embryo) showed that both isoforms are present in all tissues examined. The longer isoform has a higher expression than the shorter one in all tissues except the 14 day embryo. However the pattern is reversed for the shorter isoform as it is highly expressed only in the 14 day embryo. A Western blot experiment identified two protein isoforms from these tissues. A bigger protein (52kDa) was detected in the adult tissues whereas a smaller protein (32kDa) was only detected in the embryonic tissue. Thus these two protein isoforms are designated as the adult (52 kDa) and the embryonic isoform (32 kDa), respectively. There are very limited studies investigating the functional differences between these two isoforms with the exception of some recent finding stating that the adult isoform of AEBP2 may play a role as a transcription activator for some PcG target genes (185).

To verify the expression pattern of the two types of transcripts in primary TECs, I isolated cTEC, immature mTEC, and mature mTEC from 5 week-old wild type C57BL/6 mice. The transcripts for either isoform were quantified and compared to those in the mTEC 1c6 cell line using qRT-PCR. A robust expression of the adult isoform was observed in postnatal TEC which was consistently higher when compared to the embryonic isoform (Figure 3.1A). In addition, public available database also shows that *Aebp2* is highly expressed at different postnatal thymocyte developmental stages. In aggregate, these

analyses demonstrate that *Aebp2* expression can be detected in both postnatal TEC and thymocytes with the adult isoform being dominant in primary TEC.

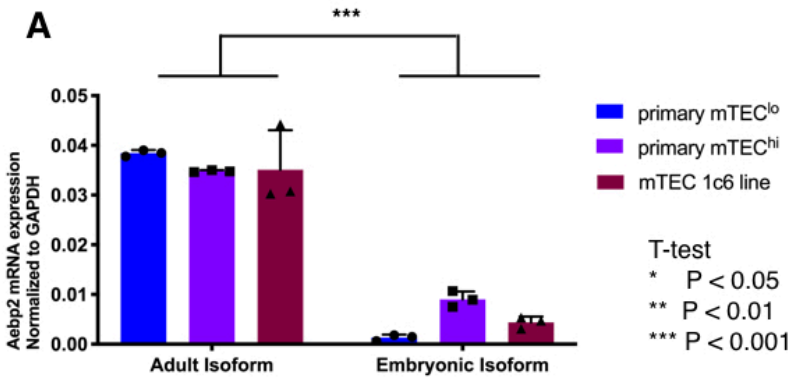

Figure 3.1: Aebp2 is expressed in the mouse both in TEC and thymocytes.

(A) PCR analysis of *Aebp2* expression in primary mouse TECs from 5 week-old mice and murine medullary TEC line. Graph represent data from two independent experiments. Each dot represents one biological sample. *** p < 0.001, ** p < 0.01 and * p < 0.05

3.2 AEBP2 physically interacts in mTEC with the PRC2 core component EZH2

The protein crystal structure of mammalian AEBP2 has shown that this protein associates with SUZ12, EZH2 and EED, the core components of PRC2 (167). I therefore investigated whether AEBP2 is also a constitutive component of the PRC2 complex in mTEC. Due to the limited availability of the primary cells for protein assays, I used a cultured mouse line, mTEC 1c6, for the following experiment. To this end, I performed a co-immunoprecipitation assay (co-IP) for AEBP2 and EZH2, respectively, followed by Western blotting (Figure 3.2). Using the mTEC 1c6 line, I demonstrated that EZH2 co-immunoprecipitates with AEBP2 (upper panel, Figure 3.2A) and, conversely, AEBP2

brings down EZH2 (upper panel, Figure 3.2B). These results demonstrate that AEBP2 physically associates in the mTEC 1c6 line with the PRC2 component EZH2 thus likely unveiling a functionally relevant interaction.

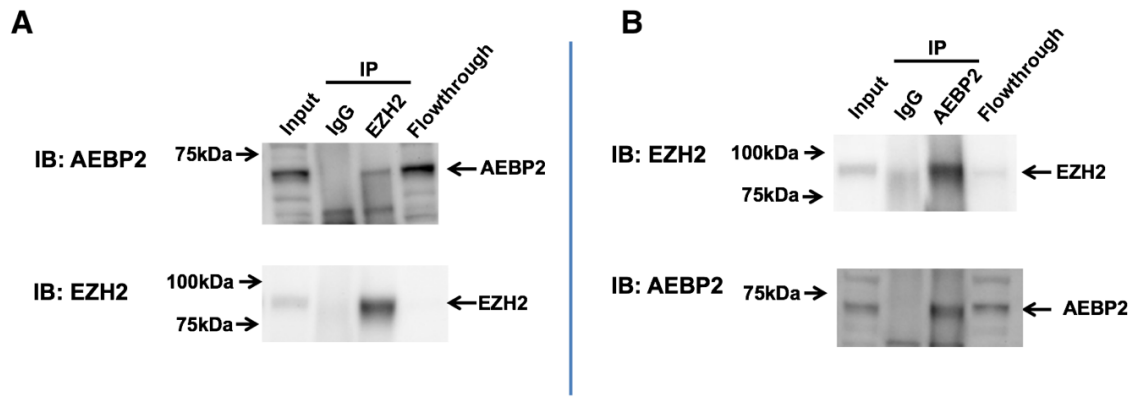

Figure 3.2: AEBP2 interacts in mTEC 1c6 with EZH2, a PRC2 core component.

(A) Co-IP for EZH2 and AEBP2 detected using Western blotting (WB). (B) Confirmation of the interaction between EZH2 and AEBP2 demonstrated in panel A by pulling down AEBP2 and detecting EZH2. The expected molecular sizes for the two proteins are indicated by an arrow on the right side of the panel. An arrow on the right side of the panel indicates the expected molecular sizes for the two proteins. This data is representative of two independent experiments.

3.3 AEBP2 association with EZH2 is independent of exons 1-3.

AEBP2 contains three zinc finger domains which are encoded from exons 2 to 4 and present in both isoforms. The third zinc finger which is encoded in sequence that spans from the end of exon 3 to exon 4 is important for DNA binding (171). Exon 5 and the following exons form the basic domain, together with the zinc finger domains, were found to interact with other PRC2 components (167). Thus we are interested in verifying whether exons 1-3 are sufficient to interact with the PRC2 core complex.

The sequence of exons1-3 was cloned into i) the pCMV vector which adds a Flag tag (C-Flag AEBP2 1-3 at the C-terminus, and ii) the pLion2FS2IP vector which introduces an in frame N-terminal Flag (N-Flag AEBP2 1-3). The plasmids were transfected into HEK293T cells to express AEBP2 1-3 with either a C- or N-terminal Flag tag. C- and N-Flag tagged, full length AEBP2 constructs were also generated to serve as controls.

As demonstrated in Figure 3.3A, the full length AEBP2 protein with a C-terminal Flag tag was successfully pulled down in an immunoprecipitation experiment using anti-Flag antibody. However it did not bring down EZH2, which suggested the C-terminus of AEBP2 was critical for the interaction with EZH2. On the other hand, a tagged protein consisting only of exons 1-3 of AEBP2 failed to be pulled down probably due to the formation of an incorrect structure that may prevent the Flag tag from being detected (upper panel, Figure 3.3B). Not surprisingly, EZH2 was not co-precipitated either (lower panel, Figure 3.3B).

The N-Flag full length AEBP2 co-precipitated with EZH2 successfully (Figure 3.3C), providing further support that the N-terminus of AEBP2 was not involved in EZH2-binding. The N-Flag AEBP2 1-3 protein could be successfully immunoprecipitated (upper panel, Figure 3.3D), but failed to bring down EZH2 (lower panel, Figure 3.3D). Taken together, these results strongly indicate that the association of AEBP2 with EZH2 mostly likely occurs via sequences that are encoded 3' of exon 3.

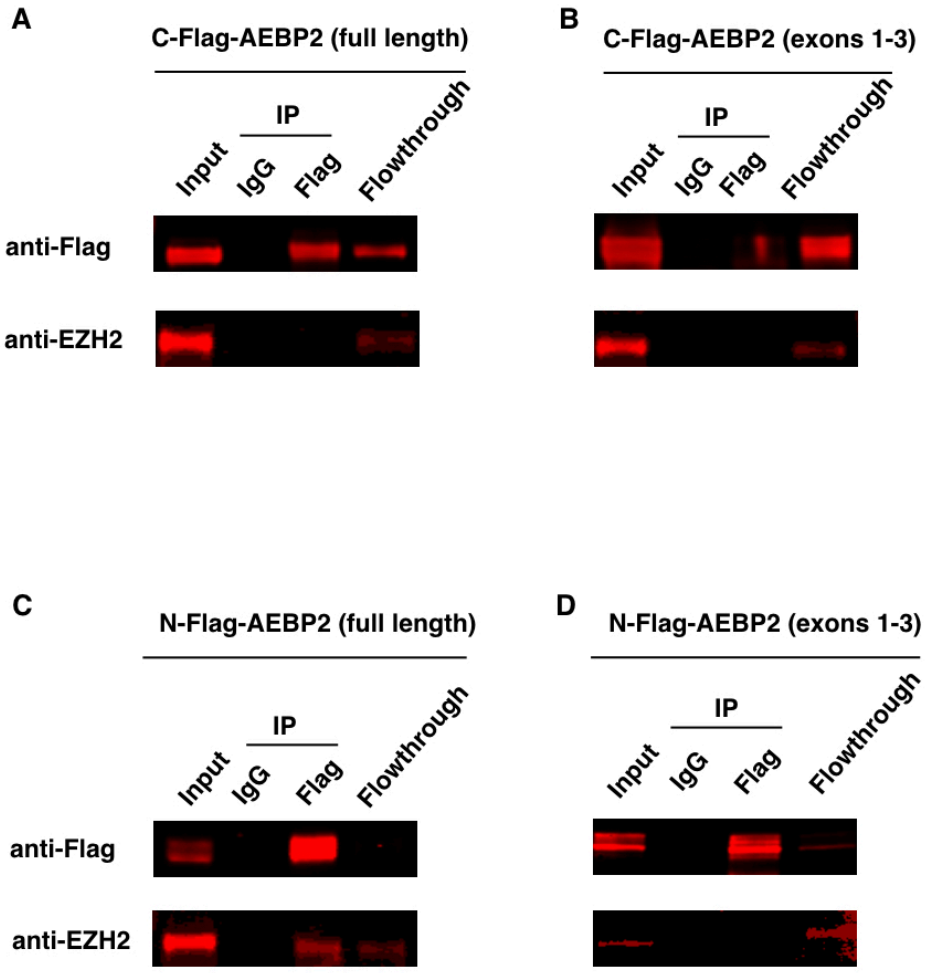

Figure 3.3: Protein encoded by exons 1-3 of AEBP2 do not associate with EZH2

(A) Co-IP for C-terminal Flag tagged full length AEBP2 and EZH2 detected by WB. (B) Co-IP for C-Flag AEBP2 exons 1-3 and EZH2. (C) Co-IP for N-Flag full length AEBP2 and EZH2. (D) Co-IP for N-Flag AEBP2 exons 1-3 and EZH2.

3.4 A potential Nuclear localization signal (NLS) in AEBP2

A recent finding showed that EZH1B, an isoform of EZH1, interacts with EED directly and is responsible for keeping the PRC2 positioned in the cytosol for its function (186). Under oxidative atrophic stress conditions, EZH1B is degraded by the proteasome and

PRC2 is released to translocate to the nucleus. This process is typically mediated by a nuclear localization signal (NLS), which is usually a Lysine-rich sequence and involves post translational modification (PTM) of the protein. Using an online NLS prediction algorithm (187), a consensus putative lysine-rich NLS sequence was found in exon 4 of AEBP2 (Figure 3.4A). Thus I was interested in demonstrating whether this sequence is essential for the targeting of AEBP2 itself to the nucleus, and further assisting PRC2 to translocate to the nucleus.

The subcellular localization of the Flag-tagged full length AEBP2 and the shorter AEBP2 1-3 protein were investigated in HEK293T cells using an overexpression system. As demonstrated in Figure 3.4B, the N-Flag full length AEBP2 successfully localized to the nucleus, where EZH2 could also be detected. In contrast, the N-Flag AEBP2 1-3 protein lacking the putative NLS sequence, exclusively localized to the cytoplasm of the transfected cells (Figure 3.4C). EZH2 was still detected in the nucleus of the transfected cells which could be explained by the endogenously expressed AEBP2 if it were to play a role in nuclear localization. To determine whether AEBP2 is required to translocate EZH2 to the nucleus, I examined the subcellular localization of EZH2 in primary TECs that are AEBP2 deficient (The mutant mouse line designated *Aebp2*$^{-/-}$ will be described in detail further below). TECs were sorted from either WT or *Aebp2*$^{-/-}$ mice by the surface expression of EpCAM and placed by cytospin on glass slides for the detection of EZH2 by immunostaining. The subcellular localization of EZH2 was identical in WT and *Aebp2*$^{-/-}$ TEC (Figure 3.4 D and E) thus inferring that AEBP2 is not responsible for EZH2's translocation to and prevalence in the nucleus.

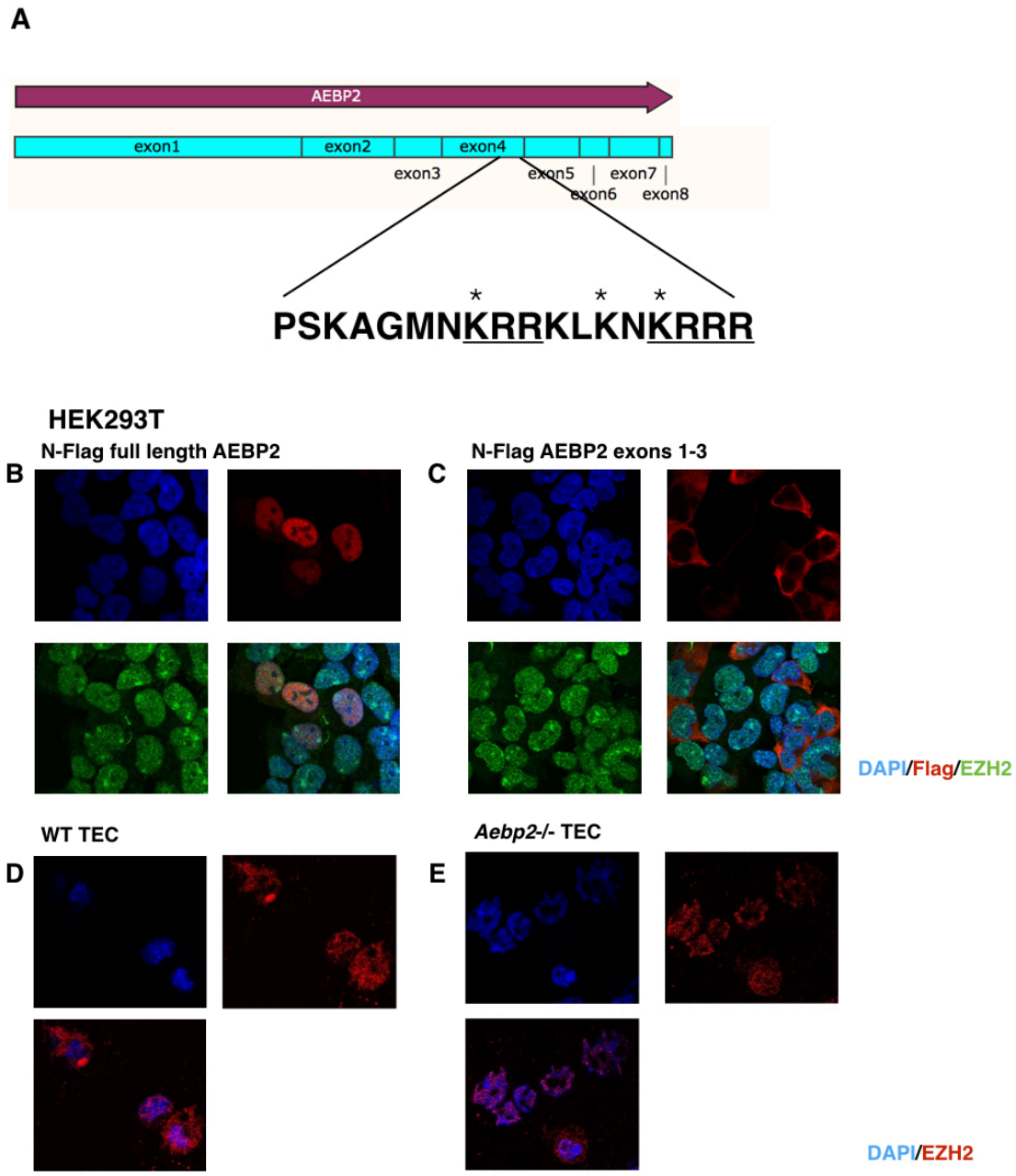

Figure 3.4: A bona fide NLS sequence in AEBP2

(A) A Lysine-rich sequence within exon 4 is predicted as NLS. * shows the Lysine residue and the underscore identifies the putative sequence that serves as a NLS. (B) Full length and (C) shortened exons of AEBP2 with N-terminal Flag tags were overexpressed in the HEK293T cell line. The subcellular localization of WT AEBP2, mutant AEBP2 and EZH2 were detected by immunofluorescence. The photomicrograph at the bottom right of the panel is a merged image of

the indicated fluorescent analyses. Primary TECs (EpCAM+) from WT (D) or *Aebp2*$^{-/-}$ (E) mice were FACS purified, placed onto glass slides, and stained for the presence of EZH2. The photomicrograph at the bottom is the merged image.

3.5 Discussion

AEBP2 is a co-factor of the PRC2 complex in many cell types including neural crest cells (188) and mouse embryonic stem cells (169). Whether it is expressed in TECs and thymocytes and acts there as a co-factor of PRC2 was not yet documented. The Co-IP assays clarified that AEBP2 is a part of PRC2 in TEC (Figure 3.2) where AEBP2 physically associates with EZH2, although the efficiency appears to be low.

When performing an IP experiment for EZH2, almost all of the EZH2 was precipitated since barely no EZH2 were detected in the flow-through fraction (lower panel, Figure 3.2A). However, the EZH2 did not bring down all the AEBP2 as there is still a detection of AEBP2 in the flow-through (upper panel, Figure 3.2A). This could be due to the efficiency of the Co-IP assay, or it might suggest a possibility that not all PRC2 complexes contain AEBP2. Indeed, different subtypes of PRC2 (i.e. PRC2.1 and PRC2.2) have been reported recently among which PRC2.2 but not PRC2.1 shows the association with AEBP2 (189).

The sequence analysis of AEBP2 predicted an NLS sequence encoded by exon4 of AEBP2. To test whether this was a functional NLS, I generated and analysed a truncated form of AEBP2 that contained sequences encoded by only exons 1-3, and examined the molecule's subcellular localization. As expected, this truncated AEBP2 was predominantly found in the cytoplasm (Figure 3.4C). To conclude that this specific sequence is a bona fide NLS, an extended analysis is required, including the cloning of this putative NLS sequence into the sequence of a reporter protein whose subcellular

localization can be easily monitored. The absence of AEBP2 in primary TEC did not disrupt the normal nuclear distribution of EZH2 (Figure 3.4 E). This may be because EZH2 has its own NLS or some other molecules assist EZH2's nuclear translocation.

Complete loss-of-function of EZH2 results in a severe thymus phenotype in early developmental stages, making it difficult to investigate the role of PRC2 in thymus with limited number of cells (Unpublished data in our group). Due to that, we decided to generate a tissue-specific knockout mouse model by CRISPR/Cas9. Deletion of exon 4 of AEBP2 will cause a frame shift resulting in a loss-of-expression of that exon and the following 3' exons.

In this chapter, the exons 1-3 of AEBP2 has been shown to be insufficient for its own nuclear localization and the binding with EZH2. Thus exon 4 could serve as a good target for the generation of tissue-specific KO mouse model. With this mouse model, we aim to investigate the loss-of-function of AEBP2 in TEC and thymocyte, respectively.

Chapter 4. Mice constitutively deficient in AEBP2 exhibit defects in thymic development

As AEBP2 was shown to be expressed in the TEC compartment in association with EZH2 in previous chapter, I next investigated the impact of *Aebp2* on thymic function in mice rendered conventionally deficient for the expression of this PRC2-associated molecule. This knockout mouse line truncates *Aebp2* transcripts for both the adult and the embryonic isoforms by inserting a splicing acceptor and stop codon before exon 2, which results in a loss of the conserved zinc finger and basic domains (169). The global loss of AEBP2 leads to a peri-natal lethality accompanied with anterior transformation in embryonic development and abnormal cardiac function.

I therefore used the mice at embryonic day 18.5 (E18.5) to analyse the TEC differentiation and TEC-mediated T cell development at early developmental stages.

4.1 Change in thymocyte maturation in the absence of AEBP2 expression

4.1.1 Constitutive AEBP deficiency causes a reduction in total thymic cellularity

Thymic lobes from wild type and homozygous mutant E18.5 embryos were isolated, dispersed into single cells, stained as indicated, and analysed by flow cytometry. A reduction in the size of the thymus between wild type and homozygotes is visible (Figure 4.1A). There were reductions in total cellularity between wild type and homozygous embryonic thymi (Figure 4.1B), which suggests that *Aebp2* deficiency could affect thymocyte maturation.

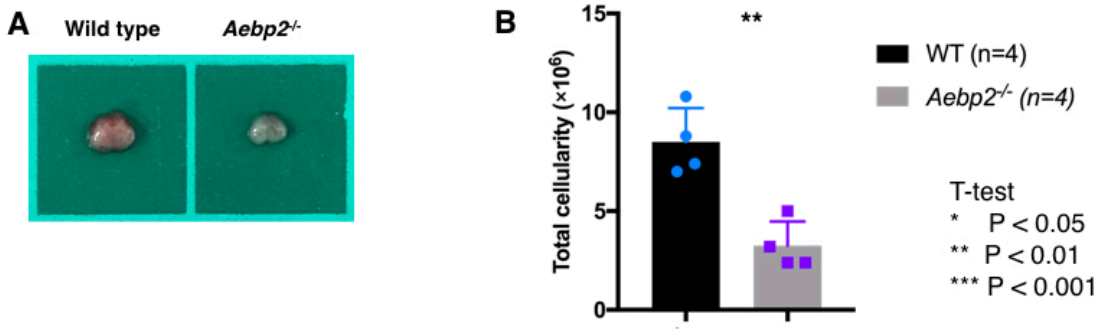

Figure 4.1: Total cellularity in E18.5 embryos

(A) The size of wild type and *Aebp2* deficient thymi are representative of each genotype. (B) Total cellularity of WT and *Aebp2*$^{-/-}$ thymic after mechanical disruption. Graphs represent data from three independent experiments. Statistics were calculated by student T-test. Columns show mean value and error bars represent standard deviation (SD). Each dot represents one biological sample. *** $p < 0.001$, ** $p < 0.01$ and * $p < 0.05$

4.1.2 A disturbed DN thymocyte development

The frequency of double negative thymocytes (Figure 4.2 A and B: DN, i.e. cells that are Lineage-, TCR-, CD4-, CD8-. See attached supplemented data for detailed gating strategy.) was increased in mutant thymic lobes when compared to wild type cells (Figure 4.2C). However the cellularity of this population was slightly reduced (Figure 4.2D) probably due to the reduction of total thymocyte cellularity (Figure 4.1B). Within the DN population, the first two earliest subpopulations (DN1: CD44+CD25-; and DN2: CD44+, CD25+) of the four double negative stages (DN1-DN4) were relatively increased (Figure 4.2E). Whilst there were no differences in the relative frequencies of DN3 and DN4 subpopulations. The decreased total cellularity (see Figure 4.1B) meant that there were significant differences in absolute cell number per thymus for DN3 and DN4

subpopulations between different genotypes (Figure 4.2F). In aggregate, these results suggested that there is a delay or partial blockage at this stage of intrathymic thymocyte development.

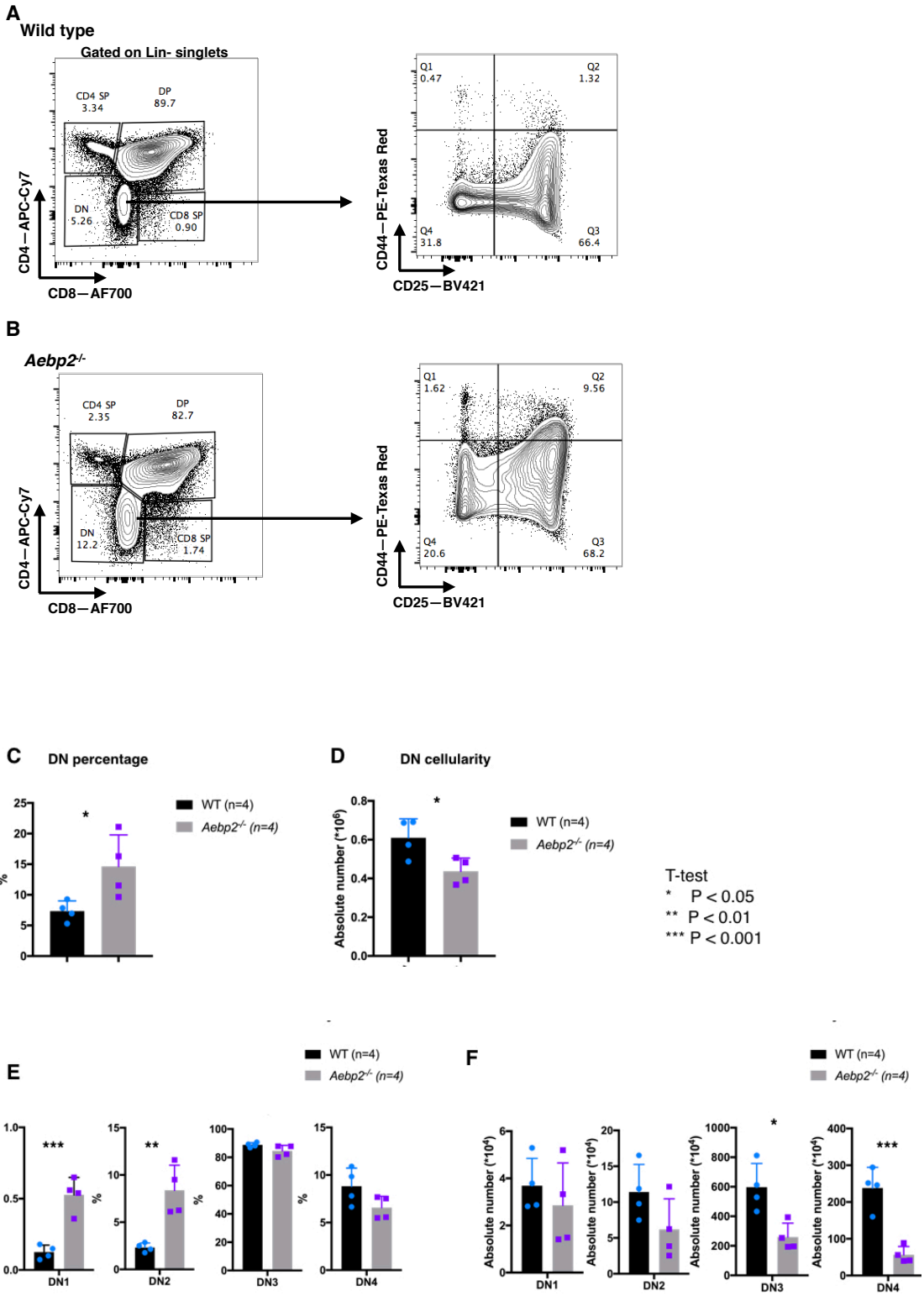

Figure 4.2: DN development in E18.5 thymus

Gating strategy of DN and its DN1-4 subpopulations in wild type (A) and *Aebp2*-deficient (B) E18.5 embryos. Percentages of DN population within total lineage- cells (C) and DN1-4 subpopulations within DN population (E) were compared between the different genotypes as indicated. The absolute number of DN (D) and DN1-4 cells (F) were also compared as indicated. Graphs represent data from three independent experiments. Statistics were calculated by student T-test. Columns show mean value and error bars represent standard deviation (SD). Each dot represents one biological sample. *** $p < 0.001$, ** $p < 0.01$ and * $p < 0.05$

4.1.3 Fewer DP cells were found in *Aebp2*-deficient E18.5 thymi

The analysis of the double positive (DP) stage of intrathymic T cell development demonstrated that fewer CD4+CD8+ thymocytes were recovered in E18.5 mutant embryos when compared to wild type littermates (Figure 4.3A). Calculating the absolute cell number of these cells furthermore demonstrated that, in comparison to wild type thymic lobes, DP thymocytes were decreased in the absence of AEBP2 expression (Figure 4.3B).

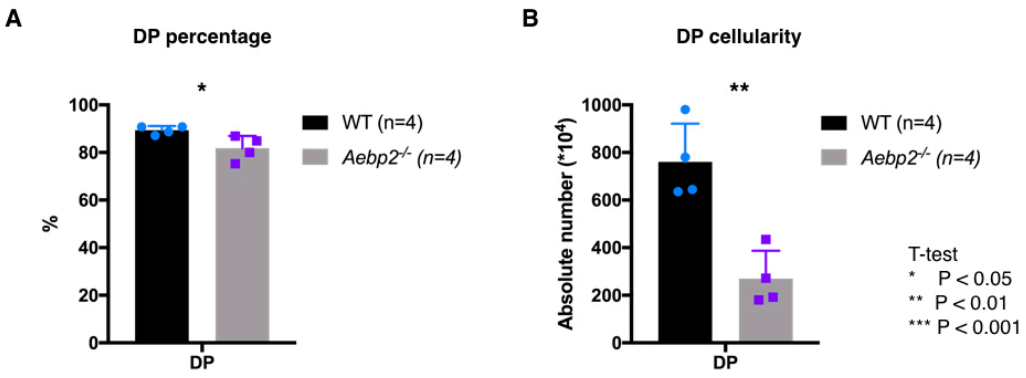

Figure 4.3: DP thymocytes were reduced in Aebp2-deficient thymi

The percentage of DP cells within in total lineage- cells (A) and absolute cell number of DP cells were compared as indicated. Graphs represent data from three independent experiments. Statistics were calculated by student T-test. Columns show mean value and error bars represent

standard deviation (SD). Each dot represents one biological sample. *** $p < 0.001$, ** $p < 0.01$ and * $p < 0.05$

Taken together, these data would suggest that the absence of AEBP2 expression disturbs the early DN development and the transition of DN to DP thymocyte, as the latter cell stage usually does not proliferate under physiological conditions.

4.2 Increased mTEC frequency in the absence of AEBP2 expression

I next sought to analyse the thymic epithelial compartment of mice either proficient or deficient for the expression of AEBP2. For this purpose, single cell suspensions were prepared by enzymatically digesting thymic lobes with liberase. The cells were stained for the cell surface expression of EpCAM, and Ly51 and for reactivity to the lectin UEA1 to identify cortical (cTEC: EpCAM+, MHCII+, Ly51+UEA1-) and medullary thymic epithelial cells (mTEC: EpCAM+, MHCII+, Ly51-UEA1+) (Figure 4.4A). Analysis by flow cytometry revealed that the frequency of cortical epithelial cells in E18.5 *Aebp2* mutant embryos was reduced compared to the wild type counterpart (Figure 4.4B). Conversely, the frequency of mTEC was increased in mice deficient in *Aebp2* expression, an opposite finding rarely observed in TEC-targeted loss of function mutations of individual components of the PRC2 core complex (data from other projects in Holländer lab). The physiological structure of E18.5 thymus was examined by IHC staining for the cTEC marker Keratin 8 (K8) and the mTEC marker Keratin 5 (K5). This demonstrated that the *Aebp2*$^{-/-}$ thymus had clear and structured cortical and medullary regions (Figure 4.4D) compared to the wild type thymus (Figure 4.4.C). Although it is difficult to quantify that, the medullary region seemed to have an advanced structure in the *Aebp2*$^{-/-}$ thymus

which could reflect the increase in the mTEC relative frequency. These observations are further supported by the RNA sequencing data presented later in this chapter.

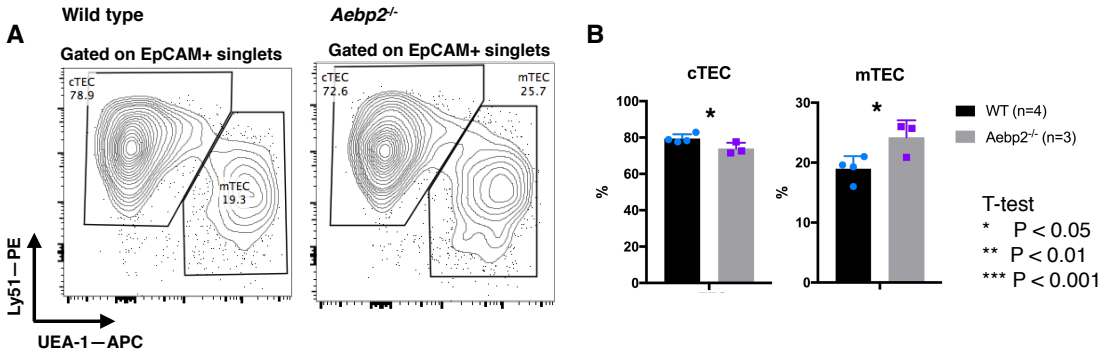

C

Wild type

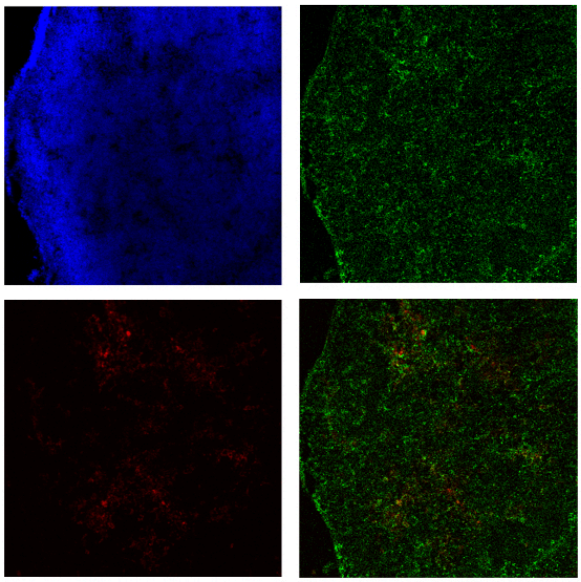

DAPI/K8/K5

D

Aebp2$^{-/-}$

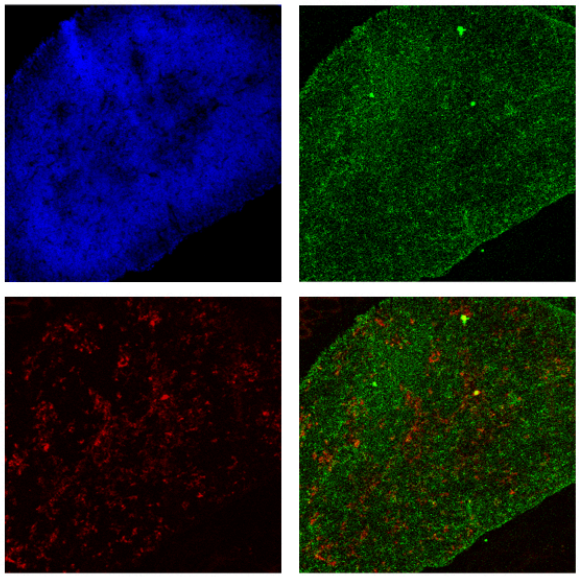

DAPI/K8/K5

Figure 4.4: An advanced mTEC development was observed in *Aebp2*$^{-/-}$ thymus

(A) The gating strategy of cTEC (Ly51+) and mTEC (UEA1+) populations was shown in both wild type and *Aebp2*$^{-/-}$ E18.5 embryos. (B) The frequency of cTEC and mTEC cells were compared as indicated. Cryosections were prepared from wild type (C) and *Aebp2*$^{-/-}$ (D) E18.5 thymi followed by staining for the cTEC marker K8 and the mTEC marker K5. The photomicrograph at the bottom right of each panel is the merged image. Graphs represent data from three independent experiments. Statistics were calculated by student T-test. Columns show mean value and error bars represent standard deviation (SD). Each dot represents one biological sample. *** $p < 0.001$, ** $p < 0.01$ and * $p < 0.05$

4.3 Transplantation of Aebp2-deficient fetal thymus tissue

Constitutive *Aebp2*$^{-/-}$ mice ubiquitously lack *Aebp2* expression. It was therefore unclear which specific cell type(s) was responsible for the observed thymic changes in this mouse. To determine whether the observed phenotypes were due to the absence of AEBP2 in TEC population, a thymus transplant experiment was conducted. In this experiment, thymic lobes harvested from either wild type or *Aebp2*$^{-/-}$ E18.5 embryos were transplanted under the kidney capsule of syngeneic adult recipient mice. This experimental setting helped address whether *Aebp2*-deficient TECs could support the development of wild type thymocyte progenitors. Moreover, this transplant system allowed for the investigation of the maturation of CD4 and CD8 single positive cells, which was difficult to assess from the embryonic thymus. Donor and recipient thymocytes could be distinguished by different CD45 alleles, where the donor WT and *Aebp2*-/- strain had a CD45.2 allele, whilst the recipient B6.SJl.CD45.1 mice had a CD45.1 allele.

4.3.1 Absence of *Aebp2* within the TEC compartment had a minor effect on total cellularity

Six weeks after transplantation, the engrafted thymic lobes were harvested from the recipient mice for analysis. The engrafted *Aebp2* deficient thymi were smaller than the wild type ones (Figure 4.5A). There was a reduction in the total cellularity in *Aebp2*$^{-/-}$ thymus compared to the wild type one (Figure 4.5B).

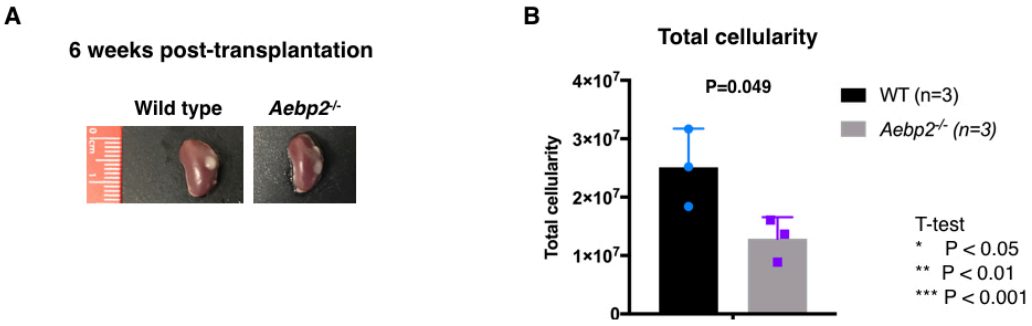

Figure 4.5: A minor reduction in cellularity was observed in *Aebp2*$^{-/-}$ thymus engrafts

(A) Representative images of the transplanted wild type and *Aebp2* deficient thymi harvested 6 weeks post-transplantation. (B) Total cell numbers were collected through mechanical digestion and compared between the different genotypes as indicated. Graphs represent data from one independent experiment. Statistics were calculated by student T-test. Columns show mean value and error bars represent standard deviation (SD). Each dot represents one biological sample. *** $p < 0.001$, ** $p < 0.01$ and * $p < 0.05$

4.3.2 Thymocyte frequencies during development were normal in *Aebp2*$^{-/-}$ thymi

During thymocyte development, DN cells up-regulate CD4 and CD8 expression to become DP cells, which eventually down-regulatte either of the two markers to become SP cells. The thymus transplantation experiment, as introduced before, allowed the phenotypical investigation of CD4 and CD8 SP cells, as the latter has not developed as a distinct population in embryonic thymus (Figure 4.6A). As previously presented for the

E18.5 analysis, the TCRβ- DN population could be sub-divided into four subpopulations based on their surface expression of CD44 and CD25 (Figure 4.6B). The frequencies of these compartments in *Aebp2*$^{-/-}$ engrafted thymi were compared to their wild type counterparts, but no significant change was observed (Figure 4.6 C and D). This suggested that *Aebp2*$^{-/-}$ TEC could still provide sufficient support for thymocyte development.

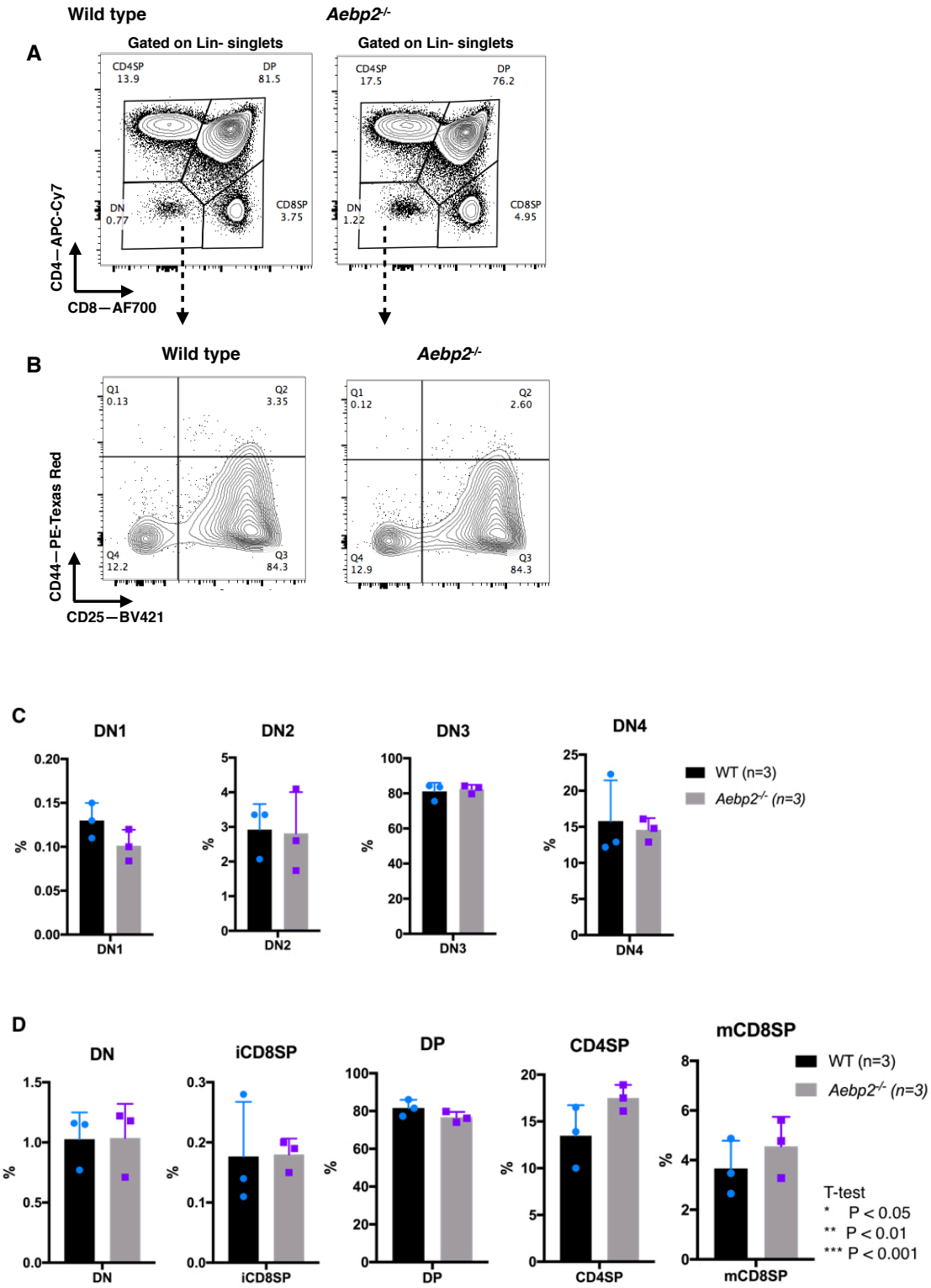
Wild type
Aebp2-/-
A
Gated on Lin- singlets
CD4SP 13.9
DP 81.5
DN 0.77
CD8SP 3.75
CD4SP 17.5
DP 76.2
DN 1.22
CD8SP 4.95
CD4—APC-Cy7
CD8—AF700
B
Q1 0.13
Q2 3.35
Q4 12.2
Q3 84.3
Q1 0.12
Q2 2.60
Q4 12.9
Q3 84.3
CD44—PE-Texas Red
CD25—BV421
C
DN1
DN2
DN3
DN4
%
WT (n=3)
Aebp2-/- (n=3)
D
DN
iCD8SP
DP
CD4SP
mCD8SP
T-test
* P < 0.05
** P < 0.01
*** P < 0.001

Figure 4.6: Frequencies of thymocyte compartments were equivalent between WT and *Aebp2*$^{-/-}$ engrafts

(A) Gating strategy of DN, DP, CD4SP, and CD8SP populations of the indicated genotypes from wild type and *Aebp2*$^{-/-}$ engrafts. (B) Gating strategy of DN1-4 subpopulations derived from TCRβ-DN cells. (C) DN1-4 subpopulations were compared between the indicated genotypes. (D) Each thymocyte compartment was compared between the indicated two genotypes. Graphs represent data from one independent experiment. Statistics were calculated by student T-test. Columns show mean value and error bars represent standard deviation (SD). Each dot represents one biological sample. *** $p < 0.001$, ** $p < 0.01$ and * $p < 0.05$

4.3.3 *Aebp2*$^{-/-}$ TECs provided a normal environment for thymocyte positive selection

T cells recognise antigen and are subsequently activated via the TCR-mediated signaling pathway. As thymocytes develop in the thymus, a crucial step is to assess their TCR-mediated competency and only the thymocytes passed the test are allowed to survive, namely positive selection. During the process of selection and further maturation, thymocytes spatio-temporally regulate their expression of several activation and maturation markers, i.e. CD69, CD5 and CD24 (190–192). As they develop, thymocytes migrate from the thymic cortex to the medulla for further negative selection.

After re-arrangement of the TCR α and β chains, TCR cell surface expression allows the thymocytes to transition from a pre-S stage (defined as TCRβ-CD69-) to the S1 stage (TCRβ^{int}CD69-). Consequent to TCR signaling, thymocytes up-regulate their CD69 expression and adopt an S2 (TCRβ^{int}CD69+) phenotype. Thymocytes that have received sufficient TCR-mediated signal adopt a TCRβ+CD69+ phenotype (designated Post-S) and eventually down-regulate CD69 expression to progress to mature (M) TCRβ+CD69- thymocytes; the gating strategy for the pre-S, S1, S2, post-S, and M stages are shown in Figure 4.7A. A minor decrease in the frequency of the cells in the S1 stage, but not other stages, was observed in *Aebp2*$^{-/-}$ thymus engrafts compared to the wild type (Figure 4.7B). The geometric mean fluorescence intensity (gMFI) of CD69 was also examined and compared between the two genotypes, and there was a small reduction only in the S5 stage in *Aebp2*$^{-/-}$ group (Figure 4.7C). These results suggested that the overall positive selection of the total thymocytes were not perturbed.

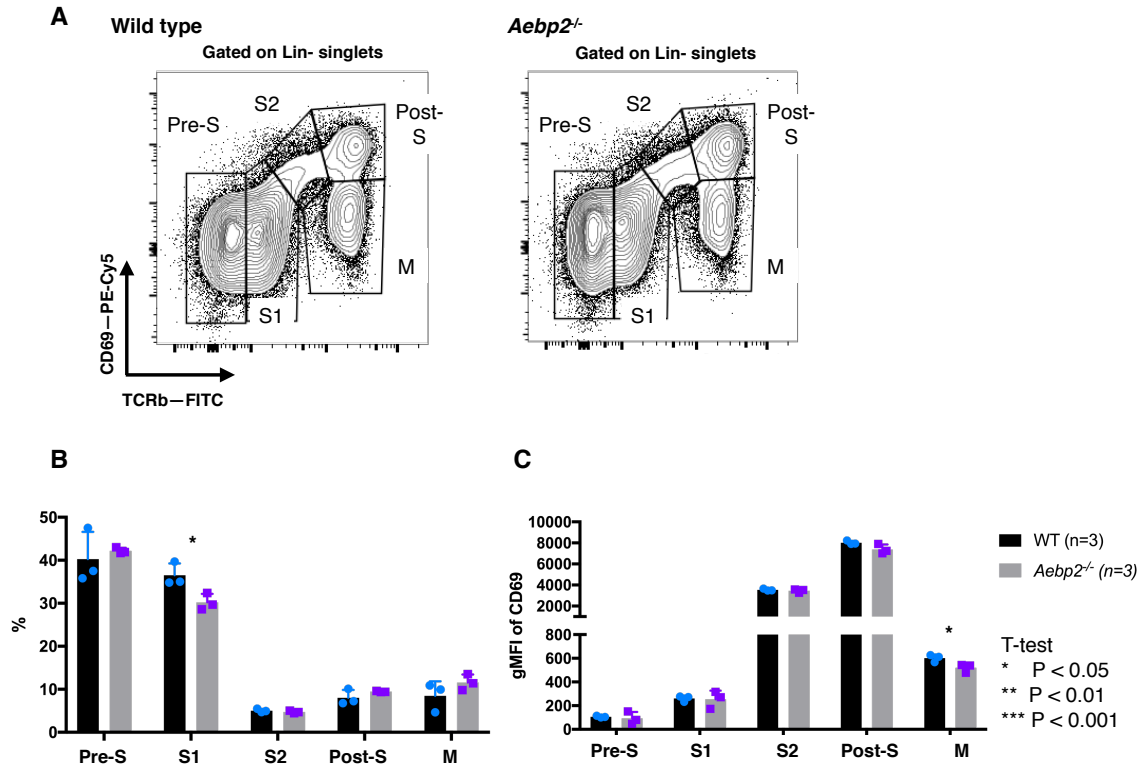

Figure 4.7: Thymocytes developing in Aebp2-/- thymus underwent normal positive selection

(A) Representative FACS plots defining different stages during positive selection: pre-S (TCRβ-CD69-), S1 (TCRβ^{int}CD69-), S2 (TCRβ^{int}CD69+), post-S (TCRβ+CD69+), and M (TCRβ+CD69-) stages. (B) Frequencies of each maturation stage was compared between indicated groups. (C) geometric mean fluorescence intensity (gMFI) of CD69 was compared between indicated groups. Each dot in bar graph represents one biological sample. *** p < 0.001, ** p < 0.01 and * p < 0.05

As a next step, I investigated the post-selectional maturation of CD4SP and CD8SP respectively. Positively selected DP thymocytes down-regulate CD4 and CD8 expression to adopt a "DPdull" phenotype before they further commit to either CD4 or CD8 lineage. With the markers introduced above, the development process was dissected into several sequential steps from DP into either CD4SP or CD8SP lineages (Figure 4.8 A and Figure 4.9 A). After commitment to CD4SP fate, the CD69+CD24+ CD4SP thymocytes started

to up-regulate CCR7 expression in order to migrate to the medulla (139). TCR and CCR7 were therefore used to separate the immature CD4 thymocytes in the cortex from the semimature CD4 thymocytes in the medulla (Figure 4.8A right panels). Within the medulla, CD4 thymocytes down-regulate CD69 and CD24 to become mature cells (Figure 4.8A left panels). The three maturation stages of CD4 thymocytes were found to be comparable between wild type and *Aebp2*$^{-/-}$ thymus engrafts (Figure 4.8B). I then examined the transition from DP thymocytes to immature, semimature and eventually mature CD4 thymocytes progressively by calculating how many cells in each stage progressed to the next stage. A mild but significant increase in the progression rate from DP to immature CD4 thymocytes was observed in thymocytes developed in *Aebp2*$^{-/-}$ thymus engrafts compared to wild type (Figure 4.8C left panel).

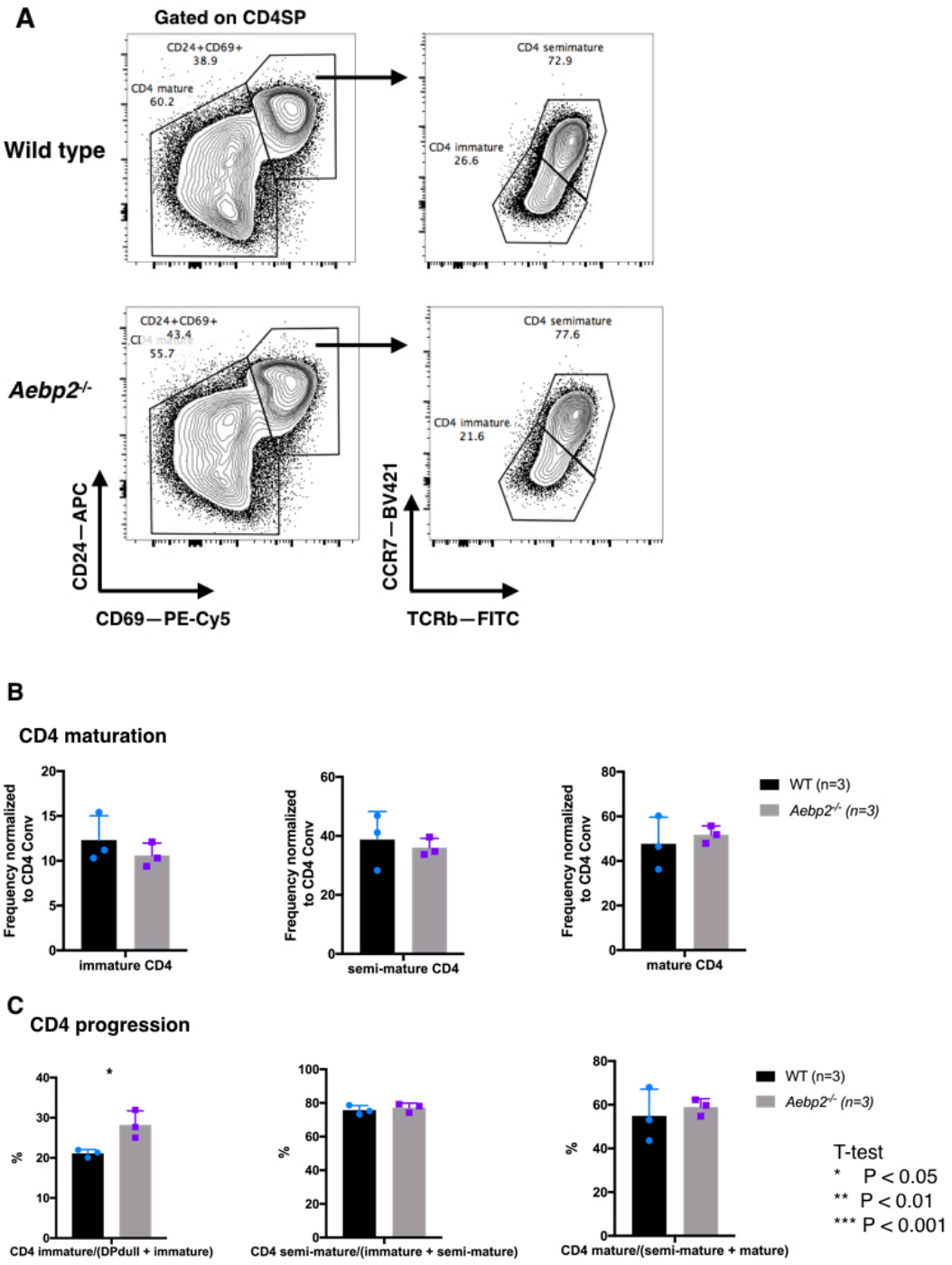

Figure 4.8: CD4 single positive thymocytes underwent normal developmental process in *Aebp2*$^{-/-}$ thymus

(A) Gating strategies of immature, semi-mature, and mature CD4 thymocytes characterized by their TCRβ, CCR7, CD24, and CD69 expression. (B) Comparison of each CD4 developmental stage between two indicated genotypes. (C) Progression analysis showing the frequency of the

cells that progressing from one stage to the next stage. The percentage of cells progressing to a particular stage was calculated dividing the percentage or number of cells within the stage of interest by that of the preceding stage, e.g CD4 immature /(DPdull + CD4 immature). Each dot in bar graph represents one biological sample. *** $p < 0.001$, ** $p < 0.01$ and * $p < 0.05$

The lineage commitment of CD4 and CD8 thymocytes is not a simple dichotomy (123). The development of CD8SP thymocytes is similar but not identical to that of CD4 lineage. DPdull thymocytes down-regulate CD8 expression to become CD4+CD8low thymocytes and prepare to migrate to the medulla. A proportion continue to become CD4SP thymocytes, whereas other CD4+CD8low thymocytes re-gain CD8 expression and down-regulate CD4 expression to commit to CD8 lineage. Because of that, immature CD8 thymocytes usually emerge in the medulla and are characterized as TCRβ+CCR7+ thymocytes (Figure 4.9A left panels). Analogous to the CD4 lineage, semimature CD8 thymocytes (CD69+CD24+) down-regulate both markers to become mature CD8 thymocytes (Figure 4.9A middle and right panels). Although there were no significant differences in each of the CD8 developmental stages between two genotypes (Figure 4.9B), an increased progression rate from DP to immature CD8 thymocytes was observed in thymocytes developed in *Aebp2*$^{-/-}$ thymus engrafts compared to wild type (Figure 4.9C left panel). This increased early stage progression also existed in CD4 lineage as shown above (Figure 4.8C left panel), which could be explained by the minor reduction in the frequency of S1 stage thymocytes (Figure 4.7B).

Taken together, these results suggested that *Aebp2*$^{-/-}$ thymus was still able to support the overall positive selection and development of the thymocytes, although there could be some minor effect on transition from DP to immature SP thymocytes.

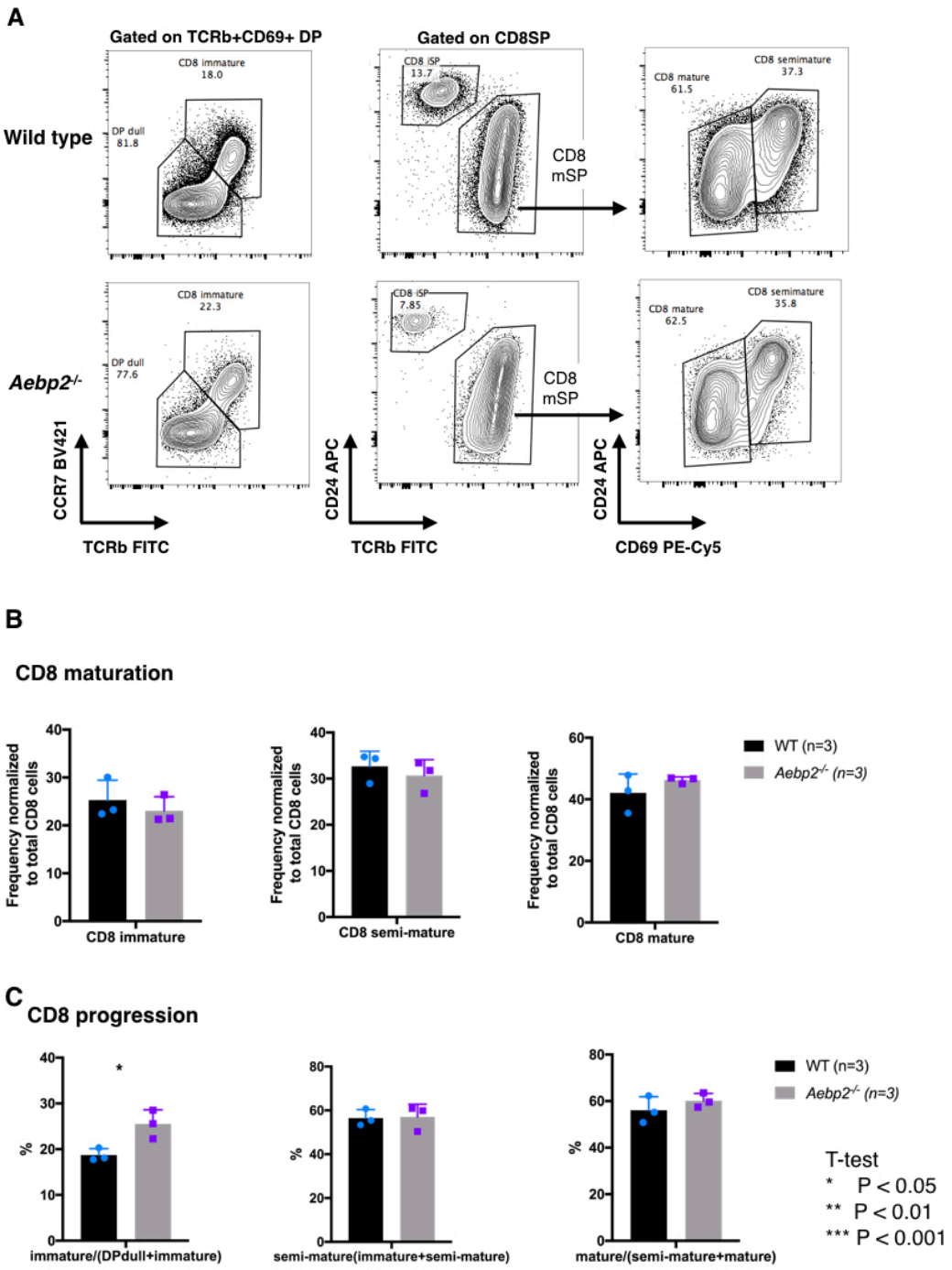

Figure 4.9: CD8 single positive thymocytes underwent normal developmental process in *Aebp2*$^{-/-}$ thymus

(A) Gating strategies of maturation stages of CD8 lineage also by their TCRβ, CCR7, CD24, and CD69 expression. (B) (C) Same statistical analysis in CD8 lineage as in CD4 lineage was conducted. Graphs represent data from one independent experiment. Statistics were calculated

by student T-test. Columns show mean value and error bars represent standard deviation (SD). Each dot in bar graph represents one biological sample. *** $p < 0.001$, ** $p < 0.01$ and * $p < 0.05$

4.3.4 *Aebp2*$^{-/-}$ TECs were able to undergo negative selection of thymocytes

Positively selected thymocytes have become mature and eventually egress to the periphery as mature T cells. However due to the random arrangement of the TCR locus, which creates a diverse pool of TCRs, a big proportion of the TCRs have the potential to recognize self-antigens and therefore could cause autoimmune diseases. These self-reactive thymocytes thus need to be eliminated or become Tregs to regulate autoimmunity, in a process known as central tolerance. Previously, negative selection was thought to take place solely in the medulla in a process largely dependent on AIRE-regulated PGE. However it has recently been demonstrated that negative selection could also occur in the cortex independent of the medulla (193). As described in the previous section, CD4 maturation can be characterized as DPdull, CD4 immature, CD4 semimature, CD4 mature stages from cortex to medulla. Four stages of negative selection, corresponding to these maturational stages have been defined as wave 1a, wave 1b, wave 2a and wave 2b, respectively (Figure 4.10A) (See supplementary data for detailed gating strategy). Thymocytes undergoing negative selection up-regulate their expression of transcription factor Helios (wave 1&2) and cell surface marker program death (PD)-1 (wave 1) (194,195). These markers were then used to assess the efficiency of wave 1 and wave 2 negative selections.

The data showed that no significant difference was observed when comparing thymocytes isolated from wild type and *Aebp2*$^{-/-}$ thymus engrafts (Figure 4.10B). The expression of Helios and PD-1 in CD8 thymocytes have not been validated as indicators for negative

selection in the literature and hence were not assessed here. Taken together, this set of data suggested that *Aebp2*$^{-/-}$ TECs were competent to induce negative selection.

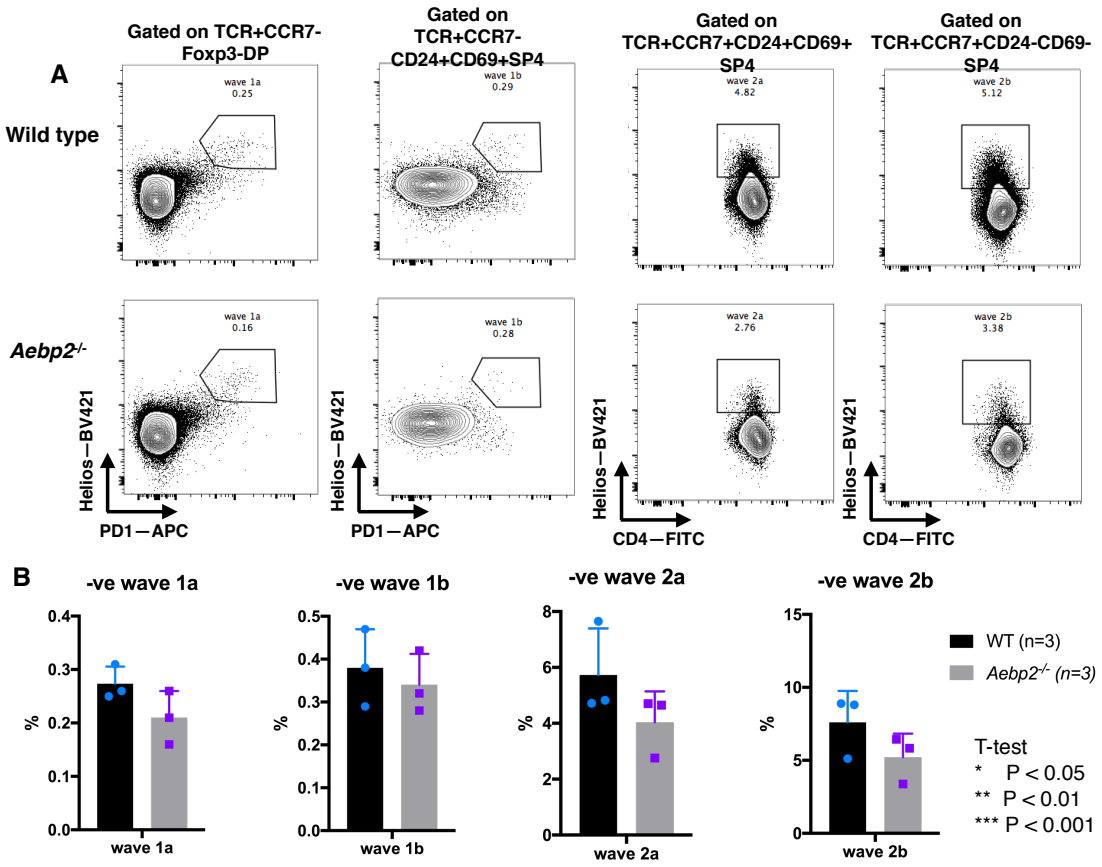

Figure 4.10: Negative selection of host thymocytes is comparable between WT and *Aebp2*$^{-/-}$ deficient thymi

(A) Gating strategies of different waves of negative selections from both cortex and medulla for both genotypes. (B) Comparison of cells undergoing negative selection from different waves between indicated genotypes. Graphs represent data from one independent experiment. Statistics were calculated by student T-test. Columns show mean value and error bars represent standard deviation (SD). Each dot in bar graph represents one biological sample. *** $p < 0.001$, ** $p < 0.01$ and * $p < 0.05$

4.4 Changes in gene expression profiles in *Aebp2*-deficient E18.5 TEC

PGE plays a vital role in mediating central tolerance of T cells. It is in part dependent on the presence of the transcriptional facilitator AIRE in a subpopulation of medullary TEC (107). Previous research from our lab has shown that AIRE regulated gene loci are typically characterized by a significant reduction in the tri-methylation of lysine 4 of histone 3 (H3K4me3) but an enrichment of tri-methylation of lysine 27 (H3K27me3) (109). This latter post-translational modification is catalysed by the Polycomb Repressive Complex 2 (PRC2). Recent structural studies have suggested that AEBP2 stabilizes the entire complex via multiple interactions between the core components, EZH2, EED, and SUZ12, thus enabling the binding of the entire PRC2 to the nucleosome (167,174,175). AIRE-targeted genes are enriched for H3K27me3 marks in the area of their transcriptional start site, which I hypothesize has been placed there by the catalytic activity of PRC2 in conjunction with AEBP2. To test this contention formally, I compared the gene expression profiles of TRA transcripts isolated from AEBP2 -proficient and -deficient TECs. This investigation will identify whether AEBP2 plays an essential role in PGE in general and which categories of genes (i.e. AIRE-dependent, AIRE-enhanced, and AIRE-independent) encoding self-antigens are affected by the absence of AEBP2.

Single cell suspensions of thymi isolated from wild type and AEBP2 deficient E18.5 embryos were stained for cell surface markers that distinguish between cortical (Ly51+ UEA1-) and medullary TEC (UEA1+Ly51+) and were then isolated using FACS-assisted cell sorting. Library preparation and QC methods were introduced in the Methods and Materials chapter (Section 2.8.1). The bioinformatic analyses was performed by Dr. Kevin Rue-Albrecht from Kennedy Institute in Oxford.

4.4.1 Both embryonic and somatic isoforms of *Aebp2* were depleted from E18.5 *Aebp2*$^{-/-}$ TECs

There are two major *Aebp2* transcripts, one encoding a bigger adult isoform (52kDa) and the other is a smaller embryonic isoform (32kDa), respectively (185). The adult isoform of AEBP2 was universally expressed in all peripheral tissues examined whereas the embryonic isoform was detected only in a subset of tissues (Figure 4.11A). In E18.5 embryos, the shorter, i.e. embryonic isoform was detected at higher copy numbers than the adult isoform in both WT cTECs and mTECs (Figure 4.11A). As expected, both isoforms were almost completely abolished in *Aebp2*$^{-/-}$ cTECs and mTECs given that the loss of exons 3' to exon 2 was engineered in these cells (169). Some transcripts of the embryonic isoform of *Aebp2* were still detected in Aebp2-/- mTECs which might be due to the leakiness of the system.

4.4.2 Mutually independent transcription of *Aebp2* and *Aire*

I first investigated whether AEBP2 was involved in the process of AIRE-regulated PGE. Previously generated RNA-seq data (109) from *Aire* KO mTECs showed that *Aebp2* was marginally up-regulated in the absence of *Aire* (Figure 4.11B). However, *Aire* expression was not altered in *Aebp2*$^{-/-}$ mTECs when compared to wild type cells (Figure 4.11C). Therefore, *Aebp2* and *Aire* expression are mutually independent and whatever impact *Aebp2* may have on PGE should be direct rather than a secondary effect resulting from a change in *Aire* expression.

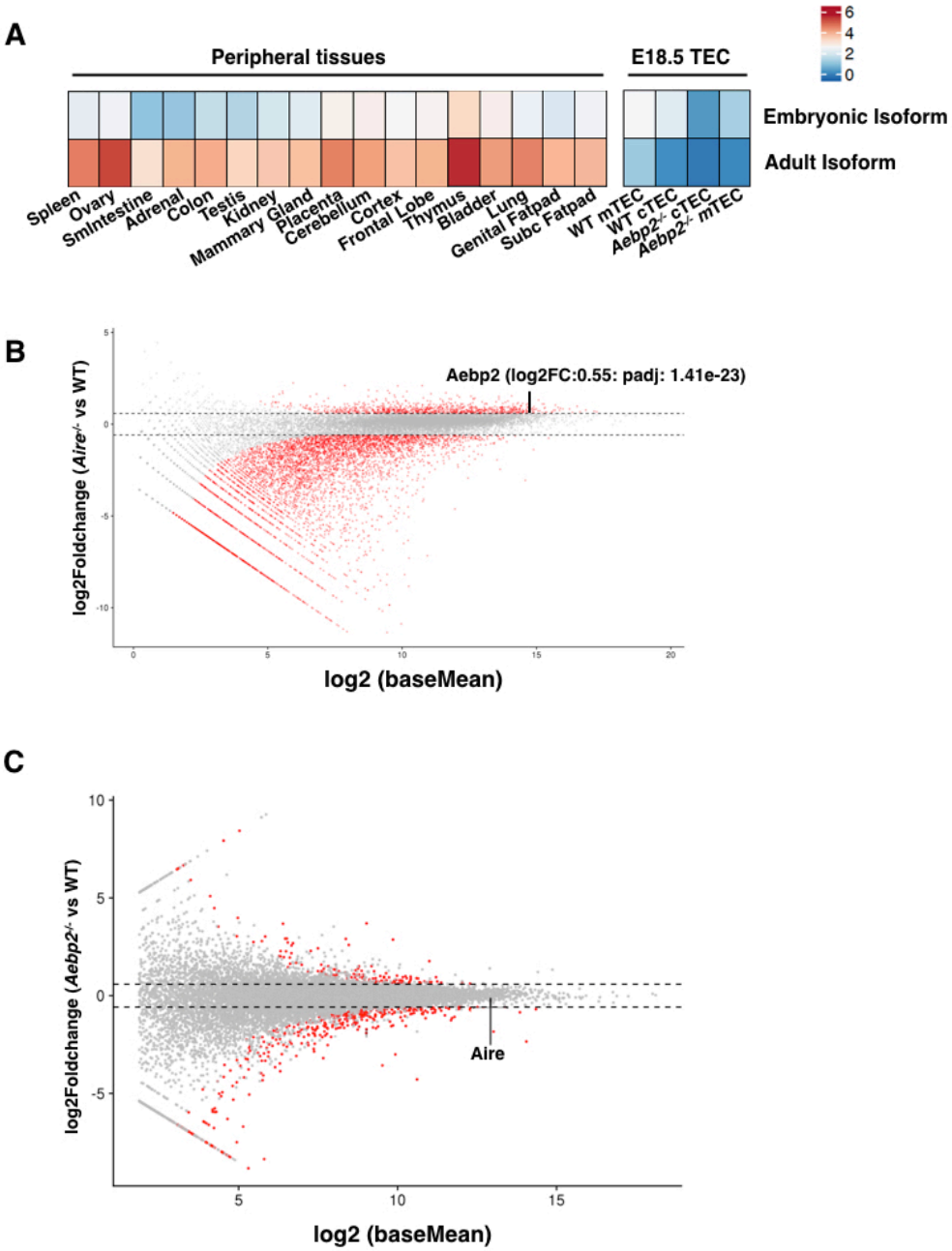

Figure 4.11: Mutually independent transcription of *Aebp2* and *Aire*

(A) Heat maps showing the transcription of *Aebp2* in indicated peripheral tissues (derived from Ensembl database) and E18.5 TECs. (B) M (log ratio) A (mean average) plot showing differences in gene expression between *Aire*$^{-/-}$ and WT mTEC^{hi}. Significantly differentially expressed genes (i.e. log2 fold change >0.5, Benjamin-Hochberg (BH) adjusted p <0.05) are coloured in red and *Aebp2* is labelled as indicated. (C) MA plot showing differences in gene expression between

Aebp2$^{-/-}$ and WT mTEC cells. Significantly differentially expressed genes (i.e. log2 fold change >0.5, BH adjusted p <0.05) are coloured in red and *Aire* is labelled as indicated.

4.4.3 AEBP2 is associated with PGE in mTECs

Both cTECs and mTECs are able to generate and present a repertoire of self-antigens to ensure negative selection of thymocytes bearing high-affinity TCRs (193). cTECs preferentially generate peptides from ubiquitous self-antigens to mediate the first wave of negative selection (193) whereas mTECs have the ability to generate almost all tissue-restricted antigens (TRAs) for the purpose of thymocyte negative selection during the second wave which is in part dependent on the expression of AIRE (107). Consistent with previous studies, the RNA-seq data detected many more tissue-restricted genes (TRGs) in mTECs than in cTECs in both wild type and *Aebp2*$^{-/-}$ mice (Figure 4.12A).

Next step, we investigated the genes differentially expressed (i.e. BH adjusted $p < 0.05$, absolute fold change > 1.5) between wild type and *Aebp2*$^{-/-}$ mTECs. A larger number of protein coding genes were down-regulated (N=544) whereas fewer genes were up-regulated (N=173) in the absence of AEBP2 in mTECs (Figure 4.12B). This observation was contrary to the expectation as PRC2 functions as repressor of gene expression, thus suggested that the presence of AEBP2 positively regulates gene expression in mTECs.

Next we investigated the 544 AEBP2-induced protein coding genes down-regulated in *Aebp2*$^{-/-}$ mTECs. Of these 206 (38%) were genes encoding TRGs, with 140 (68%) being AIRE-regulated and the remaining 66 (32%) being AIRE-independent (Figure 4.12C). To probe whether AEBP2 was involved in PGE (either in an AIRE-dependent or independent fashion), statistical analysis was conducted to investigate the significance of the overlap between AEBP2-induced TRGs and total number of TRGs that are either AIRE-induced or AIRE-independent. An odds ratio of 1 was set as a cut-off value to

define the association between two analysed groups, and BH adjusted p-value < 0.05 was used to show the significance of any overlap. The odds ratio of the overlap between AEBP2 and AIRE up-regulated TRGs (140 TRGs) was 3.2 suggesting the overlap between these two groups was greater than expected by chance (Figure 4.12C). The BH adjusted p-value was 6.2×10^{-38}, indicating that this overlap was statistically significant. The odds ratio of the overlap between AEBP2 and AIRE-independent TRGs was 2.0 and the BH adjusted p-value was calculated to be less significant with a value of 1.8×10^{-06}. Among the 173 genes up-regulated in the absence of AEBP2 (Figure 4.12B), only 30 of them were either AIRE-regulated (N=16) or -independent (N=14) TRGs and this was no more than expected changes (Figure 4.12D). Hence AEBP2 did not reveal a function to repress TRG expression. Taken together, these results suggested that AEBP2 contributed to largely AIRE-regulated and to a lesser extent AIRE-independent PGE.

According to our previous study (109), judged by their expression change in the absence of AIRE, AIRE-regulated TRG expression is divided into the categories of AIRE-dependent and AIRE-enhanced loci. As a next step, AEBP2 up- and down-regulated genes, were further classified into AIRE-dependent, AIRE-enhanced, AIRE-independent and other categories (Figure 4.12 E and F). By comparing the absolute number of up- and down-regulated protein coding genes in the absence of AEBP2, it was revealed that AEBP2 served mainly to assist TRG expression rather than suppressing it (Figure 4.12E). Also, close to 50% of the genes down-regulated in the absence of AEBP2 were AIRE-enhanced TRAs and fewer than 5% were AIRE-dependent loci (Figure 4.12F). These data suggested that AEBP2 may have different effects on TRGs that require AIRE to up-regulate their expression in comparison to TRGs that absolutely require AIRE for their transcription.

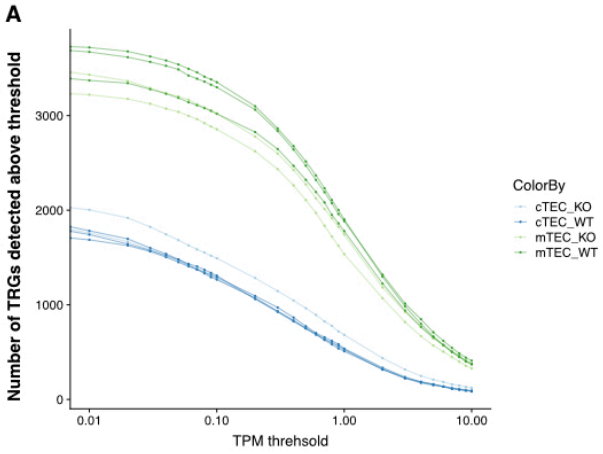
A
Number of TRGs detected above threshold
3000
2000
1000
0
0.01
0.10
1.00
10.00
TPM threhsold
ColorBy
cTEC_KO
cTEC_WT
mTEC_KO
mTEC_WT

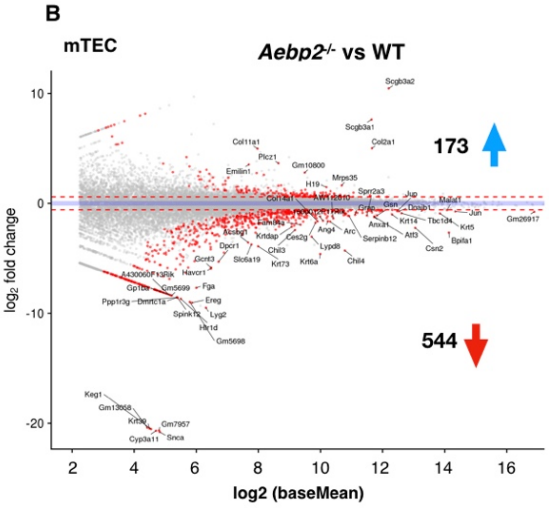
B
mTEC
Aebp2-/- vs WT
173
544
log2 fold change
log2 (baseMean)

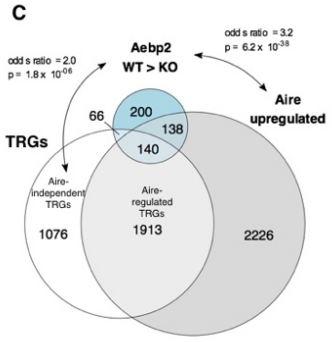
C
Aebp2
WT > KO
odd s ratio = 2.0
p = 1.8 x 10-06
odd s ratio = 3.2
p = 6.2 x 10-38
Aire
upregulated
TRGs
66
200
138
140
Aire-
independent
TRGs
1076
Aire-
regulated
TRGs
1913
2226

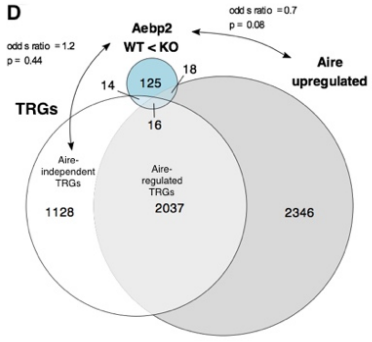
D
Aebp2
WT < KO
odd s ratio = 1.2
p = 0.44
odd s ratio = 0.7
p = 0.08
Aire
upregulated
TRGs
14
125
18
16
Aire-
independent
TRGs
1128
Aire-
regulated
TRGs
2037
2346

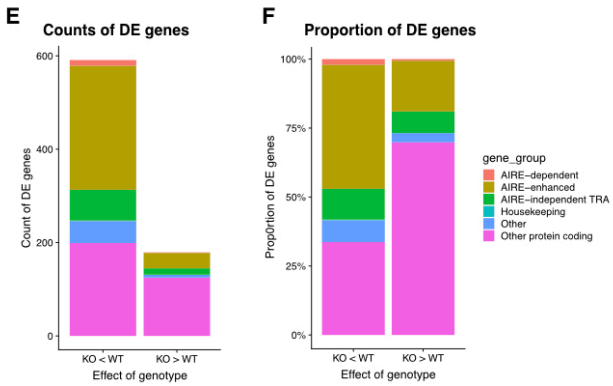
E
Counts of DE genes
Count of DE genes
600
400
200
0
KO < WT
KO > WT
Effect of genotype
F
Proportion of DE genes
PropOrtion of DE genes
100%
75%
50%
25%
0%
KO < WT
KO > WT
Effect of genotype
gene_group
AIRE−dependent
AIRE−enhanced
AIRE−independent TRA
Housekeeping
Other
Other protein coding

Figure 4.12: AEBP2 associated with PGE in mTECs

(A) The number of TRGs detected in cTECs and mTECs from WT and *Aebp2*$^{-/-}$ samples. (B) MA plot showing differences in gene expression between WT and *Aebp2*$^{-/-}$ mTECs. Significantly differentially expressed genes (BH adjusted $p < 0.05$, absolute fold change > 1.5) are coloured in red and the number of significantly up and down regulated genes are indicated next to the coloured arrow. (C) (D)The Venn diagrams compare the overlap of *Aebp2* up-regulated (C) and Aebp2 down-regulated (D) protein coding genes with Aire-induced TRGs and total TRGs. The significance of any overlapping of different populations was tested by odds ratio and BH adjusted p-value. Bar graphs show the counts (E) and the frequencies (F) of different gene groups as indicated within *Aebp2* up-regulated (KO<WT) and down-regulated (KO>WT) groups.

4.4.4 H3K27me3 marks AEBP2 induced TRGs

So far our data indicated that AEBP2 may facilitate the promiscuous expression of TRGs in mTECs. Thus, it is worthwhile to check the epigenetic status (i.e. H3K27me3 and H3K4me3 marks) of the down-regulated TRGs in mTECs in the absence of AEBP2. However due to the limited mTEC number from E18.5 thymus, it is challenging to get reliable chromatin immunoprecipitation (ChIP) results with the resolution necessary to compare the change in H3K27me3 status between WT and AEBP2 deficient mTECs. As an indirect way of examining the epigenetic status of the TRGs found to be differentially expressed in the absence of AEBP2, the level of H3K27me3 and H3K4me3 around their transcription start site (TSS) was assessed using our in-house data generated from adult WT mature mTECs (109,196). This analysis revealed that the TRGs requiring AEBP2 for their expression (blue) were marked by a higher level of repressive H3K27me3 over their gene bodies in adult WT mature mTECs compared to both AEBP2 repressed (red) and AEBP2 independent (green) TRGs (Figure 4.13A and B) and a lower level of the permissive H3K4me3 mark in a 1 kb window around their TSSs (Figure 4.13C and D).

These observations that the AEBP2 induced TRGs had a high level of H3K27me3 in adult WT mature mTECs indicated that H3K27me3 modification was important for PGE in mTECs, as concluded from the study of AIRE-induced TRGs (109).

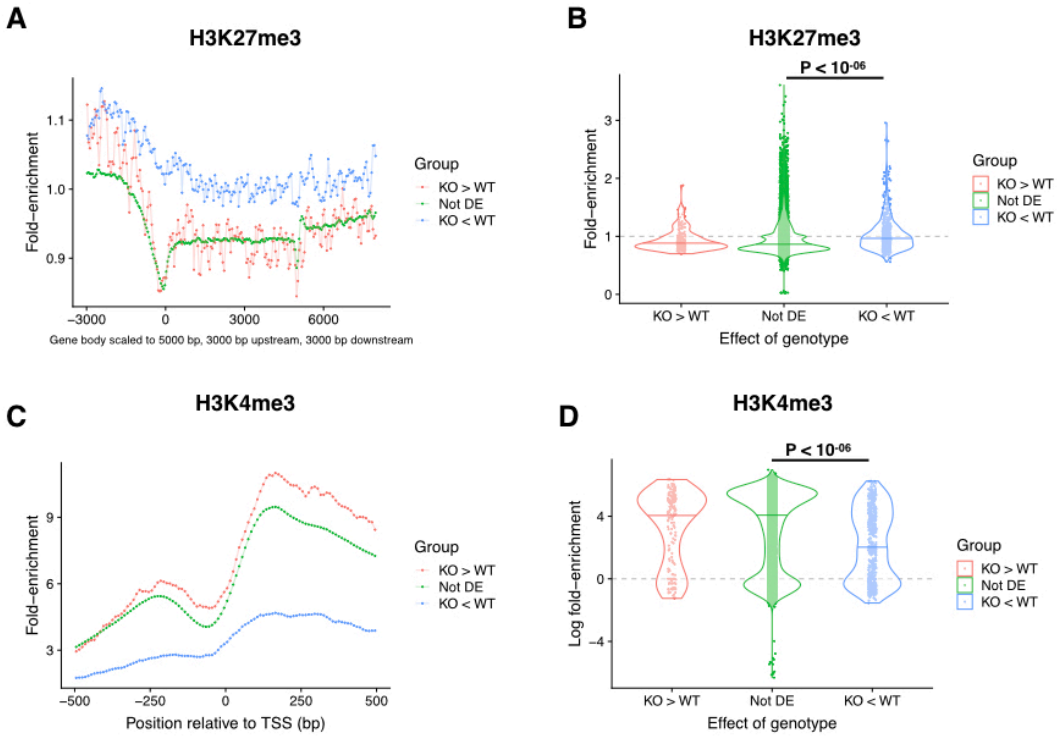

Figure 4.13: Metagene profiles and median enrichment of H3K27me3 and H3K4me3 over AEBP2 regulated genes

(A) Metagene profile and (B) median enrichment over gene bodies scaled to 5 kb for H3K27me3 histone modifications averaged across biological replicates (WT: N=3, AEBP2 KO: N=2). (C) Metagene profile and (D) median enrichment at the TSS for the H3K4me3 histone modification averaged across biological replicates (WT: N=3, AEBP2 KO: N=2). All the reads from the publicly available data obtained from 4-week-old mTEC samples (197) were trimmed to a common 50 bp and mapped to the mm10 reference genome.

4.4.5 The role of AEBP2 in TEC development

AEBP2 appeared to facilitate gene expression in mTECs. In cTECs more genes were up-regulated (N=322) than down-regulated (N=200), which was consistent with PRC2's conventional role for gene repression (Figure 4.14A).

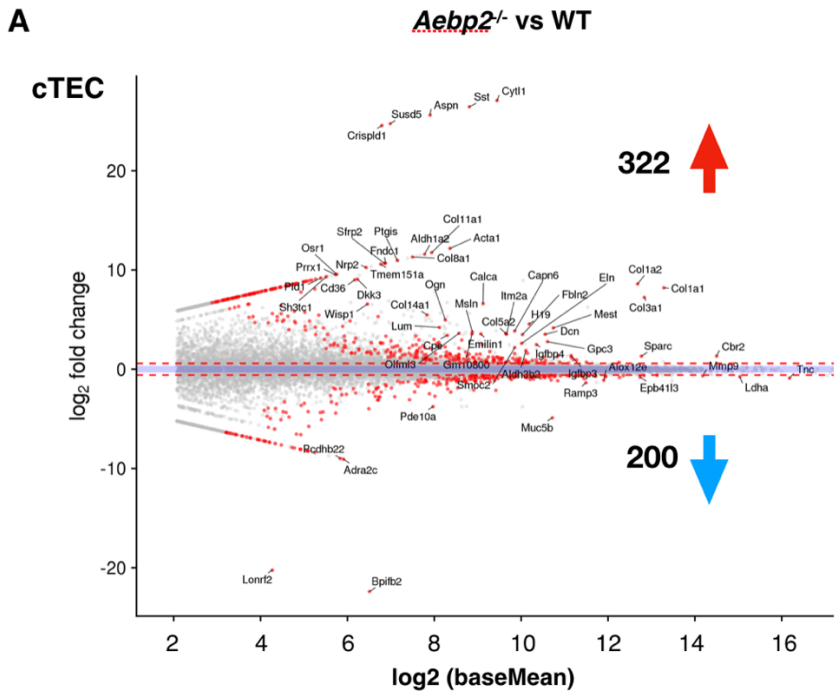

Figure 4.14: Differential gene expression in cTECs in the absence of AEBP2

(A) MA plot showing differences in gene expression between WT and *Aebp2*$^{-/-}$ cTECs. Significantly differentially expressed genes (BH adjusted $p < 0.05$, absolute fold change > 1.5) are coloured in red and the number of significantly up- and down- regulated genes are indicated next to the coloured arrow.

A gene ontogeny (GO) pathway analysis was conducted to investigate whether any pathways were affected in the absence of AEBP2 in TEC. Three criteria were applied to this analysis: 1) BH adjusted p-value had to be smaller than 0.05; 2) the odds ratio needed to be bigger than 2; 3) number of genes belonging to the pathway had to be more than 5. Using these criteria, 484 pathways were enriched from the up-regulated genes in the

absence of AEBP2 in cTECs including various developmental processes (Figure 4.15A). On the other hand, 49 pathways were enriched from the down-regulated genes in the absence of AEBP2 in cTECs (Figure 4.15B). Similarly, GO pathway analyses were also conducted for both up- and down-regulated genes in *Aebp2*$^{-/-}$ mTECs (Figure 4.15C and D). Although 173 genes were up-regulated in the absence of AEBP2 in mTECs, no pathways were enriched from them (Figure 4.15C). Meanwhile 53 pathways were enriched from the 544 down-regulated genes in the absence of AEBP2 in mTECs but none related to tissue development enriched (Figure 4.15D).

The up-regulated genes in *Aebp2*$^{-/-}$ cTECs had the most abundant pathway enrichment (N=484), reflecting the broad effect of PRC2-AEBP2 in gene repression. Furthermore, among the top 10 pathways that had been enriched, 6 were development- or morphogenesis-related (Figure 4.15A), indicating that the regulatory role of AEBP2 is essential in early tissue development. Moreover, we noticed that the epithelial cell proliferation pathway was also enriched and a large number of genes involved in this pathway were found to be up-regulated in the absence of AEBP2 in cTECs whereas in mTECs these genes did not show a consistent change comparing *Aebp2*$^{-/-}$ and wild type groups (Figure 4.15E). Thus, lack of AEBP2 in cTECs may have an effect on TEC development.

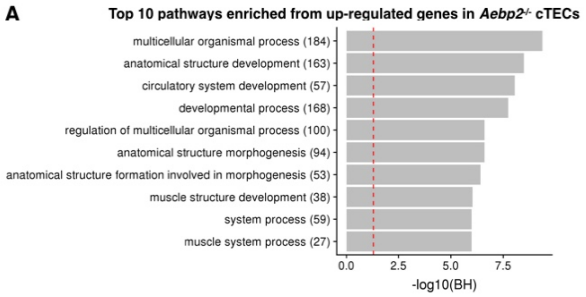
A
Top 10 pathways enriched from up-regulated genes in Aebp2-/- cTECs
multicellular organismal process (184)
anatomical structure development (163)
circulatory system development (57)
developmental process (168)
regulation of multicellular organismal process (100)
anatomical structure morphogenesis (94)
anatomical structure formation involved in morphogenesis (53)
muscle structure development (38)
system process (59)
muscle system process (27)
0.0
2.5
5.0
7.5
-log10(BH)

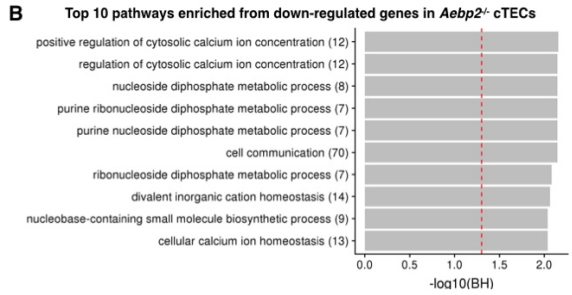
B
Top 10 pathways enriched from down-regulated genes in Aebp2-/- cTECs
positive regulation of cytosolic calcium ion concentration (12)
regulation of cytosolic calcium ion concentration (12)
nucleoside diphosphate metabolic process (8)
purine ribonucleoside diphosphate metabolic process (7)
purine nucleoside diphosphate metabolic process (7)
cell communication (70)
ribonucleoside diphosphate metabolic process (7)
divalent inorganic cation homeostasis (14)
nucleobase-containing small molecule biosynthetic process (9)
cellular calcium ion homeostasis (13)
0.0
0.5
1.0
1.5
2.0
-log10(BH)

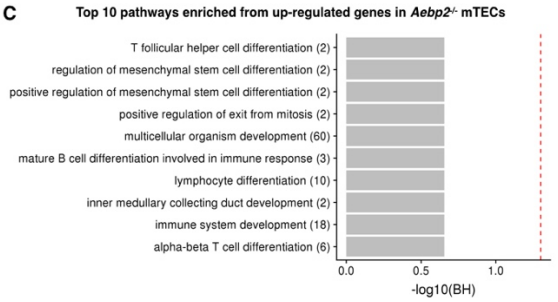
C
Top 10 pathways enriched from up-regulated genes in Aebp2-/- mTECs
T follicular helper cell differentiation (2)
regulation of mesenchymal stem cell differentiation (2)
positive regulation of mesenchymal stem cell differentiation (2)
positive regulation of exit from mitosis (2)
multicellular organism development (60)
mature B cell differentiation involved in immune response (3)
lymphocyte differentiation (10)
inner medullary collecting duct development (2)
immune system development (18)
alpha-beta T cell differentiation (6)
0.0
0.5
1.0
-log10(BH)

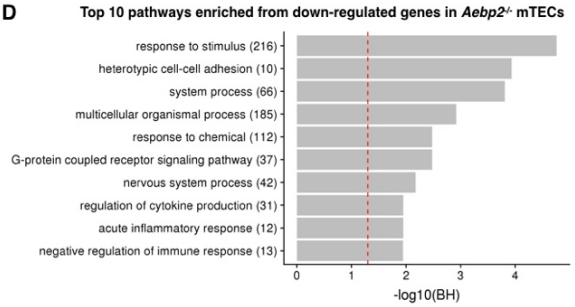
D
Top 10 pathways enriched from down-regulated genes in Aebp2-/- mTECs
response to stimulus (216)
heterotypic cell-cell adhesion (10)
system process (66)
multicellular organismal process (185)
response to chemical (112)
G-protein coupled receptor signaling pathway (37)
nervous system process (42)
regulation of cytokine production (31)
acute inflammatory response (12)
negative regulation of immune response (13)
0
1
2
3
4
-log10(BH)

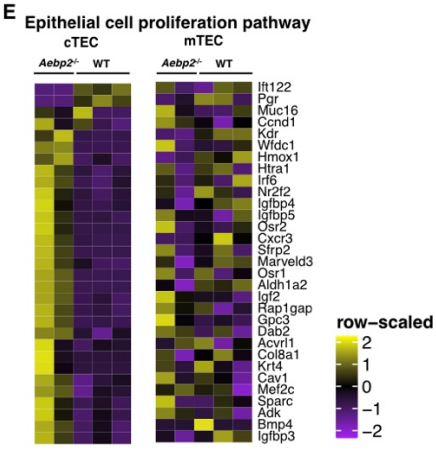
E
Epithelial cell proliferation pathway
cTEC
mTEC
Aebp2-/-
WT
Aebp2-/-
WT
Ift122
Pgr
Muc16
Ccnd1
Kdr
Wfdc1
Hmox1
Htra1
Irf6
Nr2f2
Igfbp4
Igfbp5
Osr2
Cxcr3
Sfrp2
Marveld3
Osr1
Aldh1a2
Igf2
Rap1gap
Gpc3
Dab2
Acvrl1
Col8a1
Krt4
Cav1
Mef2c
Sparc
Adk
Bmp4
Igfbp3
row−scaled
2
1
0
−1
−2

Figure 4.15: GO pathway analysis for genes differentially expressed in cTECs and mTECs in the absence of AEBP2

(A) The top 10 pathway categories enriched from up-regulated genes in *Aebp2*$^{-/-}$ cTECs. (B) The top 10 pathway categories enriched from down-regulated genes in *Aebp2*$^{-/-}$ in cTECs. (C) No pathways enriched from up-regulated genes in *Aebp2*$^{-/-}$ mTECs. (D) The top 10 pathway categories enriched from down-regulated genes in *Aebp2*$^{-/-}$ mTECs. (E) Heat map showing the transcription level of genes involved in the epithelial cell proliferation pathway comparing E18.5 cTEC and mTEC. The transcription level was shown in row-scaled value. The criteria for the GO pathway enrichment were 1) BH adjusted *P* value <0.05 (indicated as red dashed line); 2) odds ratio >2; 3) number of genes in the pathway > 5.

4.5 Discussion

Epigenetic mechanisms play vital roles in the establishment of gene expression programmes through tissue development and the maintenance of cell identity. Recent studies have reported the importance of the epigenetic landscape for TEC development and function. This includes the studies on histone post-translational methylation in mTEC development and function (i.e. negative selection) (109,196). AIRE-mediated PGE within mTEC^{hi} was demonstrated to be crucial for negative selection of self-recognizing thymocytes and hence prevention of autoimmunity (107). Previous studies originating from our laboratory have revealed that AIRE-induced TRGs in mTEC^{hi} are marked by the repressive histone modification H3K27me3 and lack the permissive mark H3K4me3 (109).

However, the overall chromatin landscape at AIRE-induced TRG loci was found to be similar between mTEC^{lo} and mTEC^{hi}, indicating that the mature mTEC chromatin landscape forms in early mTEC developmental stages and AIRE is not required for the re-patterning of chromatin in mTEC (196). These findings suggest that the repressive

H3K27me3 mark plays a role in TEC maturation and function. Although the importance of this histone modification in TEC biology, detailed function and molecular mechanism have remained elusive so far.

Due to the facts stated above, PRC2, the sole methyltransferase complex responsible for trimethylation of H3K27, was therefore believed to be involved in AIRE-regulated PGE. Unpublished data from our group shows a severe defect in total thymic cellularity and a block in mTEC maturation when PRC2 core components (i.e. EZH1/2 and EED) are knocked out in TEC specifically mediated by either *Psmb11* or *Foxn1* promoter driven Cre recombinase, both of which are expressed in early embryonic TEC stages (198). Limited TEC cellularity has, so far, restricted the deep phenotyping and functional studies for the role of PRC2 in TEC biology, in particular PGE in $mTEC^{hi}$.

AEBP2 is a co-factor of PRC2 and was demonstrated to be important for the efficient deposition of H3K27me3 mark on nucleosomes (174). As lack of AEBP2 does not abolish the methyltransferase activity of PRC2 completely, the molecule is targeted to investigate whether and how changes in H3K27me3 could affect AIRE-regulated PGE in my DPhil research. The function of AEBP2 as an epigenetic regulator in embryonic development, mouse embryonic stem cells (mESCs) and neural crest cells has been demonstrated however no studies on the thymus have been reported so far (169,188).

Due to the importance of PRC2-AEBP2 for embryonic development, a global depletion of AEBP2 in mouse caused perinatal lethality. I then focus our analysis on E18.5 thymi. In contrast to the severe defects in TEC maturation from TEC-specific KO of PRC2 core components, lack of AEBP2 causes a mild decrease in the frequency of cTECs and an increase in the frequency of mTECs (Figure 4.4B). In addition, the *Aebp2*$^{-/-}$ embryonic thymi have a more developed medullary structure (Figure 4.4D), suggesting that lack of

AEBP2 might accelerate the TEC development. Transcriptome analysis of E18.5 TECs could support this notion as the epithelial cell proliferation pathway and some other development-related pathways are found to be activated in *Aebp2*-deficient cTECs. PRC2-AEBP2 functions as a negative regulator controlling step-wise gene expression. AEBP2 deletion may not completely abolish this regulatory machinery but rather reduce this regulation mildly which could explain an early development and maturation of TECs. An enhanced TEC differentiation phenotype is also observed in TEC-specific KO of JARID2, another co-factor of PRC2 (unpublished studies in our group).

The E18.5 thymi analyses also reveal a mild reduction in total thymic cellularity (Figure 4.1) and a disturbance in early thymocyte development (Figure 4.2). Thymic lobe transplant experiment has suggested that this is a thymocyte intrinsic defect caused by lacking AEBP2 expression as normal thymic progenitors from the host home to the transplanted thymi and go through normal early thymocyte development (Figure 4.6), positive (Figure 4.7, 4.8, 4.9) and negative (Figure 4.10) selection to become mature T cells. This hypothesis is further confirmed in the following chapter by a transplantation experiment with AEBP2-deficient haematopoietic cells.

As the conventional role of AEBP2 within in the context of PRC2 is to negatively regulate gene expression, depletion of AEBP2 up-regulates the transcription of a large number of genes in cTECs as expected (Figure 4.14A). We see that many of these genes are involved in tissue development pathways (Figure 4.15A). Thus we believe that AEBP2 is required for the spatio-temporal control of tissue development, which is reflected by the phenotype that lack of AEBP2 expression enhances TEC development as discussed above. On the contrary, in mTECs more genes are down-regulated in the absence of AEBP2 (Figure 4.12B) indicating that the major role of AEBP2 in mTECs is to facilitate gene expression.

More importantly, close to 50% of these AEBP2 induced genes are AIRE-induced TRGs (Figure 4.12 C and F). This finding indicates that AEBP2 is required for AIRE-induced PGE. Although to a lesser extent, AEBP2 is also shown to up-regulate AIRE-independent TRGs (Figure 4.12C) suggesting that AEBP2 may have a broader role regulating both AIRE-regulated and AIRE-independent PGE. Although the lack of AEBP2 in mTECs affects PGE, the wave 2 negative selection mediated by *Aebp2*-deficient thymus in the transplant experiment is not affected (Figure 4.10). There are two possible explanations for that. Firstly, as negative selection is a highly dynamic process, the up-regulation of Helios and PD-1 expression may not be adequate enough to characterize all the thymocytes undergoing negative selection. Moreover this method is only validated for the assessment of negative selection of CD4 thymocytes from literature (195). Secondly, lack of AEBP2 only affects the transcription of a fraction of the total TRGs (7% of AIRE-induced ones), either due to the limited impact on H3K27me3 deposition when AEBP2 is absent or because other molecular mechanisms are also required for PGE. Hence the assays used in this study might not be sufficient to address the effect of AEBP2 in negative selection. Additional approaches such as assessing apoptosis of the negatively selected thymocytes by Annexin V staining may be necessary.

It is worth noting that AIRE is highly expressed in a fraction of mature $mTEC^{hi}$ postnatally (109), however our RNA-seq data are obtained from E18.5 thymi in which the mTECs are largely immature. Although the chromatin landscape has been established early in TEC differentiation (196), the embryonic mTEC is not the best model to study the role of AEBP2-mediated H3K27me3 mark in PGE. A TEC-specific KO of AEBP2 mouse model, which we are currently generating, is absolutely necessary to address this issue.

In summary, the data presented in this chapter demonstrate that AEBP2 negatively regulates the expression of genes related to tissue development in cTEC and positively facilitates the expression of TRGs, particularly those dependent on AIRE, in mTEC.

Chapter 5. Loss of AEBP2 affects haematopoiesis and thymocyte development

The previous chapter demonstrated that the lack of AEBP2 expression in the TEC population had a limited impact on normal thymocyte development. To further address the question whether the observed thymocyte defects in *Aebp2*$^{-/-}$ E18.5 embryo were thymocyte intrinsic, I engrafted fetal liver (FL) cells from mice at embryonic day 15.5 (E15.5) into wild type adult recipients, and analysed the development of *Aebp2*-deficient thymocytes with control WT thymocytes. FL cells at E15.5 stage contain haematopoietic stem and progenitor cells, which have the potential to develop into T cell progenitors in the thymus. For this purpose, CD45.2+ total FL cells were transplanted into lethally irradiated 6 weeks old CD45.1+ recipients. At 6 weeks post-transplantation, thymus and lymph nodes were harvested and analysed as detailed below.

5.1 The phenotype of E18.5 *Aebp2*$^{-/-}$ thymocytes is cell-intrinsic

5.1.1 A reduction of CD45.2+ donor thymocyte number was observed

The thymus size of recipients engrafted with either wild type or *Aebp2*$^{-/-}$ donor FL cells were compared. The thymus repopulated with *Aebp2*$^{-/-}$ haematopoietic cells appeared slightly smaller (Data not shown). Flow cytometric staining of both CD45.1 and CD45.2 for total thymocytes showed that both groups of recipient mice were engrafted successfully 6 weeks post-transplantation and almost all of the thymocytes were from donor, suggesting that *Aebp2*$^{-/-}$ thymocytes do not have an engraftment defect (Figure 5.1A and B). The total cell number of *Aebp2*$^{-/-}$ thymocytes was reduced compared to mice engrafted with wild type FL cells (121.1±7.27 in *Aebp2*$^{-/-}$ vs 188.6±37.92 in WT) (Figure 5.1C). This observation is in line with the results of *Aebp2*$^{-/-}$ E18.5 embryos (Figure 4.1B).

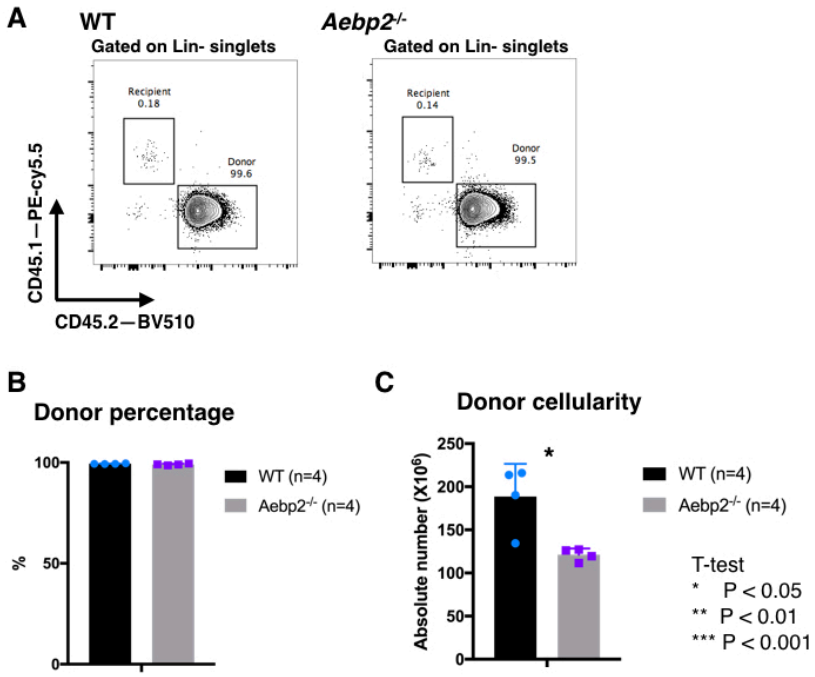

Figure 5.1: Thymi from mice transplanted with *Aebp2*$^{-/-}$ FL cells are hypocellular compared to those transplanted with WT cells

(A) Flow cytometric staining of donor (CD45.2) and recipient (CD45.1) thymocytes in 12 weeks old recipients transplanted with either wild type or *Aebp2*$^{-/-}$ E15.5 FL cells. (B) The frequencies of engrafted donor thymocytes of indicated genotypes. (C) Comparison of donor thymocyte cellularity in recipients of either wild type or *Aebp2*$^{-/-}$ FL cells. Graphs represent data from two independent experiments. Statistics were calculated by student T-test. Columns show mean value and error bars represent standard deviation (SD). Each dot in bar graph represents one biological sample. *** $p < 0.001$, ** $p < 0.01$ and * $p < 0.05$

5.1.2 Thymocyte development in the absence of AEBP2

I next investigated the relative frequencies of thymocyte subpopulations using the gating strategies previously described in Figure 4.6 A and B (Figure5.2 A and B). The frequency of DN thymocytes was comparable for both groups of transplanted recipients (Figure

5.2D). However, a closer analysis of the different DN subpopulations revealed that the DN1, DN2 and DN4 subpopulations were increased in the *Aebp2*$^{-/-}$ FL recipient whereas the DN3 subpopulation was reduced (Figure 5.2C). A reduction in frequency of DP thymocytes and increase in frequency of CD8SP but not CD4SP were observed in the *Aebp2*$^{-/-}$ FL recipient (Figure 5.2D). Although there was a disturbance in thymocyte development, the overall cell populations were not severely affected. In aggregate, these data showed defects similar to the E18.5 conventional KO thymus, confirming that a lack of AEBP2 expression had a cell-autonomous effect on thymocyte development.

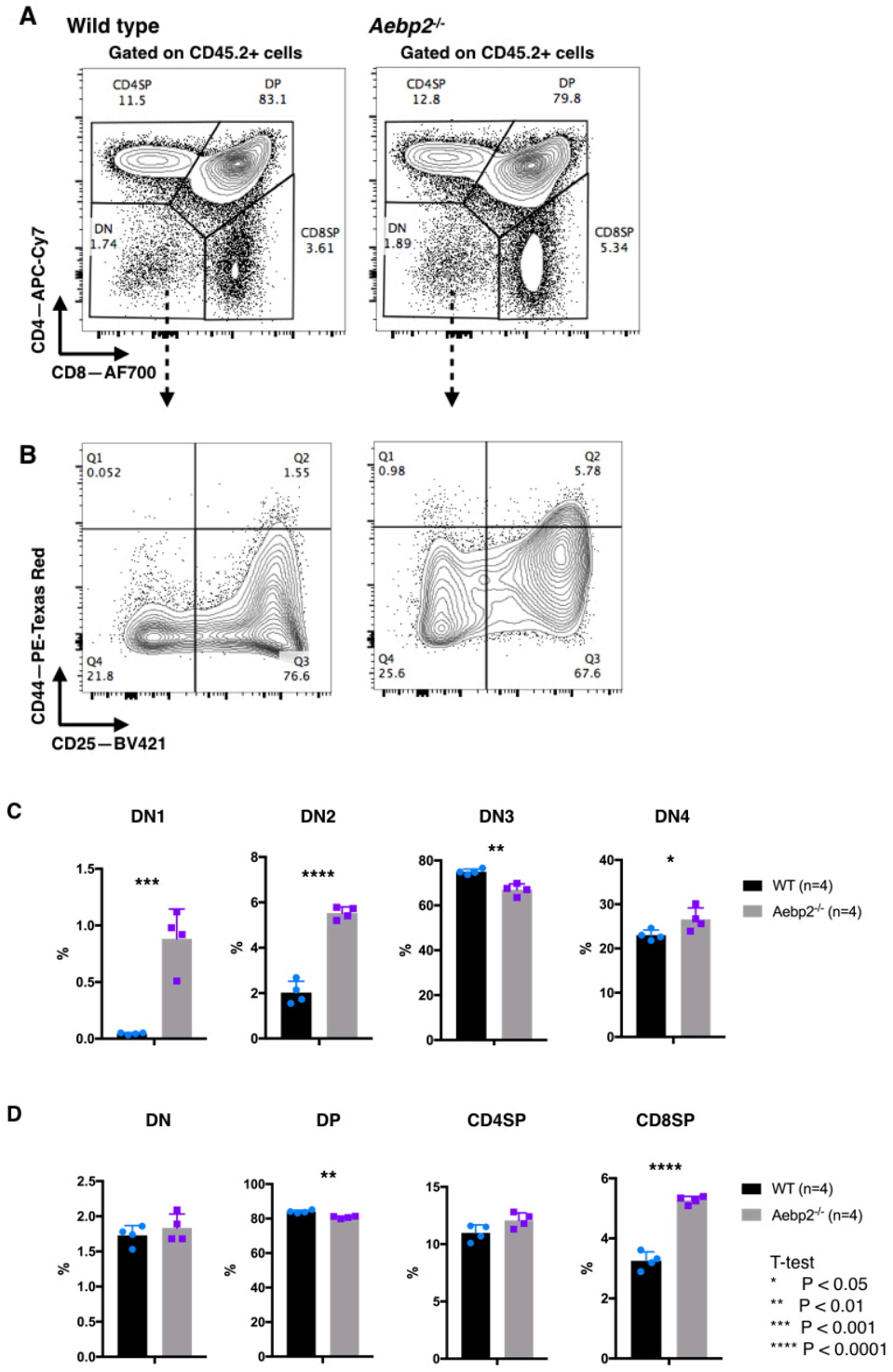

Figure 5.2: Frequencies of thymocyte subpopulations were altered in *Aebp2*$^{-/-}$ engrafts.

(A) (B) Gating strategies to identify and quantify distinct thymocyte subpopulations in mice engrafted with either wild type or *Aebp2*$^{-/-}$ FL cells. (C) (D) Thymocyte subpopulations were compared between the different genotypes as indicated. Graphs represent data from two

independent experiments. Statistics were calculated by student T-test. Columns show mean value and error bars represent standard deviation (SD). Each dot in bar graph represents one biological sample. **** $p < 0.0001$, *** $p < 0.001$, ** $p < 0.01$ and * $p < 0.05$

5.2 Engraftment of *Aebp2*$^{-/-}$ early thymic progenitors

Common lymphoid progenitors (CLPs) home to the thymus, where their commitment to a T cell fate is established (199). The most immature intrathymic progenitor cells are phenotypically defined as Lin-CD44+CD25-Kit^{hi} cells and are known as early thymic progenitors (ETPs) (200,201). Due to the significant increase in *Aebp2*$^{-/-}$ DN1 cells in the engrafted mice (Figure 5.2C), I next examined the frequency of ETPs within the same experimental system (Figure 5.3A). Indeed, a significant increase of ETPs was observed in mice engrafted with *Aebp2*$^{-/-}$ FL cells compared to recipients of wild type cells (Figure 5.3B). However the frequencies of DN2a and DN2b cells, which are the direct progeny of ETPs, were unaffected in the absence of AEBP2. It is, therefore, conceivable that cells of developmental stages upstream of ETP may indeed be affected by the loss of AEBP2. This possibility will be investigated later in this chapter.

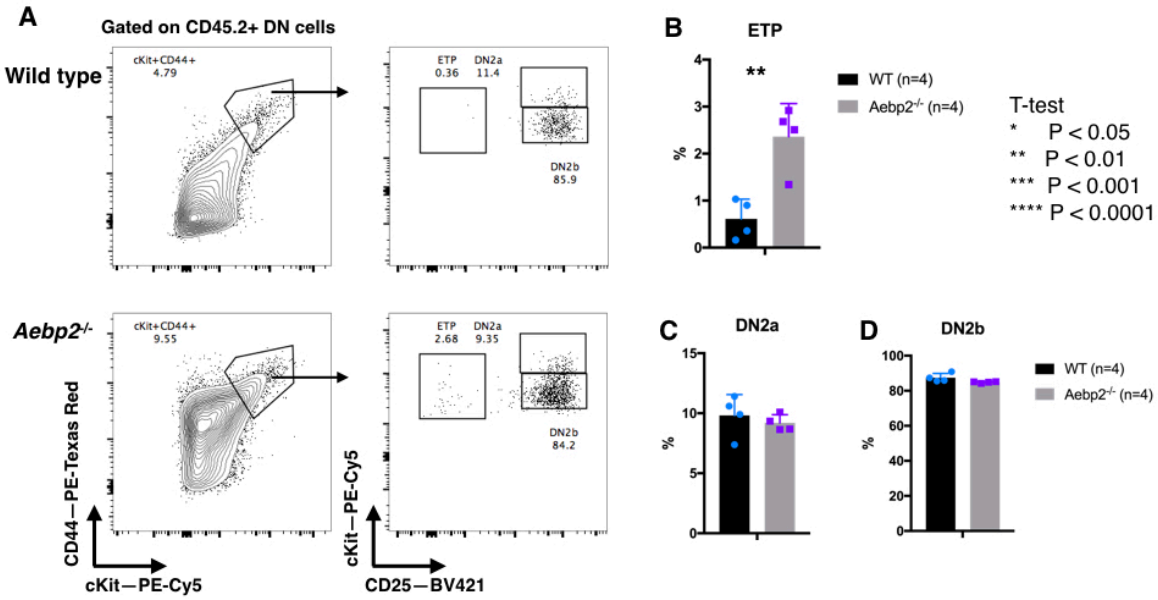

Figure 5.3: *Aebp2*$^{-/-}$ engrafts contained more ETPs compared with WT.

(A) Gating strategy to identify and quantify ETPs in mice engrafted with either wild type or *Aebp2*-deficient FL cells, respectively. (B)-(D) Relative frequencies of ETPs (B), DN2a (C) and DN2b (D) thymocyte subpopulations in the indicated FL recipients. Graphs represent data from two independent experiments. Statistics were calculated by student T-test. Columns show mean value and error bars represent standard deviation (SD). Each dot in bar graph represents one biological sample. **** p < 0.0001, *** p < 0.001, ** p < 0.01 and * p < 0.05

5.3 Both CD4 and CD8 thymocytes had an accelerated maturation when AEBP2 was absent

5.3.1 Altered positive selection for *Aebp2*$^{-/-}$ thymocytes

I next investigated whether thymocyte positive selection was affected in the absence of AEBP2. Positive selection takes place at the DP stage of thymocyte development and is characterized by changes in the surface expression of TCR and CD69. Once TCR rearrangement is finished, thymocytes start to up-regulate TCR expression followed by

CD69 up-regulation. Although TCR expression remains high, CD69 is down-regulatted when thymocytes mature. The positive selection and development of total thymocytes was therefore divided into progressive stages (i.e. Pre-S, S1-3 and M) (Figure 5.4A). There was a significant reduction in the frequency of the Pre-S thymocytes and an increase in the frequency of S1 thymocytes in the absence of AEBP2 (Figure 5.4B). Geometric mean fluorescence intensity (gMFI) of CD69 expression at both S1 and S2 stages were comparable for wild type and *Aebp2*$^{-/-}$ thymocytes, suggesting that TCR-mediated up-regulation of CD69 was not impaired in the absence of AEBP2 expression (Figure 5.4C). Taken together, these data would argue for and support a model where *Aebp2*$^{-/-}$ thymocytes could reach the S1 stage more efficiently affecting the subsequent frequencies in post-selection. However, other explanations are also possible (Figure 5.4B).

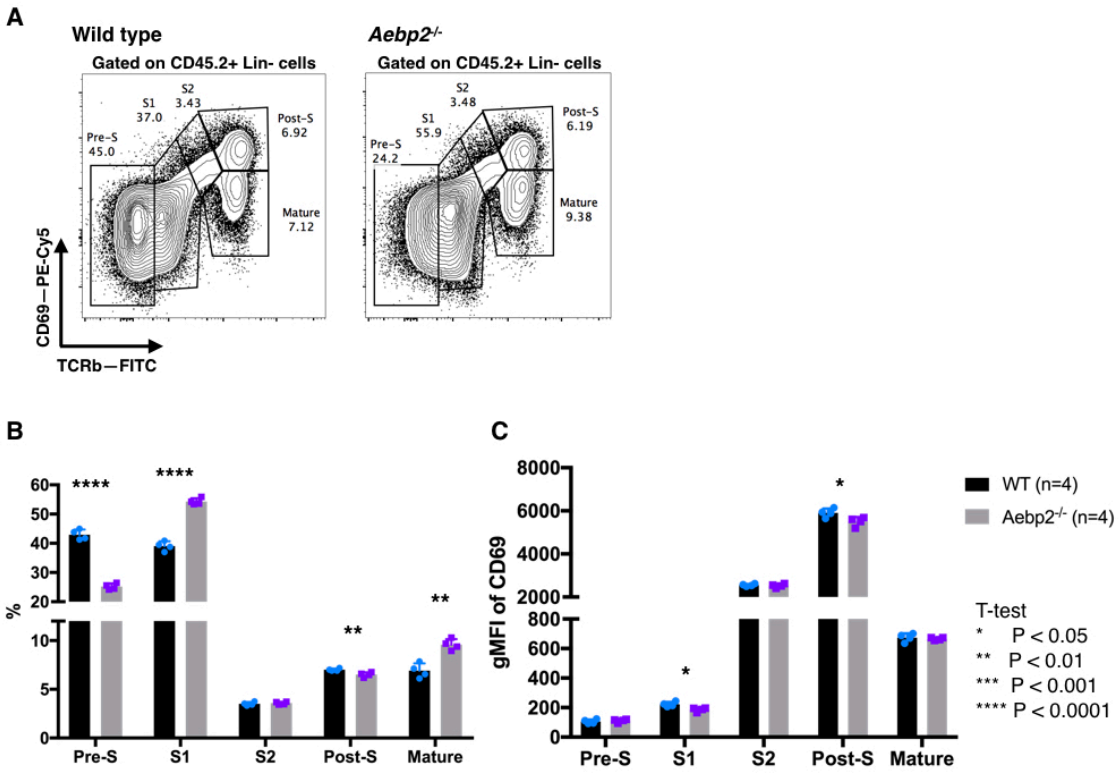

Figure 5.4: An accelerated positive selection in *Aebp2*$^{-/-}$ thymocytes

(A) Representative FACS plots showing different stages during positive selection: pre-S (TCRβ-CD69-), S1 (TCRβ^{int}CD69-), S2 (TCRβ^{int}CD69+), post-S (TCRβ+CD69+), and M (TCRβ+CD69-) stages. (B) Frequencies of the indicated maturational thymocyte stage in recipients of wild type and AEBP2 deficient FL. (C) geometric mean fluorescence intensity (gMFI) of CD69 expression. Each dot in bar graph represents one biological sample. **** $p < 0.0001$, *** $p < 0.001$, ** $p < 0.01$ and * $p < 0.05$

5.3.2 Both CD4 and CD8 thymocytes had an accelerated maturation

After successful completion of positive selection, TCRβ^{hi} DP thymocytes further develop to commit to either the CD4SP or the CD8SP lineage. The maturation of these two lineages is characterized by the expression of CCR7, CD24 and CD69 and additional markers, and typically separated into immature (CCR7-CD69+CD24+), semimature (CCR7+CD69+CD24+) and mature thymocyte (CCR7+CD69-CD24-) stages, as

depicted in Figure 5.4E for the CD4 lineage and Figure 5.4I for the CD8 lineage, respectively. The FACS plots show the staining pattern for CD4 and CD8 lineages (Figure 5.5A and 5.6A).

Although the frequency of *Aebp2*$^{-/-}$ immature CD4 thymocytes was identical to WT, the frequencies of both semi-mature and mature *Aebp2*$^{-/-}$ thymocytes were increased when compared to WT thymocytes (Figure 5.5C). A progression analysis, as previously described in Figure 4.8, was then conducted to assess the *Aebp2*$^{-/-}$ thymocyte maturation. This analysis showed a significant increase in the progression from the semimature to the mature stage among *Aebp2*$^{-/-}$ CD4 thymocytes when compared to wild type cells (Figure 5.5D right panel), which suggested that *Aebp2*$^{-/-}$ CD4 thymocytes matured more efficiently from a semimature to a mature stage than wild type cells.

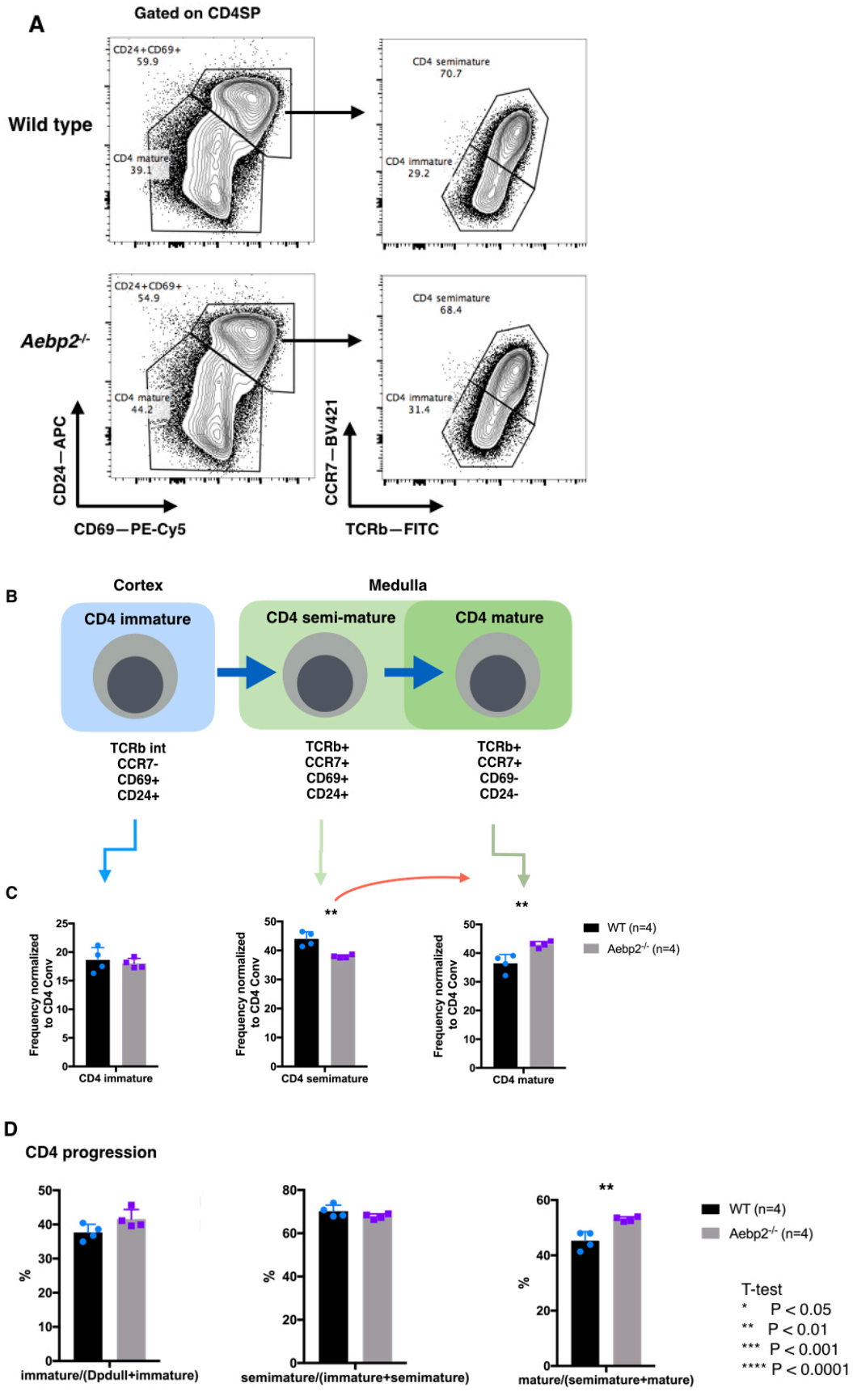
A
Gated on CD4SP
Wild type
CD24+CD69+
59.9
CD4 mature
39.1
CD4 semimature
70.7
CD4 immature
29.2
Aebp2-/-
CD24+CD69+
54.9
CD4 mature
44.2
CD4 semimature
68.4
CD4 immature
31.4
CD24—APC
CD69—PE-Cy5
CCR7—BV421
TCRb—FITC
B
Cortex
Medulla
CD4 immature
CD4 semi-mature
CD4 mature
TCRb int
CCR7-
CD69+
CD24+
TCRb+
CCR7+
CD69+
CD24+
TCRb+
CCR7+
CD69-
CD24-
C
Frequency normalized to CD4 Conv
CD4 immature
CD4 semimature
CD4 mature
**
**
WT (n=4)
Aebp2-/- (n=4)
D
CD4 progression
%
immature/(Dpdull+immature)
semimature/(immature+semimature)
mature/(semimature+mature)
**
WT (n=4)
Aebp2-/- (n=4)
T-test
* P < 0.05
** P < 0.01
*** P < 0.001
**** P < 0.0001

Figure 5.5: *Aebp2*$^{-/-}$ CD4 thymocyte development is accelerated

(A) Gating strategies to identify immature, semi-mature, and mature CD4 thymocytes using the cell surface expression of TCRβ, CCR7, CD24, and CD69. (B) Scheme of individual intrathymic maturation of the CD4 lineage. (C) CD4 developmental stages (D) Progression analysis showing the frequency of the cells that progressing from one stage to the next stage. The percentage of cells progressing to a particular stage was calculated dividing the percentage or number of cells within the stage of interest by that of the preceding stage, e.g CD4 immature /(DPdull + CD4 immature). Each dot in bar graph represents one biological sample. **** $p < 0.0001$, *** $p < 0.001$, ** $p < 0.01$ and * $p < 0.05$

Similarly, a reduction in the frequency of thymocytes at a semimature stage and an increase in the frequency of thymocytes at the mature stage were also noted for the CD8 lineage (Figure 5.6 B and C). The progression analysis for CD8 thymocytes showed that there was an increase in the progression from DPdull to immature CD8 thymocytes, and from semimature to mature CD8 thymocytes (Figure 5.6D, left and right panels), but a reduction from immature to semimature thymocytes in the *Aebp2*$^{-/-}$ CD8 thymocytes (Figure 5.6D middle panel). It is worth noting that the relative changes in thymocyte maturation were more convincing for *Aebp2*$^{-/-}$ CD8 thymocytes: CD4 vs CD8 lineage for semimature thymocytes: 6.05% ±1.27 vs 9.3 %±0.67; CD4 vs CD8 lineage for mature thymocytes: 6.55%±1.625 vs 11.66%±1.56.

Taken together, the absence of AEBP2 expression disturbs thymocyte selection and post-selectional differentiation of both the CD4 and CD8 lineages eventually leading to an increase of CD4SP and CD8SP thymocytes.

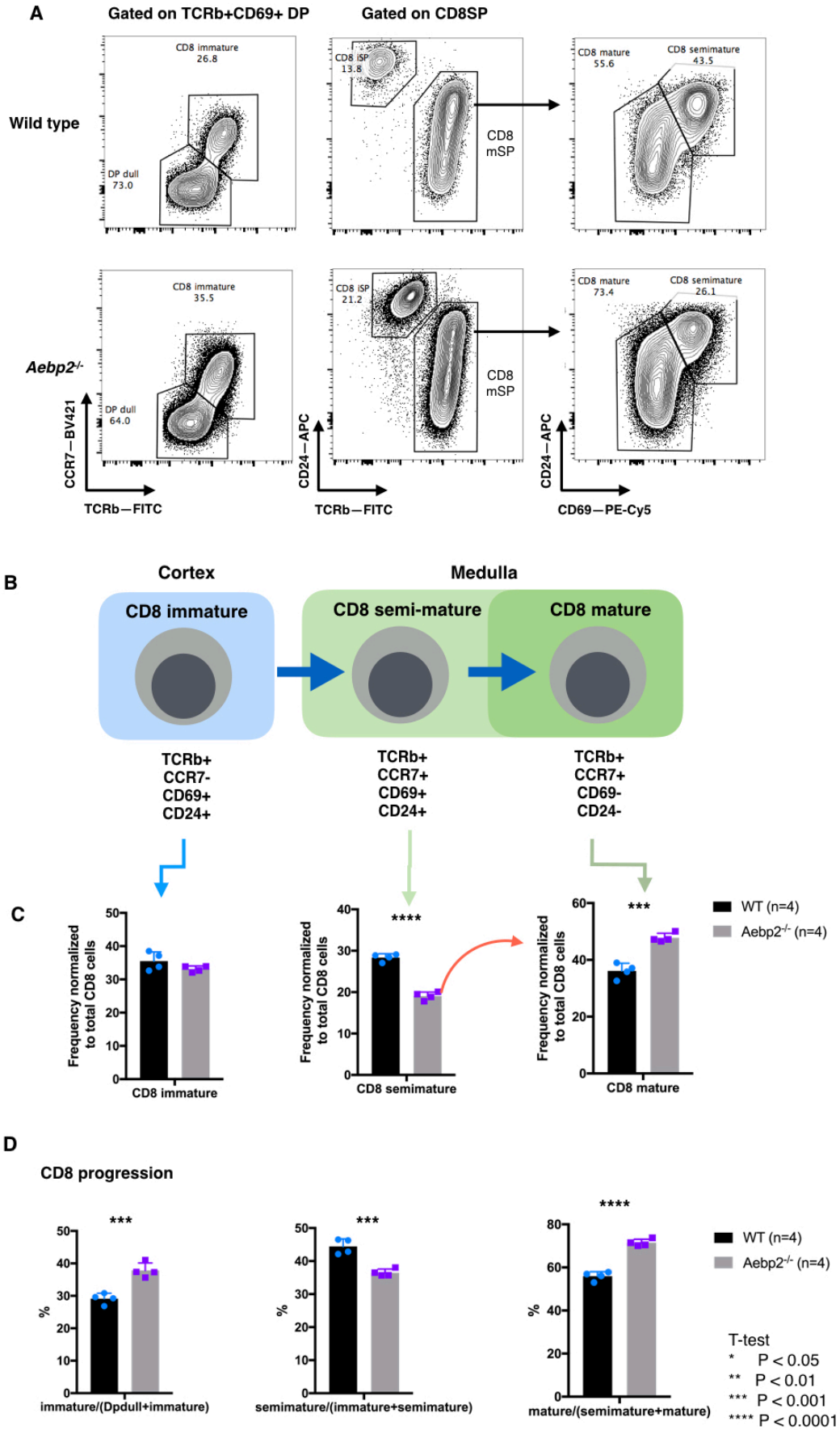
A
Gated on TCRb+CD69+ DP
Gated on CD8SP
Wild type
CD8 immature
26.8
DP dull
73.0
CD8 iSP
13.8
CD8
mSP
CD8 mature
55.6
CD8 semimature
43.5
Aebp2-/-
CD8 immature
35.5
DP dull
64.0
CD8 iSP
21.2
CD8
mSP
CD8 mature
73.4
CD8 semimature
26.1
CCR7—BV421
TCRb—FITC
CD24—APC
TCRb—FITC
CD24—APC
CD69—PE-Cy5
B
Cortex
Medulla
CD8 immature
CD8 semi-mature
CD8 mature
TCRb+
CCR7-
CD69+
CD24+
TCRb+
CCR7+
CD69+
CD24+
TCRb+
CCR7+
CD69-
CD24-
C
Frequency normalized to total CD8 cells
CD8 immature
****
CD8 semimature
***
CD8 mature
WT (n=4)
Aebp2-/- (n=4)
D
CD8 progression
***
%
immature/(Dpdull+immature)
***
semimature/(immature+semimature)
****
mature/(semimature+mature)
WT (n=4)
Aebp2-/- (n=4)
T-test
* P < 0.05
** P < 0.01
*** P < 0.001
**** P < 0.0001

Figure 5.6: *Aebp2*$^{-/-}$ CD8 thymocyte development is accelerated.

(A) Gating strategies of maturation stages of CD8 lineage also by their TCRβ, CCR7, CD24, and CD69 expression. (B) Scheme of individual intrathymic maturation of the CD8 lineage. (C) CD8 developmental stages (D) Progression analysis in CD8 lineage was conducted same as in CD4 lineage. Graphs represent data from three independent experiments. Statistics were calculated by student T-test. Columns show mean value and error bars represent standard deviation (SD). Each dot in bar graph represents one biological sample. **** $p < 0.0001$, *** $p < 0.001$, ** $p < 0.01$ and * $p < 0.05$

5.4 Absence of AEBP2 expression in T cells correlates with enhanced thymocyte negative selection

As a next step, the negative selection of the *Aebp2*$^{-/-}$ thymocytes was investigated by assessing their Helios and PD-1 expression as described in Chapter 4 (Figure 5.7A). An increase in the frequency of *Aebp2*$^{-/-}$ cells undergoing negative selection was observed in all four waves (Figure 5.7B). This suggested that the negative selection is enhanced at each maturational stage of *Aebp2*$^{-/-}$ CD4 thymocyte development.

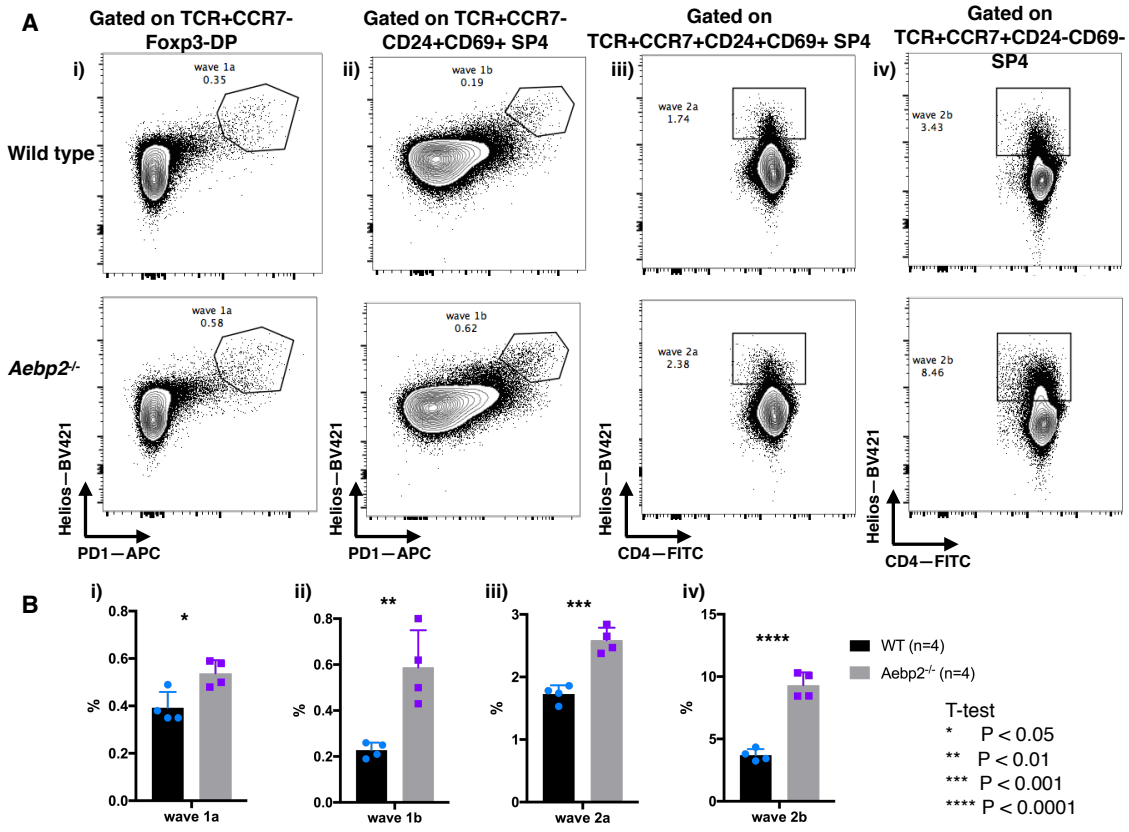

Figure 5.7: Enhanced negative selection in *Aebp2*$^{-/-}$ thymocytes

(A) Representative FACS plots showing negative selection waves in different maturation stages of thymocytes: i) wave 1a in DP dull (CD4+CD8+TCR^{pos}CCR7-); ii) wave 1b in immature CD4 (CD4+TCR^{pos}CCR7-CD24+CD69+); iii) wave 2a in semimature CD4 (CD4+TCR^{pos}CCR7+CD24+CD69+); iv) wave 2b in mature CD4 (CD4+TCR^{pos}CCR7+CD24-CD69-). (B) Frequencies of cells undergoing negative selection in difference waves were compared between indicated genotypes for CD4 lineage. Graphs represent data from three independent experiments. Statistics were calculated by student T-test. Columns show mean value and error bars represent standard deviation (SD). Each dot in bar graph represents one biological sample. **** p < 0.0001, *** p < 0.001, ** p < 0.01 and * p < 0.05

5.5 Egress of *Aebp2*-/- mature thymocytes mediated by $S1P_1$ expression

MHC-I is a cell surface marker which increases its expression along the maturation of SP thymocytes. By using MHC-I and CD69, Hogquist and colleagues developed a different strategy to assess maturation steps of medullary thymocytes (202). CCR7+ SP thymocyte maturation is described as sequentially progressing from semi-mature (SM) (MHC-I^{lo}CD69+), to mature 1 (M1) (MHC-I^{hi}CD69+) and subsequently mature 2 (M2) (MHC-I^{hi}CD69-) (Figure 5.8B)- a point at which they are capable of thymic egress. FACS gating is shown in Figure 5.8A for both wild type and *Aebp2*$^{-/-}$ thymocytes. I compared these three populations in wild type and *Aebp2*$^{-/-}$ SP thymocytes for both CD4 and CD8 lineages. The relative frequency of M2 thymocytes within these two lineages were increased in the absence of AEBP2, suggesting that the mature thymocyte egress might be affected (Figure 5.8C). Mature, egress-capable thymocytes up-regulate sphingosine-1-phosphate (S1P) receptor 1 ($S1P_1$), allowing them to migrate towards blood vessels (Figure 5.8D) (133). To further investigate the capacity of these cells to egress the thymus, I FACS sorted both CD4 and CD8 M2 stage thymocytes and measured the transcript level of $S1P_1$ by qRT-PCR. The data showed that there was a significant reduction of $S1P_1$ level in both CD4 and CD8 lineages in *Aebp2*$^{-/-}$ thymocytes (Figure 5.8E). Taken together, these data indicated that *Aebp2* deficiency altered the transcription level of $S1P_1$ for both CD4 and CD8 mature thymocytes, and eventually led to an accumulation of these cells at the M2 stage.

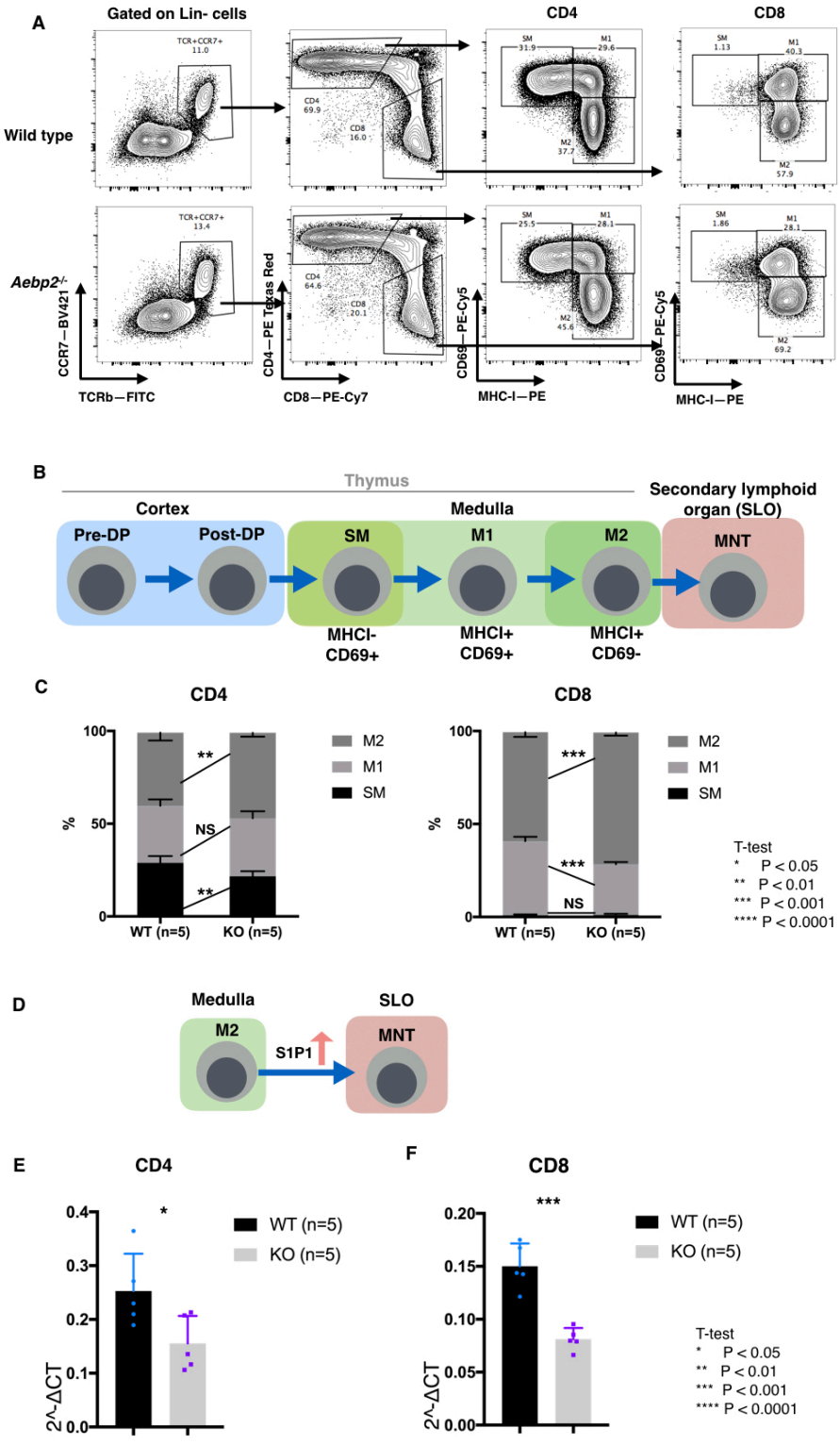

Figure 5.8: Reduced S1P$_1$ in Aebp2-/- mature thymocytes prevented their thymic egress

(A) Representative FACS plots showing different maturation stages of thymocytes within the medulla: SM (MHC-I^{lo}CD69+), M1 (MHC-I^{hi}CD69+), M2 (MHC-I^{hi}CD69-) stages. (B) A flowchart describing the progression of thymocytes from SM through M1, then to M2 sequentially before

exiting to the thymus. (C) Frequencies of SM, M1 and M2 stages were compared between the indicated genotypes for both CD4 and CD8 lineages. (D) The scheme showing that $S1P_1$ is required for thymic egress of the mature thymocytes. (E) (F) The transcription level of $S1P_1$ was compared between indicated genotypes for CD4 (E) and CD8 (F) lineages. Graphs represent data from three independent experiments. Statistics were calculated by student T-test. Columns show mean value and error bars represent standard deviation (SD). Each dot in bar graph represents one biological sample. **** $p < 0.0001$, *** $p < 0.001$, ** $p < 0.01$ and * $p < 0.05$

5.6 Peripheral T cell compartment in the absence of AEBP2

Mature thymocytes egress from the thymus to the periphery where they are described as fully functional naïve T cells. These T cells circulate throughout the host body and can be activated within the secondary lymphoid organs (i.e. LN, spleen) through interaction with cognate antigenic peptides presented by professional APCs. Although the specific functions of CD4 and CD8 naïve T cells are different as described previously, both lineages show characteristic responses to pathogens. Upon the encounter with pathogens, naïve T cells are rapidly activated and transit to effector T cells to initiate immune responses. During this process, the effector T cells undergo a robust proliferation. After the infection is eliminated, the vast majority of the effectors undergo apoptosis, with a small proportion becoming memory T cells. These cells allow for faster responses of a greater magnitude in response to a secondary exposure to their cognate antigen. In this part of the chapter, I have investigated peripheral T cell populations to assess the impact of a lack of AEBP2.

5.6.1 An increase of *Aebp2*$^{-/-}$ αβT cells in the LN

LNs were used to investigate the phenotype of *Aebp2*-deficient T cells in the periphery. As the recipient mice were lethally irradiated, most of the thymocytes from the host were depleted (Figure 5.1B and C). However, peripheral lymphocytes seemed to be, at least in part, resistant to irradiation as CD45.1+ recipient cells were observed in the LNs (Figure 5.9A i). Moreover, these lymphocytes were mainly T cells suggesting that T cells might be less susceptible to irradiation than B cells (Figure 5.9A iii). Although the frequency of the total CD45.2+ donor lymphocytes were comparable between wild type and *Aebp2*$^{-/-}$ groups (Figure 5.9B), a relative increase in the frequency of T cells and reduction of the frequency of B cells were observed in the *Aebp2*$^{-/-}$ group (Figure 5.9D), which was not expected as previous data suggested a thymic egress defect caused by Aebp2 deficiency.

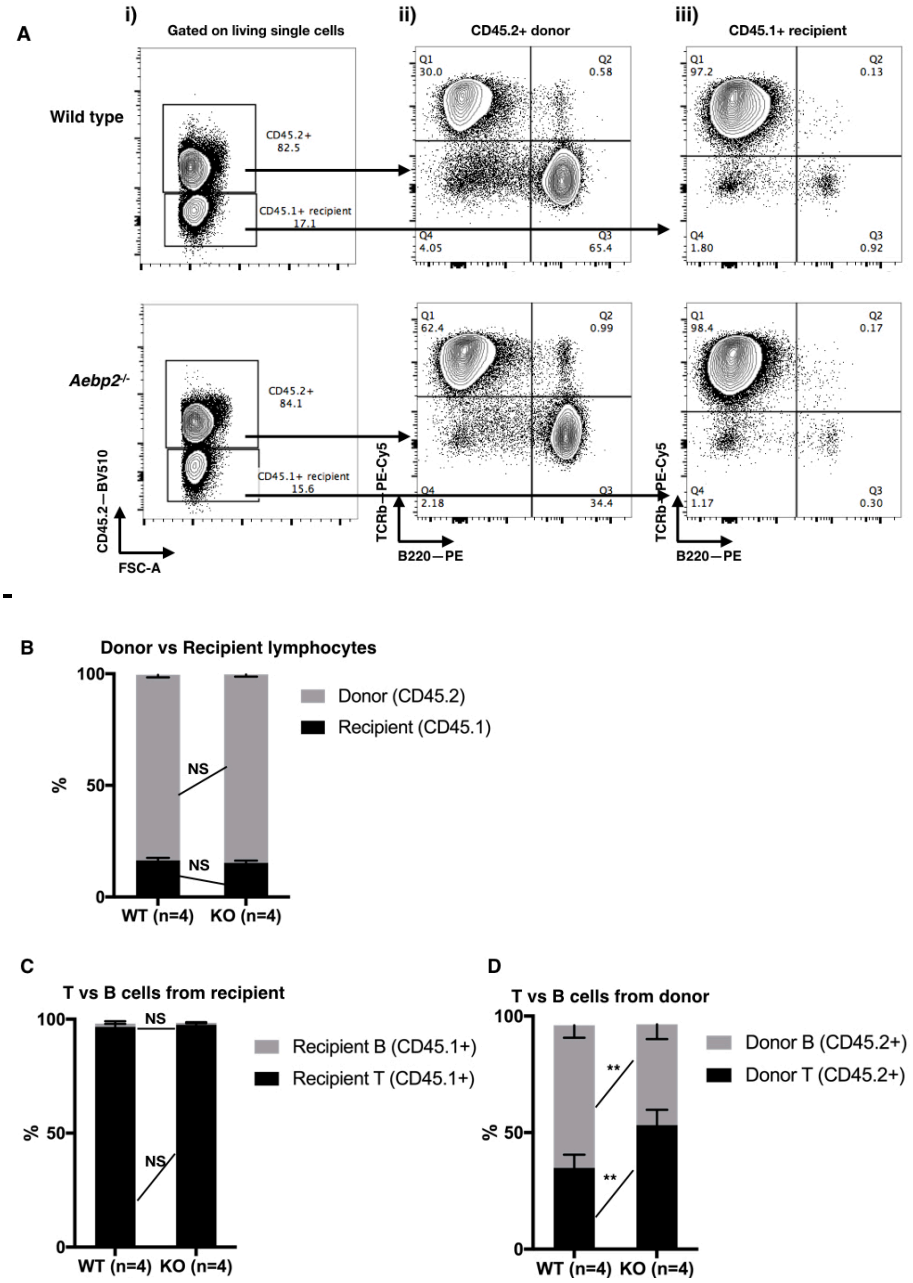

Figure 5.9: An increased peripheral T cell frequency in the absence of AEBP2

(A) Representative FACS plots showing T cells and B cells from either recipient (ii) or recipient (iii) in LNs. (B) The frequencies of donor and recipient lymphocytes in LNs were compared between indicated groups. (C) The frequencies of host (CD45.1+) T and B cells were compared between indicated groups. (D) The frequencies of donor (CD45.2+ T and B cells were compared between indicated groups. Graphs represent data from three independent experiments. Statistics were calculated by student T-test. Columns show mean value and error bars represent standard deviation (SD). **** $p < 0.0001$, *** $p < 0.001$, ** $p < 0.01$ and * $p < 0.05$

To understand what caused the increase in T cell frequency, CD4 and CD8 SP cells were investigated by checking their naïve, effector, and memory subpopulations characterized by the surface expression of CD62L and CD44 (Figure 5.10A). When comparing CD4 as well as CD8 T cells between wild type and *Aebp2*$^{-/-}$ groups, an increase of CD8 T cell frequency relative to the reduction of CD4 T cells was observed (Figure 5.10B). Within CD4 T cells, the naïve to memory ratio was not changed between wild type and *Aebp2*$^{-/-}$ groups (Figure 5.10C). However, within the CD8 T cells, I saw a reduction in the frequency of naïve T cells and an increase in the frequency of central memory T cells (Figure 5.10D). This skew from naïve to memory T cells suggested that *Aebp2*$^{-/-}$ CD8 naïve T cells might be more susceptible to pathogenic stimulus and prone to progress to memory T cells. Previous research revealed that CD8 T cells undergo extensive clonal expansion responding to infection whereas CD4 T cells showed a more restricted proliferation pattern (203). The naïve-to-memory shift of CD8 T cell could be accompanied by an enhanced cell proliferation causing the increase in the frequency of the total T cells (Figure 5.9D) as well as the increase in the relative frequency of CD8 T cells within total T cells (Figure 5.10B).

Taken together, a lack of AEBP2 expression might affect the susceptibility of CD8 T cells to pathogens in the periphery.

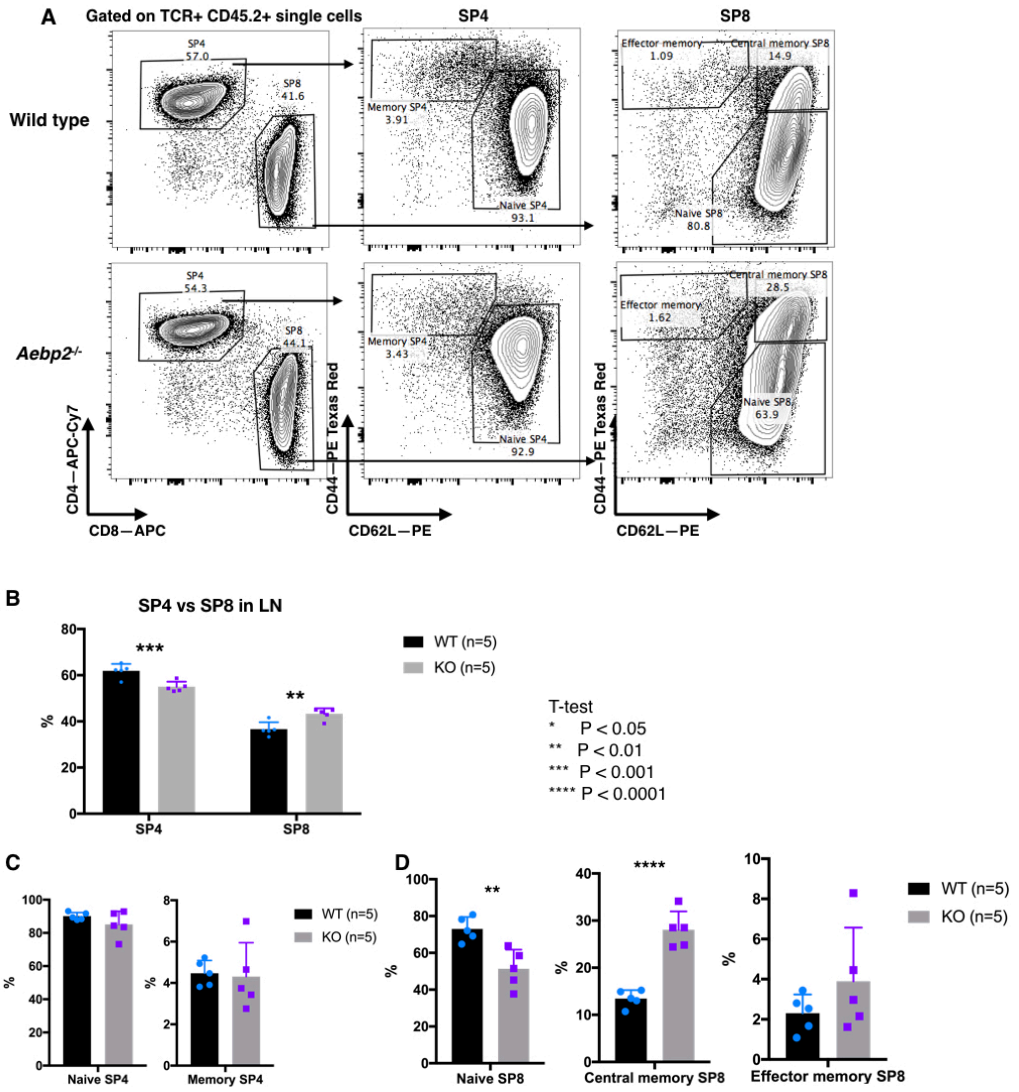

Figure 5.10: A naïve-to-memory shift in *Aebp2*$^{-/-}$ CD8 T cells

(A) Representative FACS plots showing the gating strategy for naïve CD4 (CD62L+CD44-), memory CD4 (CD62L-CD44+), naïve CD8 (CD62L+CD44-), central memory CD8 (CD62+CD44+), and effector memory (CD62L-CD44+) T cells. (B) The frequencies of CD4 as well as CD8 T cells were compared between indicated groups. (C) The frequencies of naïve as well as memory CD4 T cells were compared between indicated groups. (D) The frequencies of naïve, central memory, as well as effector memory CD8 T cells were compared between indicated groups. Graphs represent data from three independent experiments. Statistics were calculated by student T-test. Columns show mean value and error bars represent standard deviation (SD). Each dot in bar graph represents one biological sample. **** $p < 0.0001$, *** $p < 0.001$, ** $p < 0.01$ and * $p < 0.05$

5.6.2 A reduction of the peripheral Treg population in the absence of AEBP2

Tregs, formerly known as suppressor T cells, are a subpopulation of CD4 T cells in the periphery regulating or suppressing the immune response. Previous research has shown that Tregs can inhibit T cell proliferation and cytokine production to prevent autoimmunity (204). Tregs are usually characterized by the surface expression of CD25 and nuclear expression of transcription factor FOXP3. Within the Tregs, ICOS and CD103 are used to identify a subpopulation with high suppressive function (205). I next investigated Tregs and their subpopulations in the LN.

Tregs from both wild type and *Aebp2*$^{-/-}$ engrafts were gated as CD4+CD25+Foxp3+ by flow cytometry (Figure 5.11A). There was a clear reduction in the frequency of Tregs in *Aebp2*$^{-/-}$ engrafts compared with wild type (7.75%±0.44 in WT vs 3.50%±0.18 in *Aebp2*$^{-/-}$) (Figure 5.11B). Moreover, among the four subpopulations, as defined by ICOS and CD103 expression, the relative frequency of ICOS+CD103- and ICOS+CD103+ populations were significantly reduced, whereas that of the ICOS-CD103+ Tregs were increased in *Aebp2*$^{-/-}$ engrafts (Figure 5.11C). No difference in the frequency of the ICOS-CD103- subpopulation was observed between two genotypes (Figure 5.11C).

A reduction of the Treg frequency especially the relative frequency of ICOS+CD103+ subpopulation in the absence of AEBP2 could result in a suppression defect, which requires functional examination.

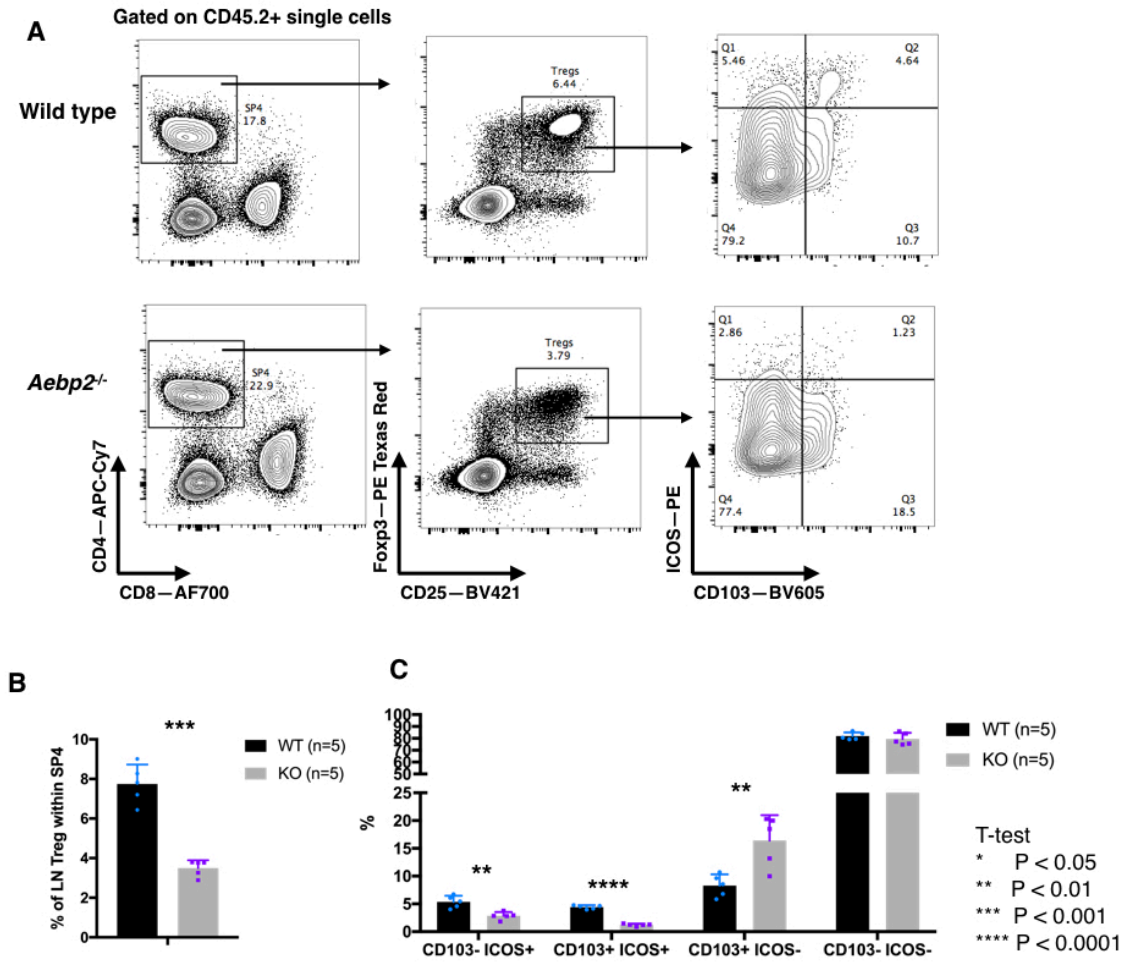

Figure 5.11: A reduction of Tregs in the LN in the absence of AEBP2.

(A) Representative FACS plots showing the gating strategy for total Tregs in the LN (CD4+CD25+FOXP3+) and the four subpopulations defined by the expression of ICOS and CD103. (B) The frequency of Tregs within CD4 T cells were compared between indicated groups. (C) The frequencies of Treg subpopulations were compared between indicated groups. Graphs represent data from three independent experiments. Statistics were calculated by student T-test. Columns show mean value and error bars represent standard deviation (SD). Each dot in bar graph represents one biological sample. **** $p < 0.0001$, *** $p < 0.001$, ** $p < 0.01$ and * $p < 0.05$

5.7 Competitive advantage in *Aebp2*$^{-/-}$ haematopoietic cells.

5.7.1 Competitive advantage was observed in *Aebp2*$^{-/-}$ thymocytes

As a way to investigate the growth potential of *Aebp2*$^{-/-}$ thymocytes, I included wild type CD45.1/2 FL cells as competitors into the transplantation system. As seen in the scheme in Figure 5.12A, same number of CD45.2+ wild type or *Aebp2*$^{-/-}$ donor FL cells as well as CD45.1/2 competitor cells were injected intravenously into lethally irradiated CD45.1+ recipients. Six weeks post-transplantation, both the thymocytes and mature T cells were investigated for their growth activities. For the groups receiving either wild type or *Aebp2*$^{-/-}$ donor cells, the recipient CD45.1+ thymocytes had been depleted thoroughly as the remaining frequency of this population was less than 1% (Figure 5.12B). Compared to the ratio of CD45.2+ wild type donor versus CD45.1/2 competitor, which remained nearly 50% to 50%, the ratio of CD45.2+ *Aebp2*$^{-/-}$ donor versus CD45.1/2 competitor was significantly skewed toward the CD45.2+ *Aebp2*$^{-/-}$ donor side (85% to 15%) (Figure 5.12C). This suggested that the *Aebp2*$^{-/-}$ thymocytes had a strong competitive advantage against the wild type competitors. The comparison between the thymocyte subpopulations showed that, the *Aebp2*$^{-/-}$ thymocytes gradually lost the competitive advantage as they mature as the ratios of *Aebp2*$^{-/-}$ donor versus competitor cells were reducing from DN1 towards mature CD4 and CD8 SP thymocytes compared to the wild type donor (Figure 5.12D).

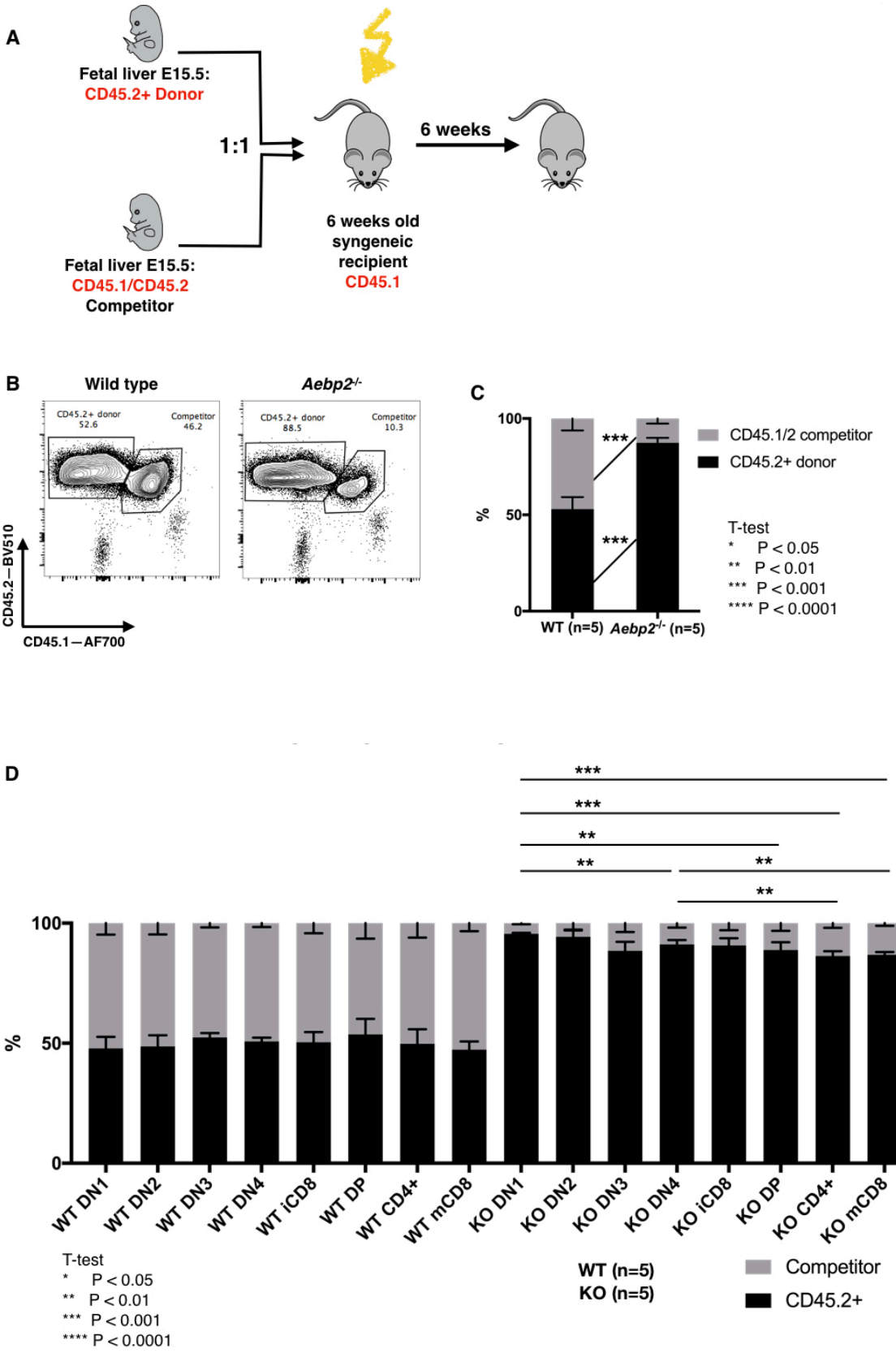
A
Fetal liver E15.5:
CD45.2+ Donor
1:1
Fetal liver E15.5:
CD45.1/CD45.2
Competitor
6 weeks old
syngeneic
recipient
CD45.1
6 weeks
B
Wild type
Aebp2-/-
CD45.2+ donor
52.6
Competitor
46.2
CD45.2+ donor
88.5
Competitor
10.3
CD45.2—BV510
CD45.1—AF700
C
100
50
0
%
***
***
CD45.1/2 competitor
CD45.2+ donor
T-test
* P < 0.05
** P < 0.01
*** P < 0.001
**** P < 0.0001
WT (n=5)
Aebp2-/- (n=5)
D
***
***
**
**
**
**
100
50
0
%
WT DN1
WT DN2
WT DN3
WT DN4
WT iCD8
WT DP
WT CD4+
WT mCD8
KO DN1
KO DN2
KO DN3
KO DN4
KO iCD8
KO DP
KO CD4+
KO mCD8
T-test
* P < 0.05
** P < 0.01
*** P < 0.001
**** P < 0.0001
WT (n=5)
KO (n=5)
Competitor
CD45.2+

Figure 5.12: A growth advantage of the thymocytes in the absence of AEBP2.

(A) Scheme showing the design of the competition experiment. (B) Representative FACS plots showing the staining for CD45.1 and CD45.2 markers. (C) The ratios of CD45.2+ donor versus CD45.1/2 competitor cells for total thymocytes were compared between indicated groups. (D) The ratios of CD45.2+ donor versus CD45.1/2 competitor cells for individual thymocyte subpopulations were compared within both wild type and *Aebp2*$^{-/-}$ groups. Graphs represent data from three independent experiments. Statistics were calculated by student T-test. Columns show mean value and error bars represent standard deviation (SD). **** $p < 0.0001$, *** $p < 0.001$, ** $p < 0.01$ and * $p < 0.05$

5.7.2 Competitive advantage commenced in haematopoietic stem and progenitor cells (HSPCs)

As the competitive advantage was observed in DN1 stage already, and to a greater extent than any other populations within the thymus, I was then interested in checking whether the phenotype existed in the earlier haematopoietic progenitor stage and how broadly this phenotype was affected.

In mouse, HSCs are usually found in the Lin^{-}Sca-1^{+}c-Kit^{+} (LSK) population, and characterized by their expression of CD150 and CD48, and the absence of Flt3 (CD150^{+}CD48^{-}Flt3^{-}) (206). The subsequent MPP2, MPP3 and MPP4 populations are defined as CD150^{+}CD48^{+}Flt3^{-}, CD150^{-}CD48^{+} Flt3^{-}, and CD150^{-}CD48^{-}Flt3^{+}, respectively. Bone marrow cells were harvested from the transplanted mice and stained for the markers introduced above to differentiate haematopoietic stem and progenitor cell (HSPC) populations (Figure 5.13A). The data showed that there is a higher percentage of HSC and MPP4 populations, and a reduction in the frequency of MPP2 population in *Aebp2*$^{-/-}$ donor cells compared to wild type (Figure 5.13B).

Although different HSPC populations showed changes in relative frequencies in different directions, an increased ratio of donor versus competitor was observed across all four populations in the *Aebp2*$^{-/-}$ engrafts (Figure 5.13C). This indicated that the competitive advantage of thymocytes already started at the HSPC stage. It is worth noting that the ratio of donor versus competitor from HSPC populations was not as high as the one in thymocytes in *Aebp2*$^{-/-}$ engrafts (Figure 5.12C). This might suggest that the growth phenotype became more advanced from HSPC stage through thymocytes in the absence of AEBP2.

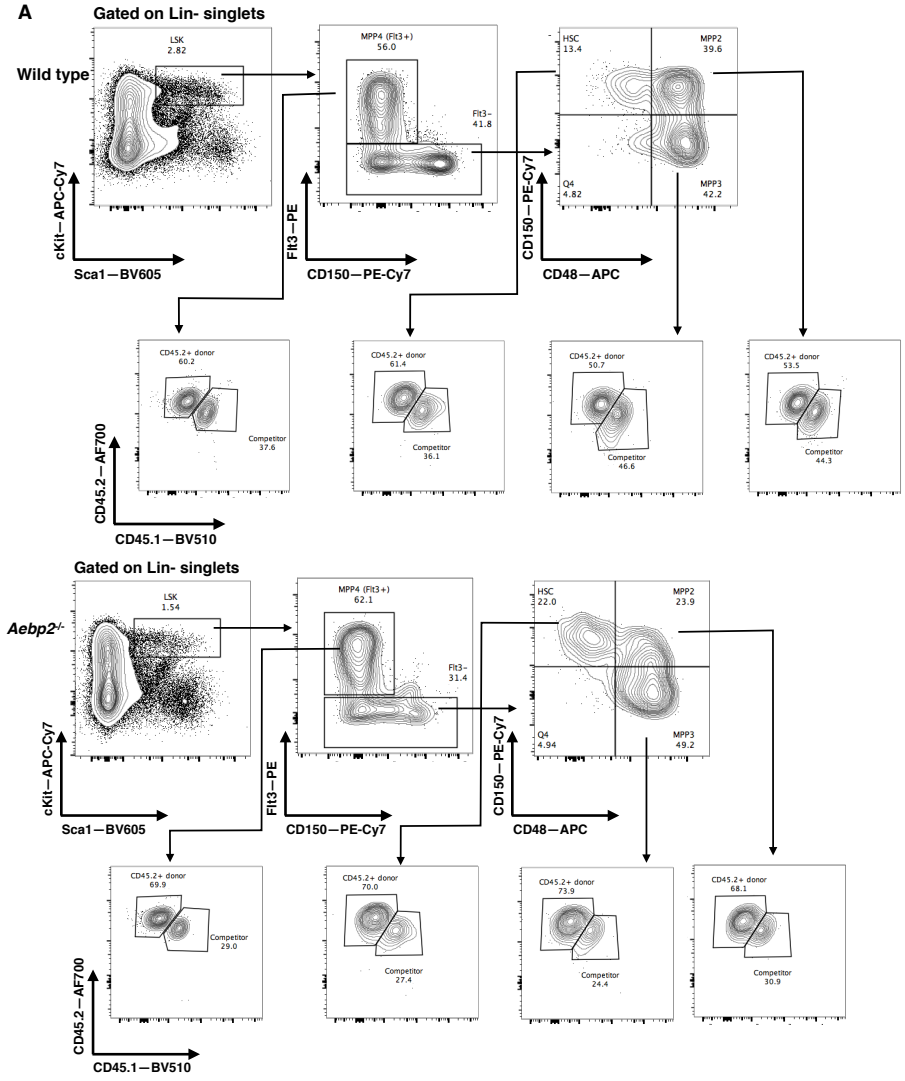
A
Gated on Lin- singlets
Wild type
LSK
2.82
MPP4 (Flt3+)
56.0
Flt3-
41.8
HSC
13.4
MPP2
39.6
Q4
4.82
MPP3
42.2
cKit—APC-Cy7
Sca1—BV605
Flt3—PE
CD150—PE-Cy7
CD150—PE-Cy7
CD48—APC
CD45.2+ donor
60.2
Competitor
37.6
CD45.2+ donor
61.4
Competitor
36.1
CD45.2+ donor
50.7
Competitor
46.6
CD45.2+ donor
53.5
Competitor
44.3
CD45.2—AF700
CD45.1—BV510
Gated on Lin- singlets
Aebp2-/-
LSK
1.54
MPP4 (Flt3+)
62.1
Flt3-
31.4
HSC
22.0
MPP2
23.9
Q4
4.94
MPP3
49.2
cKit—APC-Cy7
Sca1—BV605
Flt3—PE
CD150—PE-Cy7
CD150—PE-Cy7
CD48—APC
CD45.2+ donor
69.9
Competitor
29.0
CD45.2+ donor
70.0
Competitor
27.4
CD45.2+ donor
73.9
Competitor
24.4
CD45.2+ donor
68.1
Competitor
30.9
CD45.2—AF700
CD45.1—BV510

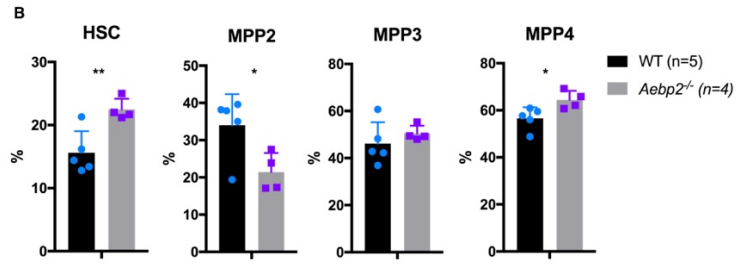
B
HSC
MPP2
MPP3
MPP4
WT (n=5)
Aebp2-/- (n=4)
%

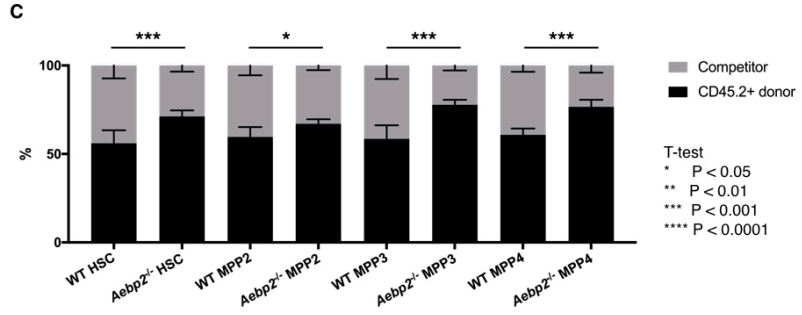
C
***
*
***
***
%
Competitor
CD45.2+ donor
T-test
* P < 0.05
** P < 0.01
*** P < 0.001
**** P < 0.0001
WT HSC
Aebp2-/- HSC
WT MPP2
Aebp2-/- MPP2
WT MPP3
Aebp2-/- MPP3
WT MPP4
Aebp2-/- MPP4

Figure 5.13: Growth advantage commenced in HSPCs in the absence of AEBP2.

(A) Representative FACS plots showing the gating strategy for HSC ($CD150^+CD48^-Flt3^-$), MPP2 ($CD150^+CD48^+Flt3^-$), MPP3 ($CD150^-CD48^+Flt3^-$) and MPP4 ($CD150^-CD48^+Flt3^+$) subpopulations from $Lin^-Sca\text{-}1^+c\text{-}Kit^+$ (LSK) cells for both wild type and *Aebp2*$^{-/-}$ engrafts. $CD45.2^+$ and CD45.1/2 populations were stained in each HSPC populations. (B) The frequencies of HSC, MPP2, MPP3 and MPP4 populations were compared between recipients engrafted with wild type and *Aebp2*$^{-/-}$ donor cells. (C) The ratios of CD45.2+ donor versus CD45.1/2 competitor cells for individual HSPC subpopulations were compared between indicated genotypes. Each dot in bar graph represents one biological sample. Statistics were calculated by student T-test. Columns show mean value and error bars represent standard deviation (SD). **** $p < 0.0001$, *** $p < 0.001$, ** $p < 0.01$ and * $p < 0.05$

5.7.3 Competitive advantage in the absence of AEBP2 affected myeloid progenitor cells in the adult bone marrow

Myeloid blood cells derive from HSCs and develop within the bone marrow in the adult. Previous research has identified $Lin^-c\text{-}Kit^+Sca\text{-}1^-$ common myeloid progenitor (CMP) that can give rise to all myeloid lineages (207). The CMP gives rise to either megakaryocyte/erythrocyte or granulocyte/macrophage progenitors. The commitment to either of these two lineages is mutually exclusive. As myeloid-primed MPP2 and MPP3 populations seemed to have increased frequency of *Aebp2*$^{-/-}$ donor cells compared to wild type, I then investigated whether CMP and the subsequent myeloid cell lineages were affected as illustrated in Figure 5.14A (208). The hierarchical development from CMP to several myeloid lineage-restricted progenitors can be characterized by cell surface markers: Fcγ receptor-II/III (FcγR), CD150, CD105, and CD41. As shown in the gating strategies of different myeloid progenitors in Figure 5.14B, CMP gives rise to either Pre MegE ($CD41^-Fc\gamma R^-CD150^+CD105^-$) or Pre GM ($Fc\gamma R^-CD150^-CD105^-$) cells. Pre MegE

is a mixed progenitor population, which produces either Pre CFU-E ($CD41^{-}FcγR^{-}CD150^{+}CD105^{+}$) or MkP ($CD41^{+}CD150^{+}$) cells. Pre CFU-Es generate almost only erythroid colonies (CFU-E ($CD41^{-}FcγR^{-}CD150^{-}CD105^{+}$)) whereas MkPs are exclusively committed to megakaryocyte generation. On the other hand, Pre GM ($FcγR^{-}CD150^{-}CD105^{-}$) gives rise to GMP ($CD41^{-}FcγR^{+}$), which eventually commit to either granulocytes or macrophages. All these progenitor populations were investigated for their donor-versus-competitor ratio between wild type and *Aebp2*$^{-/-}$ engrafts. The frequency of the $Lin^{-}c\text{-}Kit^{+}Sca\text{-}1^{-}$ population was increased in *Aebp2*$^{-/-}$ engrafts (Figure 5.14C) suggesting that the CMPs were affected in the absence of AEBP2. Indeed, all individual myeloid progenitor populations from *Aebp2*$^{-/-}$ engrafts showed a competitive advantage similar to what has been observed in HSPCs and thymocytes (Figure 5.14D). As almost all erythroid cells were $CD45^{-}$, it was difficult to investigate their growth ability in the absence of AEBP2 with CD45 expression. Similar to HSPC compartment, the skewing of the ratio of donor versus competitor was not as high as that of the thymocytes in the *Aebp2*$^{-/-}$ engrafts (Figure 5.12C). This may suggest that the growth advantage affected the lymphoid cells to a greater extent compared to the myeloid cells.

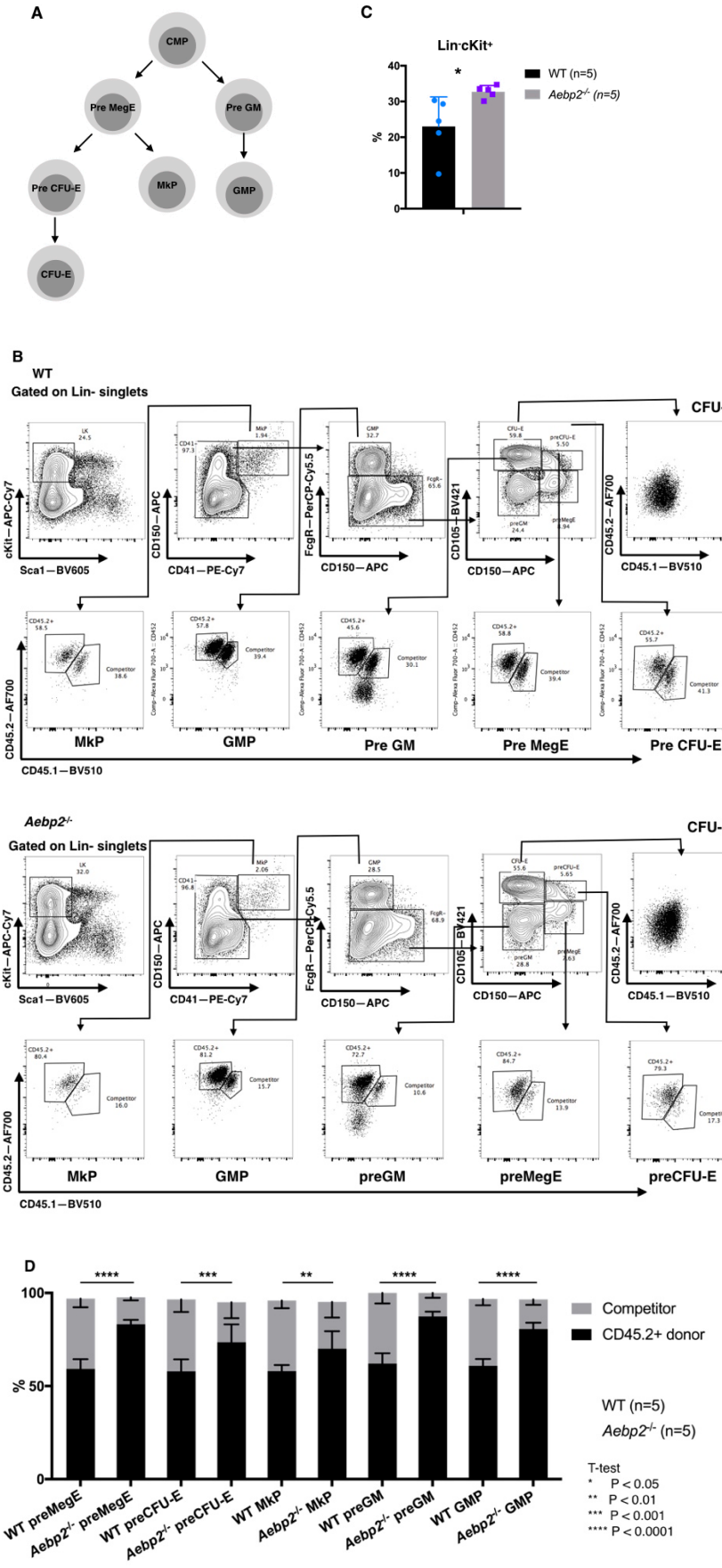
A
CMP
Pre MegE
Pre GM
Pre CFU-E
MkP
GMP
CFU-E
C
Lin-cKit+
WT (n=5)
Aebp2-/- (n=5)
%
B
WT
Gated on Lin- singlets
CFU-E
cKit—APC-Cy7
Sca1—BV605
CD150—APC
CD41—PE-Cy7
FcgR—PerCP-Cy5.5
CD150—APC
CD105—BV421
CD150—APC
CD45.2—AF700
CD45.1—BV510
MkP
GMP
Pre GM
Pre MegE
Pre CFU-E
Aebp2-/-
Gated on Lin- singlets
CFU-E
preGM
preMegE
preCFU-E
D
Competitor
CD45.2+ donor
WT (n=5)
Aebp2-/- (n=5)
T-test
* P < 0.05
** P < 0.01
*** P < 0.001
**** P < 0.0001
WT preMegE
Aebp2-/- preMegE
WT preCFU-E
Aebp2-/- preCFU-E
WT MkP
Aebp2-/- MkP
WT preGM
Aebp2-/- preGM
WT GMP
Aebp2-/- GMP

Figure 5.14: Growth advantage in the absence of AEBP2 affected myeloid progenitor cells. (A) Schematic diagram showing the hierarchy of lineage commitment of myeloid progenitor cells. (B) Representative FACS plots showing the gating strategy of Pre MegE (CD41-FcγR-CD150+CD105-), Pre CFU-E (CD41-FcγR-CD150+CD105+), MkP (CD41+CD150+), CFU-E (CD41-FcγR-CD150-CD105+), Pre GM (FcγR-CD150-CD105-) and GMP (CD41-FcγR+) for both wild type and *Aebp2*$^{-/-}$ engrafts. (C) The frequencies of the Lin^{-}c-Kit^{+}Sca-1^{-} population were compared between indicated genotypes. (D) The ratios of CD45.2+ donor versus CD45.1/2 competitor cells for individual myeloid progenitor populations were compared between indicated genotypes. Graphs represent data from three independent experiments. Statistics were calculated by student T-test. Columns show mean value and error bars represent standard deviation (SD). **** $p < 0.0001$, *** $p < 0.001$, ** $p < 0.01$ and * $p < 0.05$

5.7.4 Competitive advantage in the absence of AEBP2 affected haematopoietic cells in the periphery

As shown in previous subchapters, the lack of AEBP2 had a broad effect on the proliferative ability in early haematopoiesis and thymocyte development stages. To investigate whether the terminally differentiated cells in the periphery had the similar phenotype, I then investigated the T and B cells from LN, as well as the granulocytes and macrophages from spleen in the recipients. T cells (TCRβ^{+}) and B cells (B220^{+}) were gated from total living lymphocytes and checked for the ratio of donor versus competitor, respectively (Figure 5.15A). The result showed that both lineages had a significantly higher ratio of donor versus competitor in recipients engrafted with *Aebp2*$^{-/-}$ cells compared to wild type (Figure 5.15B). This indicated that the terminally differentiated T and B cells still retained the competitive advantage.

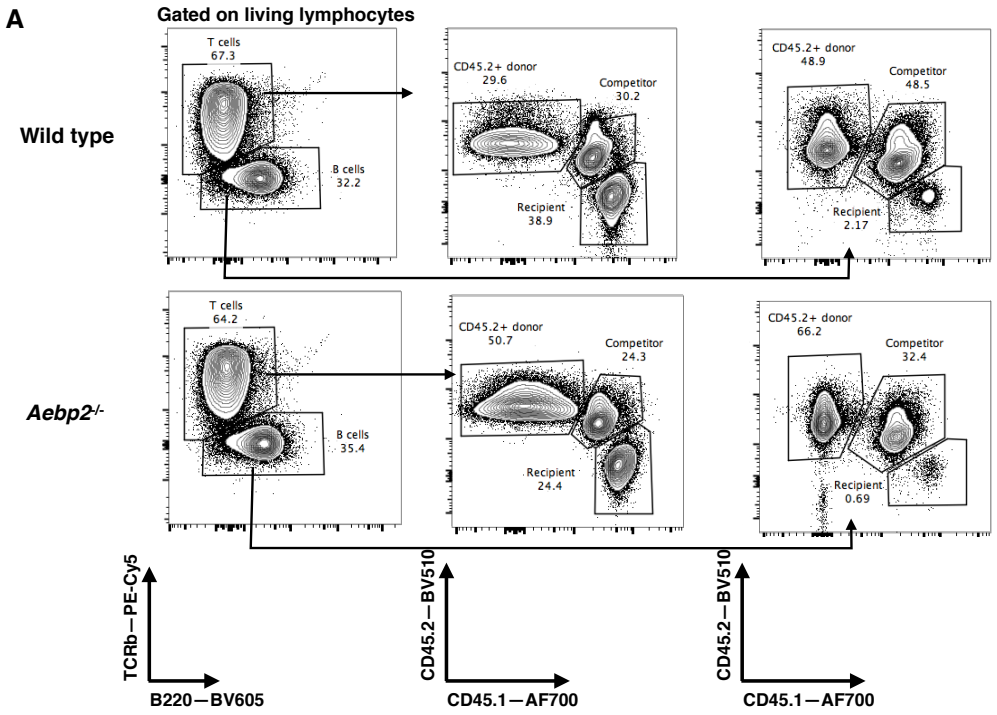

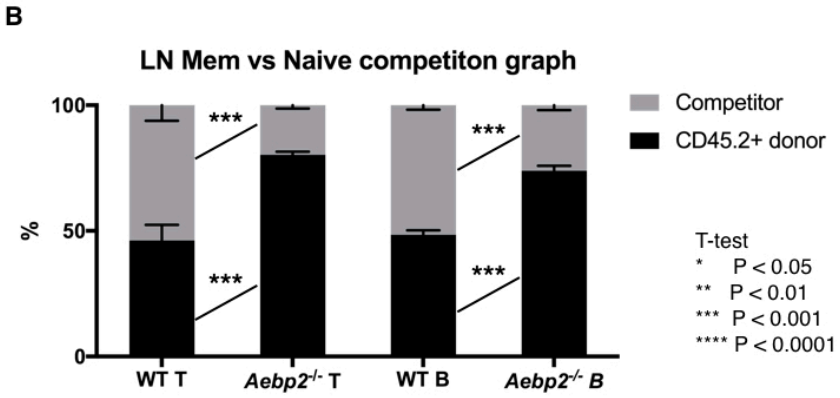

Figure 5.15: Growth advantage in the absence of AEBP2 affected lymphoid cells in the LN. (A) Representative FACS plots showing the gating strategy of T and B cells for their CD45.1 vs CD45.2 expression for both wild type and *Aebp2*$^{-/-}$ engrafts. (B) The ratios of CD45.2+ donor versus CD45.1/2 competitor cells for T as well as B cells were compared between indicated genotypes. Graphs represent data from three independent experiments. Statistics were calculated by student T-test. Columns show mean value and error bars represent standard deviation (SD). **** $p < 0.0001$, *** $p < 0.001$, ** $p < 0.01$ and * $p < 0.05$

On the other hand, granulocytes and macrophages in the spleen were characterized by their expression of Gr-1 and CD11c, respectively (Figure 5.16A). Although the relative frequencies of granulocytes and macrophages were not changed in the spleen (Figure 5.16B), both lineages showed a similar competitive advantage (Figure 5.16 C and D). Taken together, the investigation of peripheral haematopoietic cells showed that both myeloid and lymphoid cells had an increased growth ability when lacking AEBP2 expression, which started from the HSPC stage in the bone marrow.

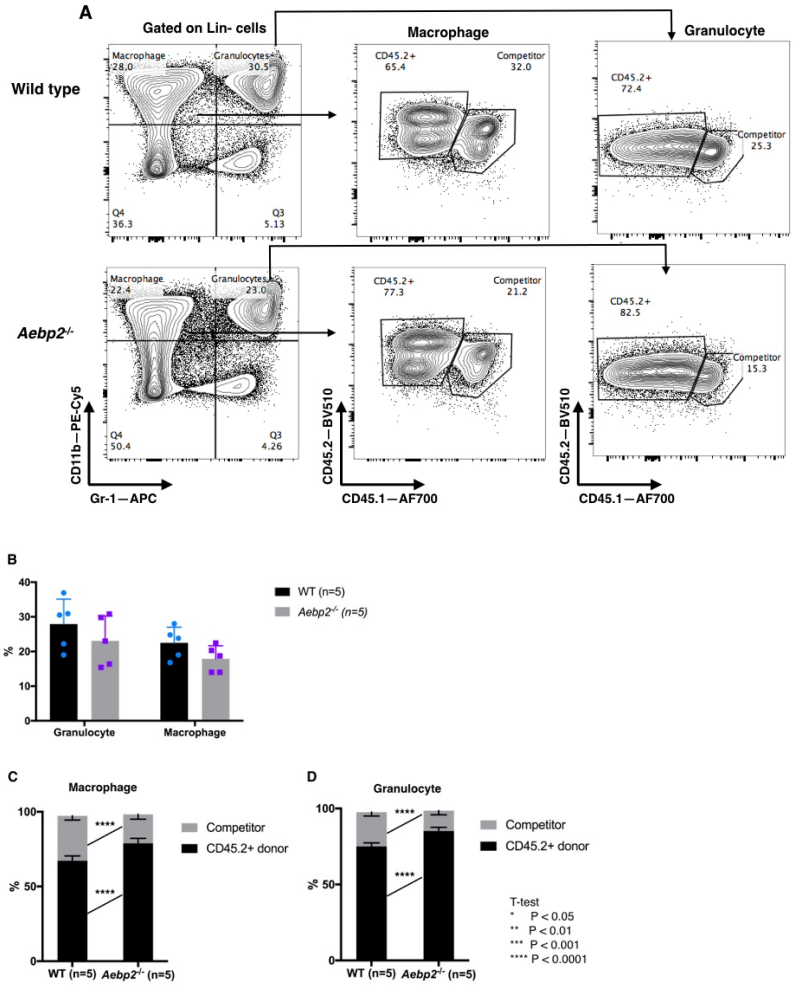

Figure 5.16: Growth advantage in the absence of AEBP2 affected myeloid cells in the spleen.

(A) Representative FACS plots showing the gating strategy of granulocytes and macrophages for their CD45.1 vs CD45.2 expression for both wild type and *Aebp2*$^{-/-}$ engrafts. (B) The frequencies

of granulocytes as well as macrophages were compared between indicated phenotypes. (C) The ratios of CD45.2+ donor versus CD45.1/2 competitor cells for granulocytes as well as macrophages were compared between indicated genotypes. Graphs represent data from two independent experiments. Statistics were calculated by student T-test. Columns show mean value and error bars represent standard deviation (SD). Each dot in bar graph represents one biological sample. **** $p < 0.0001$, *** $p < 0.001$, ** $p < 0.01$ and * $p < 0.05$

5.7.5 Competitive advantage of long-term HSCs in the absence of AEBP2

It is commonly accepted that the stable engraftment at 16-week post-transplantation is the minimal standard for determining the self-renewal ability of long-term HSCs. I next examined whether lack of AEBP2 affected long-term HSCs in terms of their repopulating ability, and if so, whether this phenotype would be propagated upon a secondary recipient. To address these questions, a serial transplantation experiment was conducted: 2.5 million CD45.2+ (donor) FL cells from either wild type or *Aebp2*$^{-/-}$ E15.5 embryos were mixed with the same amount of CD45.1/2 (competitor) wild type FL cells and injected intravenously into lethally irradiated CD45.1+ recipient. 16 weeks post-transplantation, 1000 donor-derived bone marrow HSCs sorted by flow cytometry from each primary recipient, and 1000 CD45.1/2 bone marrow HSCs from wild type mice, together with 200,000 CD45.1+ unfractionated bone marrow cells as supporting cells, were injected intravenously into lethally irradiated CD45.1+ secondary recipients. Another 16 weeks later, the ratio of donor- versus competitor-derived cells in the bone marrow of secondary recipients were examined. Gating strategies of HSC and MPP2-4 populations in primary recipients and secondary recipients were shown in Figure 5.17A and C. The ratios of donor-to-competitor cells in all four populations were significantly increased in recipients engrafted with *Aebp2*$^{-/-}$ cells compared to the wild type counterpart in primary recipients

(Figure 5.17B). This indicated that the *Aebp2*$^{-/-}$ long-term HSCs had a growth advantage over wild type HSCs. In secondary recipients, HSC and MPP3 populations retained the advantage (Figure 5.17D). This suggested that the *Aebp2*$^{-/-}$ HSCs taken from the primary recipients did not exhaust in their growth ability and continued to outcompete competitors in the secondary recipients. However, both wild type and *Aebp2*$^{-/-}$ donor cells gave rise to comparable amount of MPP2 cells to CD45.1/2 competitors. As only 100 cells were acquired on average from MPP2 population of each recipient mouse whereas 300-500 cells were acquired from other populations, it might not be accurate to calculate the ratio of donor- versus competitor-derived MPP2. There seemed to be a trend of increase in donor-to-competitor ratio in MPP4 population, however probably due to the large variance in each experimental group, the increase was not statistically significant (Figure 5.17D).

Taken together, the serial transplantation experiment showed that long-term HSCs gained a competitive advantage in the absence of AEBP2 and this enhanced repopulating ability could be stably propagated upon secondary transplantation.

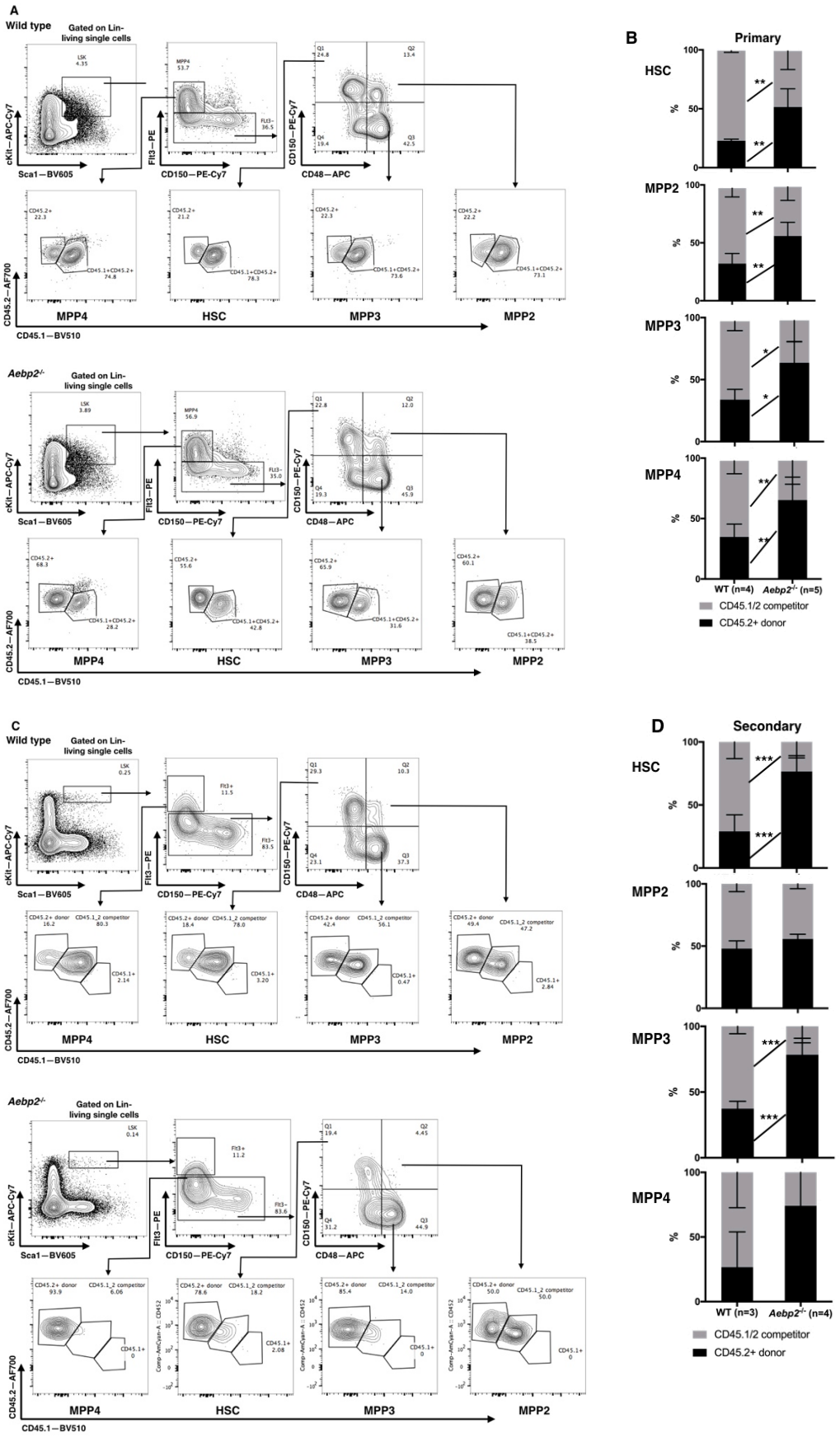
A
Wild type
Gated on Lin- living single cells
Aebp2-/-
cKit—APC-Cy7
Sca1—BV605
Flt3—PE
CD150—PE-Cy7
CD48—APC
CD45.2—AF700
CD45.1—BV510
MPP4
HSC
MPP3
MPP2
B
Primary
HSC
MPP2
MPP3
MPP4
WT (n=4)
Aebp2-/- (n=5)
CD45.1/2 competitor
CD45.2+ donor
C
D
Secondary
WT (n=3)
Aebp2-/- (n=4)

Figure 5.17: Growth advantage affected long term HSCs in the absence of AEBP2.

(A) Representative FACS plots showing the gating strategy for HSC ($CD150^+CD48^-Flt3^-$), MPP2 ($CD150^+CD48^+Flt3^-$), MPP3 ($CD150^-CD48^+Flt3^-$) and MPP4 ($CD150^-CD48^+Flt3^+$) subpopulations from $Lin^-Sca\text{-}1^+c\text{-}Kit^+$ (LSK) cells for both wild type and *Aebp2*$^{-/-}$ engrafts in primary transplanted recipient 16 weeks post-transplantation. $CD45.2^+$ and CD45.1/2 populations were stained in each HSPC populations. (B) The ratios of CD45.2+ donor versus CD45.1/2 competitor cells for individual HSPC populations were compared between indicated genotypes for primary transplantation. (C) Representative FACS plots showing the gating strategy for HSC and MPP2-4 populations for both wild type and *Aebp2*$^{-/-}$ engrafts in secondary transplanted recipient 16 weeks post-transplantation. $CD45.2^+$ and CD45.1/2 populations were stained in each HSPC populations. (D) The ratios of CD45.2+ donor versus CD45.1/2 competitor cells for individual HSPC populations were compared between indicated genotypes for secondary transplantation. Graphs represent data from one independent experiment. Statistics were calculated by student T-test. Columns show mean value and error bars represent standard deviation (SD). **** $p < 0.0001$, *** $p < 0.001$, ** $p < 0.01$ and * $p < 0.05$

5.7.6 Myeloid progenitor cells showed growth advantage after serial transplantation

MPP2 as introduced previously is a myeloid-primed progenitor population (13). Gating strategies for myeloid progenitors in secondary recipients are shown in Figure 5.18A. In all lineages analyzed here, *Aebp2*$^{-/-}$ donor cells made a significantly higher contribution to the progenitor compartment than wild type donors (Figure 5.18B). These data indicated that lack of AEBP2 had a systematic effect on all myeloid progenitor lineages in terms of their growth ability in a serial transplantation system. The reason why it was not seen in the MPP2 population might be due to that the low cell number acquired in that population did not reflect the real ratio of donor-to-competitor cells.

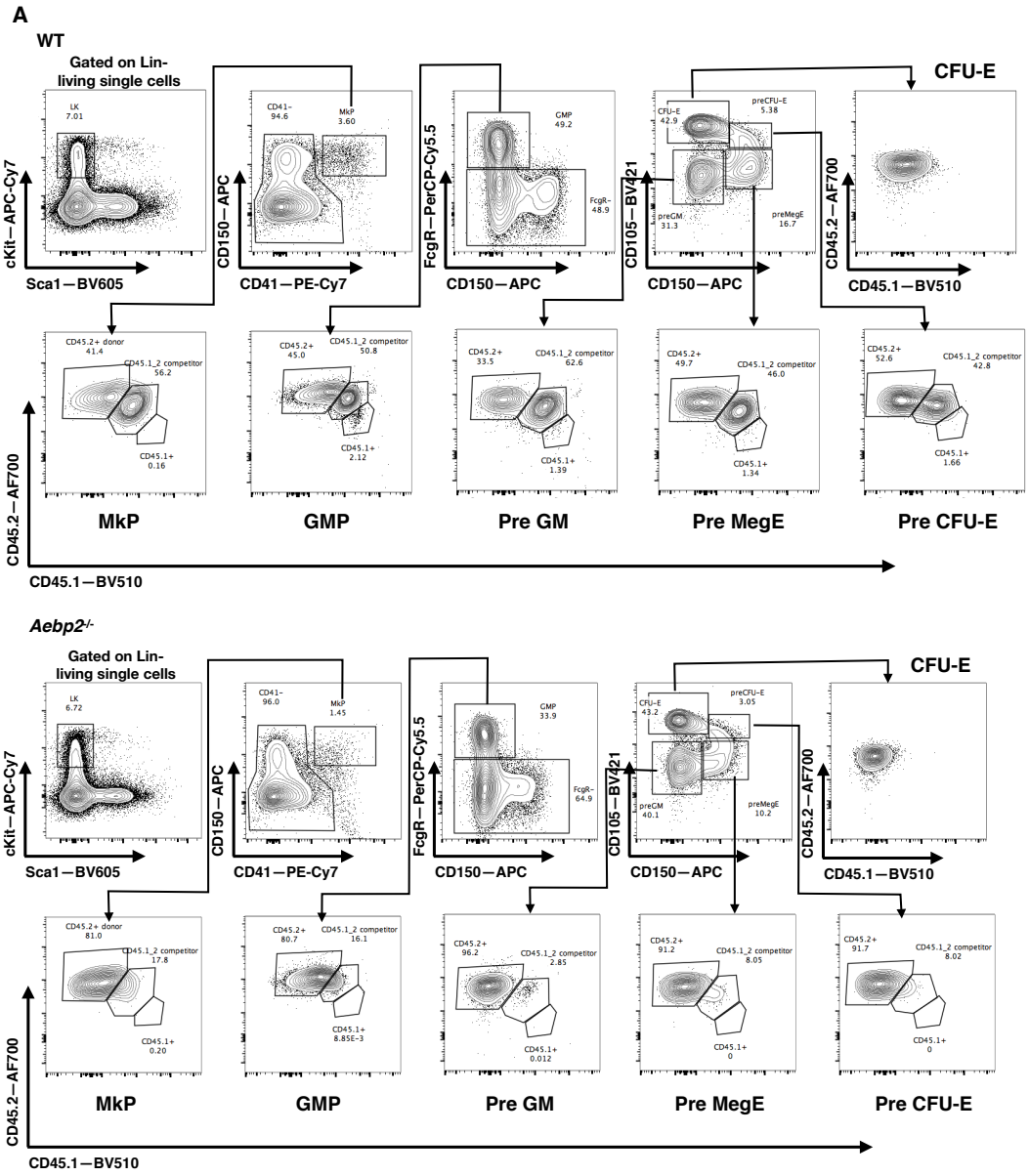
A
WT
Gated on Lin-
living single cells
CFU-E
cKit—APC-Cy7
Sca1—BV605
CD150—APC
CD41—PE-Cy7
FcgR—PerCP-Cy5.5
CD150—APC
CD105—BV421
CD150—APC
CD45.2—AF700
CD45.1—BV510
CD45.2—AF700
CD45.1—BV510
MkP
GMP
Pre GM
Pre MegE
Pre CFU-E
Aebp2-/-
Gated on Lin-
living single cells
CFU-E
cKit—APC-Cy7
Sca1—BV605
CD150—APC
CD41—PE-Cy7
FcgR—PerCP-Cy5.5
CD150—APC
CD105—BV421
CD150—APC
CD45.2—AF700
CD45.1—BV510
CD45.2—AF700
CD45.1—BV510
MkP
GMP
Pre GM
Pre MegE
Pre CFU-E

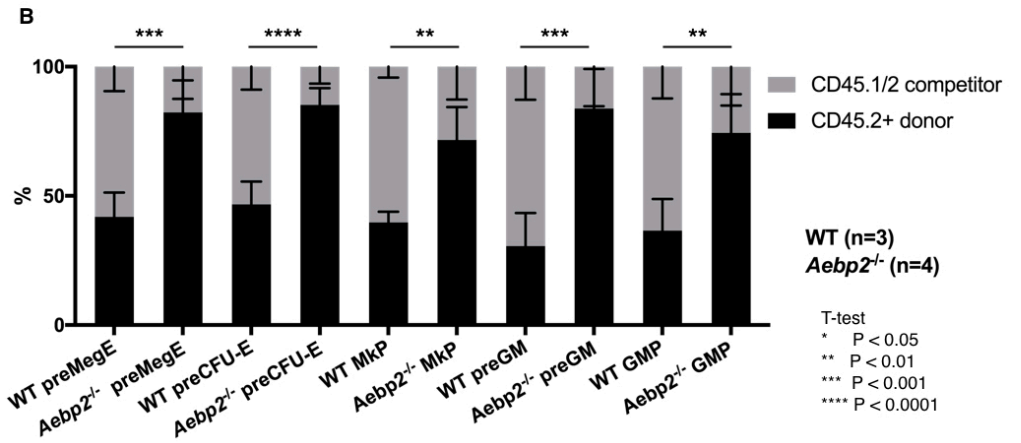
B
***
****
**
***
**
100
50
0
%
CD45.1/2 competitor
CD45.2+ donor
WT (n=3)
Aebp2-/- (n=4)
T-test
* P < 0.05
** P < 0.01
*** P < 0.001
**** P < 0.0001
WT preMegE
Aebp2-/- preMegE
WT preCFU-E
Aebp2-/- preCFU-E
WT MkP
Aebp2-/- MkP
WT preGM
Aebp2-/- preGM
WT GMP
Aebp2-/- GMP

Figure 5.18: Growth advantage in the absence of AEBP2 affected myeloid progenitor cells after secondary transplantation.

(A) Representative FACS plots showing the gating strategy of Pre MegE (CD41-FcγR-CD150+CD105-), Pre CFU-E (CD41-FcγR-CD150+CD105+), MkP (CD41+CD150+), CFU-E (CD41-FcγR-CD150-CD105+), Pre GM (FcγR-CD150-CD105-) and GMP (CD41-FcγR+) for both wild type and *Aebp2*$^{-/-}$ engrafts after secondary transplantation. (B) The ratios of CD45.2+ donor versus CD45.1/2 competitor cells for individual myeloid progenitor populations were compared between indicated genotypes. Graphs represent data from one independent experiments. Statistics were calculated by student T-test. Columns show mean value and error bars represent standard deviation (SD). **** $p < 0.0001$, *** $p < 0.001$, ** $p < 0.01$ and * $p < 0.05$

5.7.7 *Aebp2*$^{-/-}$ fetal HSCs are more proliferative compared to the wild type HSCs

As FL cells were used as donor cells in the primary transplantations, I then tried to investigate whether the *Aebp2*$^{-/-}$ FL cells are more proliferative compared to wild type ones. For this purpose, a colony assay was performed to assess the proliferation of single fetal HSCs. The same gating strategy for HSCs was applied to the FL cells (Figure 5.19A). Wild type and *Aebp2*$^{-/-}$ single HSCs were FACS sorted directly into 60-well Terasaki plate containing culture media supplemented with granulocyte-monocyte cytokines. The density of cells was evaluated after 9 days in culture. The flow cytometry analysis showed that the percentage of the LSK cells was significantly reduced in the *Aebp2*$^{-/-}$ group compared to wild type (Figure 5.19B). However, the frequency of HSC population within LSK was increased in the absence of AEBP2, which could suggest a better proliferation of HSCs in vivo (Figure 5.19C). After 9 days in culture, I saw that there were much more wells that had colonies covering 10-50% of the wells in the *Aebp2*$^{-/-}$ group compared to wild type (Figure 5.19D). This suggested that *Aebp2*$^{-/-}$ HSCs grew better compared to

wild type ones, which is in line with for the observed growth advantage in previous transplantation experiments.

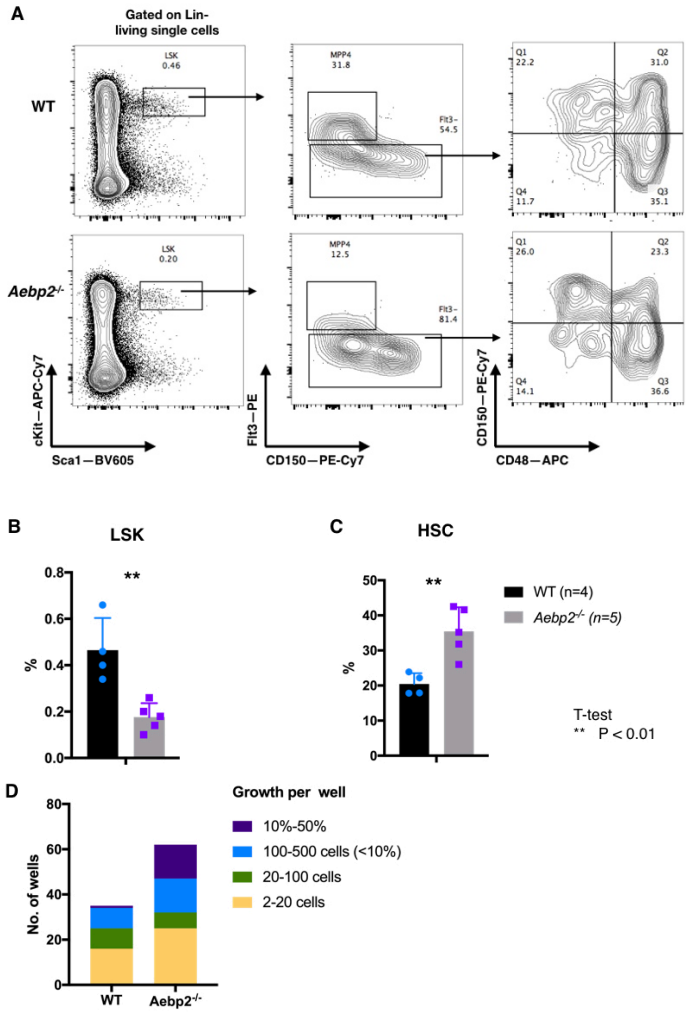

Figure 5.19: In vitro culture of single fetal HSCs.

(A) Representative FACS plots showing the gating strategy of fetal HSCs for both wild type and *Aebp2*$^{-/-}$ groups. (B) The frequencies of LSK population were compared between indicated genotypes. (C) The frequencies of HSC population were compared between indicated genotypes. (D) In vitro culture assay of single fetal HSCs from wild type and *Aebp2*$^{-/-}$ groups. Graphs showing flow cytometry analysis of the FL HSC represent data from two independent experiments. The result of in vitro culture of single fetal HSCs represent data from one independent experiment. Statistics were calculated by student T-test. Columns show mean value and error bars represent standard deviation (SD). Each dot in bar graph represents one biological sample. **** $p < 0.0001$, *** $p < 0.001$, ** $p < 0.01$ and * $p < 0.05$

5.7.8 The engraftment advantage of *Aebp2*$^{-/-}$ HSCs may be caused by an early activation of the Aurora Kinase A (Aurka)

In order to determine the molecular mechanism by which the AEBP2 depletion promotes HSC self-renewal, 500 HSCs from WT and *Aebp2*$^{-/-}$ E15.5 FL tissues were sorted for bulk RNA sequencing. The bioinformatic analysis was performed by Dr. Adam Handel. Among the differentially expressed genes comparing WT and *Aebp2*$^{-/-}$ groups, Aurora Kinase A (*Aurka*), a cell proliferation-related gene, was robustly up-regulated in the absence of AEBP2 (Figure 5.20).

In addition to *Aurka*, a few other genes involved in mitosis and cell cycling (i.e. *Bub1b* (209), *Nup133* (210), and *Dlgap5* (211)) were also up-regulated in *Aebp2*$^{-/-}$ HSCs (Figure 5.18). In particular, DLGAP5 is a mitotic spindle protein involved in the formation of tubulin polymers. The association of DLGAP5 with mitotic spindle can be stabilized by AURKA-mediated phosphorylation (211). Therefore, up-regulation of these genes in HSCs caused by AEBP2 deletion may be responsible for the enhanced repopulating ability observed in long-term HSCs in our experiments.

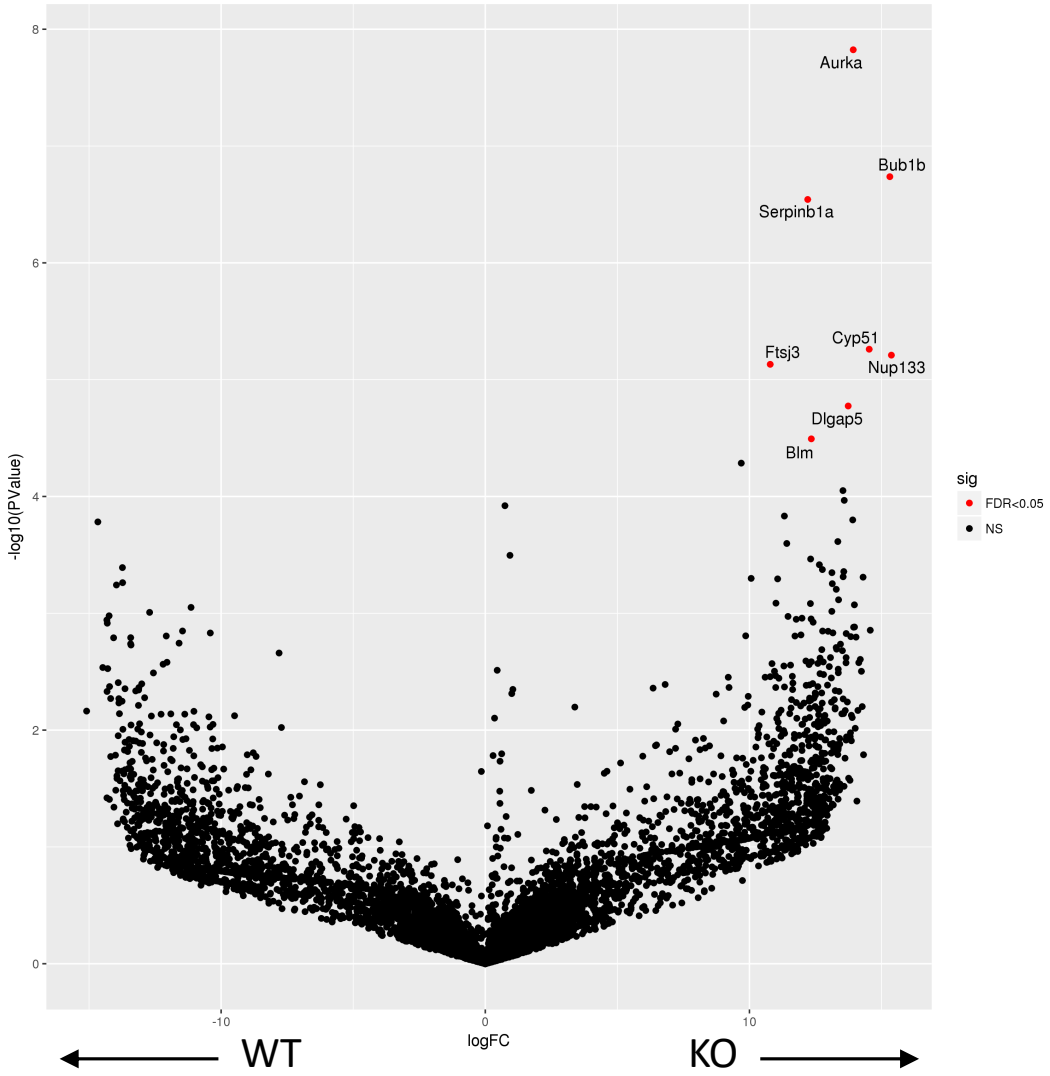

Figure 5.20: Differential gene expression analysis for HSCs

(A) Differential gene expression analysis comparing WT (n=3) and *Aebp2*$^{-/-}$ (n=3) HSCs. Significance was reported (Highlighted in red) if the false discovery rate (estimated by Benjamini Hochberg) was less than 0.05.

5.8 Discussion

PRC2-mediated H3K27me3 is responsible for gene silencing which is essential in various cell lineages to maintain their identities and regulate cell development (159). The regulatory function of PRC2 has been studied in many aspects of T cell development,

differentiation and activation (179,183,212,213). However the role of PRC2 in these processes remains elusive due to the controversial conclusions derived from loss-of-function studies of the PRC2 components. This is partially due to the multiplicity of the histone H3-independent EZH2 protein substrates (214–217). For instance, EZH2 was shown to be present in T cell cytosol, where it contributes to TCR-driven actin polymerization (179). As EZH2 is the catalytic core part of PRC2 and depletion of it led to almost complete abolishment of H3K27me3 mark, the lymphoid cell developments are blocked in very early stages (179).

JARID2, a cofactor of PRC2, is also reported to be interact with the repressive H3K9me3 methyltransferases GLP/G9a and SETDB1 (218–220). It has been shown to be up-regulated during thymocyte positive selection and CD4-Cre driven depletion of JARID2 display an increase of immature invariant natural killer T (iNKT) cells and innate-like CD8+ cells (213). This phenotype is due to that the absence of JARID2 decreases the repressive H3K9me3 level at the *Zbtb16* locus and hence increases the expression of this gene. AEBP2, as a cofactor of the PRC2 complex, has been shown to interact with multiple PRC2 components and assist the more efficient nucleosome targeting of the complex (167,175). The role of AEBP2 in gene regulation has to date not been studied in developing and mature T cells. As AEBP2 is exclusively involved in PRC2 (169), it is then a good target to study the role and molecular mechanism of PRC2 in T cell development and differentiation.

A series of haematopoietic cell transplant experiments have been conducted to demonstrate the cell autonomous defect of lacking AEBP2 in early thymocyte development (Figure 5.2C), mirroring the phenotypes in AEBP2 conventional KO E18.5 thymi (Figure 4.1 and 4.2). Unlike the EZH2-KO model which has an almost complete

block in DN to DP transition (179), a significant although reduced number of thymocytes still can progress to DP stage (Figure 5.2D), suggesting that either AEBP2 is not absolutely required for the early development of thymocytes or a compensation mechanism is triggered when AEBP2 is absent. Indeed, two subtypes of PRC2 complexes have been reported: one is defined as PRC2.2 by the association with AEBP2 and JARID2, and the other is designated as PRC2.1 by the association with PCL proteins (189). It is revealed that AEBP2 depletion may cause the formation of a hybrid PRC2 complex in which AEBP2 is replaced by PCL proteins (169). Nevertheless, the possible hybrid PRC2 complex is not as efficient as the conventional PRC2.2 as accelerated positive and negative selection processes are observed when AEBP2 is absent (Figure 5.4-5.7), which suggests that the spatio-temporal regulation of gene expression required for thymocyte development is compromised.

Mature thymocytes up-regulate $S1P_1$ expression, which is required for the thymic egress. In the absence of AEBP2, I see an increase in the frequency of CD4 and CD8 thymocytes and a reduction of the transcription level of $S1P_1$ for both CD4 and CD8 thymocytes in M2 stage (Figure 5.8C, E and F). This is initially considered as a sign of the defect in thymic egress of mature thymocytes. However, as the total thymic cellularity is slightly reduced and no sign is observed for lymphopenia in the periphery (data not shown), it seems that the thymic egress is not impaired in the absence of AEBP2. One explanation about the changed $S1P_1$ level could be that the transcription level change of a gene does not always correlate with its protein level, which is more functionally relevant. The $S1P_1$ protein level needs to be investigated in the absence of AEBP2 to stress the question whether there is a thymus egress defect. The reason why the frequency of M2 stage thymocytes is increased could be explained by the accelerated maturation of thymocytes.

Our data also reveal that the lack of AEBP2 causes a skewing of naïve to central memory CD8 T cells (Figure 5.10D) in the lymph nodes. In addition, the frequency of Treg population in the lymph nodes is reduced by approximately 50% in the absence of AEBP2 (Figure 5.11B). Furthermore, the frequency of $CD103^{+}ICOS^{+}$ subpopulation, which has a strong suppressive capacity within the Tregs (205), is also reduced in the absence of AEBP2. These data suggest that not only the development of T cells is accelerated, but their functions might also be affected in the absence of AEBP2. The proliferation of these *Aebp2*-deficient CD8 T cells as well as the suppression ability of *Aebp2*-deficient peripheral Tregs were investigated however the results seem to be contradictory between experiments (Data not shown). This could be partially due to limitation in harvesting enough donor T cells from the transplantation system to perform the functional assays as host T cells could not be cleanly depleted due to the resistance of the peripheral organs to irradiation.

Similar to thymocyte development and maturation, haematopoiesis is also a process that requires spatio-temporally restrict regulation of gene expression. The molecular role of PRC2 in haematopoiesis has been studied in detail by targeting the individual core components (e.g. EZH1/2 and EED) (221). However due to the redundancy of *Ezh* homologs and difficulties in distinguishing the canonical versus noncanonical functions of PRC2, the clear function of PRC2 in haematopoiesis remains incompletely defined (179,186,222,223).

In the study of the role of AEBP2 in thymocyte development, I notice that the lack of AEBP2 expression make the thymocytes engraft better than the wild type ones as shown in the transplant experiment with competitor cells (Figure 5.10). Subsequent analysis of the bone marrow HSPCs and myeloid lineages revealed that this growth advantage

originated from the HSCs and this feature can be propagated upon a secondary transplantation of adult bone marrow HSCs (Figure 5.17 B and D).

Transcriptome analysis of the *Aebp2*$^{-/-}$ HSCs shows the up-regulation of a few genes (i.e. *Aurka, Bub1b*, *Nup133*, and *Dlgap5*) (Figure 5.20), which are found to be involved in cell mitosis and proliferation. As a member of the family of serine/threonine protein kinases, *Aurka* plays an vital role in mitosis and meiosis (224). Previous studies have shown that *Aurka* was required for haematopoiesis as *Aurka* deletion led to pancytopenia and hypocellularity of mouse bone marrow (225). In addition, transplantation of *Aurka-/-* bone marrow cells showed a severely compromised competition ability. Aurora kinases were found overexpressed in several tumor cell lines (226–228). In particular, overexpression of *Aurka* can promote tumorigenesis as *Aurka* overexpressed cell lines formed tumors after being injected into nude mice (226,227,229). Recent studies also showed that *Aurka* is a direct target of MAPK pathway which is important for cell proliferation (230,231). All these evidences indicate that the up-regulation of *Aurka* may force cells into a faster proliferation state. Although the up-regulation of these genes at transcript level and protein level need to be validated by other methods (i.e. qRT-PCR and Western blot), it is likely that this gene is the molecular reasons for the growth advantage in *Aebp2*$^{-/-}$ HSPCs.

Chapter 6. Conclusions and Future works

The work presented in this thesis focused on the investigation of the role of AEBP2 in thymic development and maturation as well as haematopoiesis. This was addressed by studying the AEBP2 constitutively KO mouse model and two transplantation systems, i.e. thymic lobe transplant and haematopoietic cell transplant. The aim of these mouse models was to cause changes in the PRC2-AEBP2 mediated H3K27me3 landscape in different cell lineages which then could be phenotypically and functionally studied.

6.1 The role of AEBP2 in TEC development and function

6.1.1 Conclusions

The function of AEBP2 in the TEC development and maturation including effects on PGE was investigated with a loss-of-function study of AEBP2. Our data demonstrate that lacking AEBP2 expression increases the mTEC frequency and causes an advanced mTEC structure at E18.5 stage, which seems to be an accelerated maturation (see Chapter 4.2). This finding indicates the role of AEBP2 as a negative regulator for stepwise tissue development.

Bulk RNA-seq analysis for E18.5 cTEC and mTEC populations shows that gene transcription is changed in two different directions when AEBP2 is absent: more protein coding genes are up-regulated in cTECs, which is consistent with AEBP2's normal repressive role on gene expression, whereas more protein coding genes are down-regulated in mTECs suggesting that AEBP2 facilitates gene expression in mTECs (see Chapter 4.3).

Gene ontogeny pathway analysis highlights the up-regulation of several tissue development processes in cTECs which could explain the reduction of cTECs and the

subsequent increase of mTECs, as mTECs develop from cTECs. On the other hand, close to 50% of the AEBP2 up-regulated protein coding genes are demonstrated to be TRGs and significantly overlap with both AIRE- and non-AIRE- induced TRGs. These data strongly indicate that AEBP2 is required for the PGE in mTECs.

Taken together, AEBP2 has been shown to be involved in both the TEC development and induction of PGE processes with different mechanisms.

6.1.2 Future work

Due to the limited TEC numbers in embryonic thymi it is very challenging to investigate the histone landscape changes for the AEBP2 up-regulated TRGs by normal assays, such as ChIP. Recently a new technique called CUT&RUN or Chromatin ImmunoCleavage sequencing (CHIC-seq) was developed to study the in situ genome-wide histone landscape profiling with high signal-to-noise ratio for low cell numbers (even at single cell level) (232). At the moment I am trying to optimize this new technique for the embryonic cells from my mouse model.

In parallel, a mouse model with TEC targeted loss of AEBP2 expression is currently being generated by CRISPR Cas9 technique with the help of Philip Hublitz in the our institute. The role and molecular mechanism of AEBP2 in TEC maturation and PGE in postnatal thymus can then be investigated with this mouse model.

As both AIRE and TRAs are only expressed in a fraction of $mTEC^{hi}$, population level analysis might not be adequate to reflect H3K27me3 landscape for cells expressing a certain TRA. Hence single cell level transcriptome analysis is required for this purpose. Alternatively, an $mTEC^{hi}$ population expressing a specific TRA on the cell surface can be FACS sorted followed by ChIP-seq analysis for H3K27me3 profiling.

In addition, as AEBP2 has been shown to be important for PGE, mice with a TEC-targeted AEBP2-deletion will be aged and monitored for signs of autoreactivity and autoimmunity. For this purpose, I will investigate the serum of mice for the presence of autoantibodies and screen typical organs of autoimmunity for T cell infiltration (e.g. salivary glands, thyroid, liver, stomach, pancreas) and analyze the T cell antigen receptor repertoire using next generation sequencing to detail V-J-D-usage and the composition of the CDR3 region at single cell level.

6.2 The role of AEBP2 in haematopoiesis and thymocyte development

6.2.1 Conclusions

The role of AEBP2 in thymocyte development was initially investigated with a constitutive knockout mouse model, which was perinatally lethal. My results show that the absence of AEBP2 has a limited effect in early thymocyte development and most of the DN thymocytes still manage to develop to DP thymocytes in E18.5 thymi (see Chapter 4.1). These results indicate that loss of AEBP2 does not abolish the PRC2 function completely, which is the case that has been reported from the studies of PRC2 core components (179,221). Indeed, fetal haematopoietic cell transplant experiments demonstrate that the overall development of *Aebp2*$^{-/-}$ T cells is not severely impaired (see Figure 5.4B).

A closer phenotypical investigation of both the positive and negative selections of thymocytes shows that both processes are accelerated or enhanced in the absence of AEBP2 (see Figure 5.4-5.7). This could be due to the early activation of regulatory molecules required for each process, as PRC2-AEBP2 plays a role in gene repression. This is reflected by the fact that the frequency of total αβ T cells is increased in the

absence of AEBP2, probably due to the more efficient thymocyte maturation. In addition, the analysis also reveals that lack of AEBP2 expression causes a reduction in the frequency of Tregs by approximately 50% as well as a naïve to memory skew in CD8 T cells in the periphery, indicating that AEBP2 has an additional role in the regulation of mature T cell phenotypes. Functional assays such as in vitro Treg suppression assay and CD8 proliferation assays are currently under optimization in order to address these issues. By including competitor cells into the transplant experiment I see that the absence of AEBP2 cause a very robust competition advantage starting from long-term HSCs and this advantage does not exhaust in a secondary recipient (see Figure 5.17D). Bulk RNA-seq analysis of the HSCs reveal that *Aurka*, a kinase involved in cell cycling and proliferation, along with a few other molecules also involved in cell mitosis are up-regulated in *Aebp2*$^{-/-}$ HSCs. This could explain why there is a robust growth advantage in *Aebp2*$^{-/-}$ haematopoietic cells. RNA sequencing was also conducted for MPP4 cells which preferentially give rise to lymphoid cells however *Aurka* and other cell cycle-related genes were not found to be up-regulated in *Aebp2*-deficient cells (Data not shown). There are two explanations for that. Firstly, the background noise of the RNA-seq is high so we may not be able to capture the differential expression of *Aurka* between wild type and *Aebp2*$^{-/-}$ MPP4 cells. Secondly, *Aurka* may have already been highly up-regulated in MPP4 cells as they need for them to proliferate robustly and AEBP2 is not required for the control of *Aurka* at this stage.

To sum up, our results indicate that AEBP2 is an important gene expression regulator that maintains normal cell development, as lack of AEBP2 affects various stages during haematopoiesis as well T cell development and maturation.

6.2.2 Future work

Although *Aurka* was found to be up-regulated in *Aebp2*$^{-/-}$ HSCs from the RNA-seq data, the changes in both transcription level and protein level need to be further validated by other methods, e.g. qRT-PCR and Western blot. Due to the fact that the HSCs are a rare cell population and the cell number is limited in transplantation system, it is very challenging to perform protein assay with the cells. The similar limitation also affects the functional studies of *Aebp2*$^{-/-}$ peripheral T cells as previously discussed.

On that note, we are currently generating the mouse model with haematopoietic cell targeted loss of AEBP2 expression, this may help solve the cell number issues and provide more direct evidences about the effect of AEBP2 in haematopoiesis and T cell development.

Reference

1. Laurenti E, Göttgens B. From haematopoietic stem cells to complex differentiation landscapes. Nature. 2018;553(7689):418–26.
2. Jacobson LO, Simmons EL, Marks EK, Eldredge JH. Recovery from radiation injury. Science (80-). 1951;113(2940):510–1.
3. Notta F, Doulatov S, Laurenti E, Poeppl A, Jurisica I, Dick JE. Isolation of single human hematopoietic stem cells capable of long-term multilineage engraftment. Science (80-). 2011;333(6039):218–21.
4. Oguro H, Ding L, Morrison SJ. SLAM family markers resolve functionally distinct subpopulations of hematopoietic stem cells and multipotent progenitors. Cell Stem Cell. 2013;13(1):102–16.
5. Benveniste P, Frelin C, Janmohamed S, Barbara M, Herrington R, Hyam D, et al. Intermediate-Term Hematopoietic Stem Cells with Extended but Time-Limited Reconstitution Potential. Cell Stem Cell. 2010;6(1):48–58.
6. Dykstra B, Kent D, Bowie M, McCaffrey L, Hamilton M, Lyons K, et al. Long-Term Propagation of Distinct Hematopoietic Differentiation Programs In Vivo. Cell Stem Cell. 2007;1(2):218–29.
7. Sanjuan-Pla A, Macaulay IC, Jensen CT, Woll PS, Luis TC, Mead A, et al. Platelet-biased stem cells reside at the apex of the haematopoietic stem-cell hierarchy. Nature. 2013;502(7470):232–6.
8. Yamamoto R, Morita Y, Ooehara J, Hamanaka S, Onodera M, Rudolph KL, et al. Clonal analysis unveils self-renewing lineage-restricted progenitors generated directly from hematopoietic stem cells. Cell. 2013;154(5):1112–26.
9. Müller-Sieburg CE, Cho RH, Thoman M, Adkins B, Sieburg HB. Deterministic regulation of hematopoietic stem cell self-renewal and differentiation. Blood. 2002;100(4):1302–9.
10. Yu VWC, Yusuf RZ, Oki T, Wu J, Saez B, Wang X, et al. Epigenetic Memory Underlies Cell-Autonomous Heterogeneous Behavior of Hematopoietic Stem Cells. Cell. 2016;167(5):1310-1322.e17.
11. Challen GA, Boles NC, Chambers SM, Goodell MA. Distinct Hematopoietic Stem Cell Subtypes Are Differentially Regulated by TGF-β1. Cell Stem Cell. 2010;6(3):265–78.
12. Carrelha J, Meng Y, Kettyle LM, Luis TC, Norfo R, Alcolea V, et al. Hierarchically related lineage-restricted fates of multipotent haematopoietic stem cells. Nature. 2018;554(7690):106–11.
13. Pietras EM, Reynaud D, Kang YA, Carlin D, Calero-Nieto FJ, Leavitt AD, et al. Functionally Distinct Subsets of Lineage-Biased Multipotent Progenitors Control Blood Production in Normal and Regenerative Conditions. Cell Stem Cell. 2015;17(1):35–46.
14. Cabezas-Wallscheid N, Klimmeck D, Hansson J, Lipka DB, Reyes A, Wang Q, et al. Identification of regulatory networks in HSCs and their immediate progeny via integrated proteome, transcriptome, and DNA methylome analysis. Cell Stem Cell. 2014;15(4):507–22.
15. Dakic A, Metcalf D, Di Rago L, Mifsud S, Wu L, Nutt SL. PU.1 regulates the commitment of adult hematopoietic progenitors and restricts granulopoiesis. J Exp Med. 2005;201(9):1487–502.
16. Iwasaki H, Mizuno SI, Wells RA, Cantor AB, Watanabe S, Akashi K. GATA-1 converts lymphoid and myelomonocytic progenitors into the

megakaryocyte/erythrocyte lineages. Immunity. 2003;19(3):451–62.
17. Laiosa C V., Stadtfeld M, Graf T. Determinants of Lymphoid-Myeloid Lineage Diversification. Annu Rev Immunol. 2006;24(1):705–38.
18. Rosenbauer F, Owens BM, Yu L, Tumang JR, Steidl U, Kutok JL, et al. Lymphoid cell growth and transformation are suppressed by a key regulatory element of the gene encoding PU.1. Nat Genet. 2006;38(1):27–37.
19. Iwasaki-Arai J, Iwasaki H, Miyamoto T, Watanabe S, Akashi K. Enforced granulocyte/macrophage colony-stimulating factor signals do not support lymphopoiesis, but instruct lymphoid to myelomonocytic lineage conversion. J Exp Med. 2003;197(10):1311–22.
20. Kondo M, Scherer DC, Miyamoto T, King AG, Akashi K, Sugamura K, et al. Cell-fate conversion of lymphoid-committed progenitors by instructive actions of cytokines. Nature. 2000;407(6802):383–6.
21. King AG, Kondo M, Scherer DC, Weissman IL. Lineage infidelity in myeloid cells with TCR gene rearrangement: A latent developmental potential of proT cells revealed by ectopic cytokine receptor signaling. Proc Natl Acad Sci U S A. 2002;99(7):4508–13.
22. Cumano A, Godin I. Ontogeny of the Hematopoietic System. Annu Rev Immunol. 2007;25(1):745–85.
23. James Palis MCY. Yolk-sac hematopoiesis The first blood cells of mouse and man. Exp Hematol. 2001;29:927–36.
24. Wong PM, Chung SW, Eaves CJ, Chui DH. Ontogeny of the mouse hemopoietic system. Prog Clin Biol Res. 1985;193:17–28.
25. Charbord P, Tavian M, Coulombel L, Luton D, San Clemente H, Humeau L, et al. Early ontogeny of the human hematopoietic system. C R Seances Soc Biol Fil. 1995;189(4):601–9.
26. Müller AM, Medvinsky A, Strouboulis J, Grosveld F, Dzierzakt E. Development of hematopoietic stem cell activity in the mouse embryo. Immunity. 1994;1(4):291–301.
27. Medvinsky A, Dzierzak E. Definitive hematopoiesis is autonomously initiated by the AGM region. Cell. 1996;86(6):897–906.
28. de Bruijn MFTR. Definitive hematopoietic stem cells first develop within the major arterial regions of the mouse embryo. EMBO J. 2000;19(11):2465–74.
29. Ivanovs A, Rybtsov S, Welch L, Anderson RA, Turner ML, Medvinsky A. Highly potent human hematopoietic stem cells first emerge in the intraembryonic aorta-gonad-mesonephros region. J Exp Med. 2011;208(12):2417–27.
30. Gekas C, Dieterlen-Lièvre F, Orkin SH, Mikkola HKA. The placenta is a niche for hematopoietic stem cells. Dev Cell. 2005;8(3):365–75.
31. Kumaravelu P, Hook L, Morrison AM, Ure J, Zhao S, Zuyev S, et al. Quantitative developmental anatomy of definite haematopoietic stem cells/long-term repopulating units (HSC/RUs): Role of the aorta-gonad-mesonephros (AGM) region and the yolk sac in colonisation of the mouse embryonic liver. Development. 2002;129(21):4891–9.
32. Roger A. Fleischman R.Philip Custer BM. Totipotent hematopoietic stem cells: Normal self-renewal and differentiation after transplantation between mouse fetuses. Cell. 1982;30:351–9.
33. Mikkola HKA, Orkin SH. The journey of developing hematopoietic stem cells. Development. 2006;133(19):3733–44.

34. Inra CN, Zhou BO, Acar M, Murphy MM, Richardson J, Zhao Z, et al. A perisinusoidal niche for extramedullary haematopoiesis in the spleen. Nature. 2015;527(7579):466–71.
35. Lefrançais E, Ortiz-Muñoz G, Caudrillier A, Mallavia B, Liu F, Sayah DM, et al. The lung is a site of platelet biogenesis and a reservoir for haematopoietic progenitors. Nature. 2017;544(7648):105–9.
36. Becker AJ, Mcculloch EA, Siminovitch L, Till JE. The Effect of Differing Demands for Blood Cell Production on DNA Synthesis by Hemopoietic Colony-Forming Cells of Mice. Blood. 1965;26(3):296–308.
37. Schofield R. a Comparative Study of the Repopulating Potential of Grafts From Various Haemopoietic Sources: Cfu Repopulation. Cell Prolif. 1970;3(2):119–30.
38. Micklem HS, Ford CE, Evans EP, Ogden DA, Papworth DS. Competitive in vivo proliferation of foetal and adult haematopoietic cells in lethally irradiated mice. J Cell Physiol. 1972;79(2):293–8.
39. Shivdasanl RA, Mayer EL, Orkin SH. Absence of blood formation in mice lacking the T-cell leukaemia oncoprotein tal-1/SCL. Nature. 1995;373(6513):432–4.
40. Robb L, Lyons I, Li R, Hartley L, Köntgen F, Harvey RP, et al. Absence of yolk sac hematopoiesis from mice with a targeted disruption of the scl gene. Proc Natl Acad Sci U S A. 1995;92(15):7075–9.
41. Benz C, Copley MR, Kent DG, Wohrer S, Cortes A, Aghaeepour N, et al. Hematopoietic stem cell subtypes expand differentially during development and display distinct lymphopoietic programs. Cell Stem Cell. 2012;10(3):273–83.
42. Morrison SJ, Hemmati HD, Wandycz AM, Weissman IL. The purification and characterization of fetal liver hematopoietic stem cells. Proc Natl Acad Sci U S A. 1995;92(22):10302–6.
43. Rebel VI, Miller CL, Eaves CJ, Lansdorp PM. The repopulation potential of fetal liver hematopoietic stem cells in mice exceeds that of their adult bone marrow counterparts. Blood. 1996;87(8):3500–7.
44. Rebel VI, Miller CL, Thornbury GR, Dragowska WH, Eaves CJ, Lansdorp PM. A comparison of long-term repopulating hematopoietic stem cells in fetal liver and adult bone marrow from the mouse. Exp Hematol. 1996;24(5):638–48.
45. Fleming WH, Alpern EJ, Uchida N, Ikuta K, Spangrude GJ, Weissman IL. Functional heterogeneity is associated with the cell cycle status of murine hematopoietic stem cells. J Cell Biol. 1993;122(4):897–902.
46. Bowie MB, McKnight KD, Kent DG, McCaffrey L, Hoodless PA, Eaves CJ. Hematopoietic stem cells proliferate until after birth and show a reversible phase-specific engraftment defect. J Clin Invest. 2006;116(10):2808–16.
47. Bowie MB, Kent DG, Dykstra B, McKnight KD, McCaffrey L, Hoodless PA, et al. Identification of a new intrinsically timed developmental checkpoint that reprograms key hematopoietic stem cell properties. Proc Natl Acad Sci U S A. 2007;104(14):5878–82.
48. Hayakawa K, Hardy RR, Herzenberg LA, Herzenberg LA. Progenitors for Ly-1 b cells are distinct from progenitors for other b cells. J Exp Med. 1985;161(6):1554–68.
49. Pang DJ, Neves JF, Sumaria N, Pennington DJ. Understanding the complexity of γδ T-cell subsets in mouse and human. Vol. 136, Immunology. 2012. p. 283–90.

50. Havran WL, Allison JP. Developmentally ordered appearance of thymocytes expressing different T-cell antigen receptors. Nature. 1988;335(6189):443–5.
51. Ikuta K, Kina T, MacNeil I, Uchida N, Peault B, Chien Y hsiu, et al. A developmental switch in thymic lymphocyte maturation potential occurs at the level of hematopoietic stem cells. Cell. 1990;62(5):863–74.
52. McKinney-Freeman S, Cahan P, Li H, Lacadie SA, Huang HT, Curran M, et al. The transcriptional landscape of hematopoietic stem cell ontogeny. Cell Stem Cell. 2012;11(5):701–14.
53. Kiel MJ, Iwashita T, Yilmaz ÖH, Morrison SJ. Spatial differences in hematopoiesis but not in stem cells indicate a lack of regional patterning in definitive hematopoietic stem cells. Dev Biol. 2005;283(1):29–39.
54. Copley MR, Babovic S, Benz C, Knapp DJHF, Beer PA, Kent DG, et al. The Lin28b-let-7-Hmga2 axis determines the higher self-renewal potential of fetal haematopoietic stem cells. Nat Cell Biol. 2013;15(8):916–25.
55. Yuan J, Nguyen CK, Liu X, Kanellopoulou C, Muljo SA. Lin28b reprograms adult bone marrow hematopoietic progenitors to mediate fetal-like lymphopoiesis. Science (80-). 2012;335(6073):1195–200.
56. Boehm T, Swann JB. Origin and Evolution of Adaptive Immunity. Annu Rev Anim Biosci. 2014;2(1):259–83.
57. Boehm T, Hess I, Swann JB. Evolution of lymphoid tissues. Trends Immunol. 2012;33(6):315–21.
58. Busslinger M. Transcriptional Control of Early B Cell Development. Annu Rev Immunol. 2004;22(1):55–79.
59. Hozumi K, Mailhos C, Negishi N, Hirano KI, Yahata T, Ando K, et al. Delta-like 4 is indispensable in thymic environment specific for T cell development. J Exp Med. 2008;205(11):2507–13.
60. Koch U, Fiorini E, Benedito R, Besseyrias V, Schuster-Gossler K, Pierres M, et al. Delta-like 4 is the essential, nonredundant ligand for Notchl during thymic T cell lineage commitment. J Exp Med. 2008;205(11):2515–23.
61. Schatz DG. V(D)J recombination. Immunol Rev. 2004;200:5–11.
62. Al-Lazikani B, Lesk AM, Chothia C. Standard conformations for the canonical structures of immunoglobulins. J Mol Biol. 1997;273(4):927–48.
63. Clambey ET, Davenport B, Kappler JW, Marrack P, Homann D. Molecules in medicine mini review: The αβ T cell receptor. J Mol Med. 2014;92(7):735–41.
64. Brinkman CC, Rouhani SJ, Srinivasan N, Engelhard VH. Correction: Peripheral Tissue Homing Receptors Enable T Cell Entry into Lymph Nodes and Affect the Anatomical Distribution of Memory Cells. J Immunol. 2013;191(12):6292–6292.
65. Huse M. The T-cell-receptor signalling network. J Cell Sci. 2009;122(9):1269–73.
66. Germain RN. MHC-dependent antigen processing and peptide presentation: Providing ligands for T lymphocyte activation. Cell. 1994;76(2):287–99.
67. Bluestone JA, MacKay CR, O'Shea JJ, Stockinger B. The functional plasticity of T cell subsets. Nat Rev Immunol. 2009;9(11):811–6.
68. Mosmann TR, Cherwinski H, Bond MW, Giedlin MA, Coffman RL. Two types of murine helper T cell clone. I. Definition according to profiles of lymphokine activities and secreted proteins. J Immunol [Internet]. 1986;136(7):2348–57. Available from: http://www.ncbi.nlm.nih.gov/pubmed/2419430
69. Ivanov II, McKenzie BS, Zhou L, Tadokoro CE, Lepelley A, Lafaille JJ, et al.

The Orphan Nuclear Receptor RORγt Directs the Differentiation Program of Proinflammatory IL-17+ T Helper Cells. Cell. 2006;126(6):1121–33.
70. Bouchery T, Kyle R, Ronchese F, Le Gros G. The differentiation of CD4+ T-helper cell subsets in the context of helminth parasite infection. Vol. 5, Frontiers in Immunology. 2014.
71. Bending D, De La Peña H, Veldhoen M, Phillips JM, Uyttenhove C, Stockinger B, et al. Highly purified Th17 cells from BDC2.5NOD mice convert into Th1-like cells in NOD/SCID recipient mice. J Clin Invest. 2009;119(3):565–72.
72. Lee YK, Turner H, Maynard CL, Oliver JR, Chen D, Elson CO, et al. Late Developmental Plasticity in the T Helper 17 Lineage. Immunity. 2009;30(1):92–107.
73. Zhou L, Chong MMW, Littman DR. Plasticity of CD4+ T Cell Lineage Differentiation. Immunity. 2009;30(5):646–55.
74. Pennock ND, White JT, Cross EW, Cheney EE, Tamburini BA, Kedl RM. T cell responses: Naïve to memory and everything in between. Am J Physiol - Adv Physiol Educ. 2013;37(4):273–83.
75. Takahama Y. Journey through the thymus: Stromal guides for T-cell development and selection. Nat Rev Immunol. 2006;6(2):127–35.
76. Shores EW, Van Ewijk W, Singer A. Disorganization and restoration of thymic medullary epithelial cells in T cell receptor-negative scid mice: Evidence that receptor-bearing lymphocytes influence maturation of the thymic microenvironment. Eur J Immunol. 1991;21(7):1657–61.
77. van Ewijk Elisabeth W. Shores AS. Crosstalk in the mouse thymus. Immunol Today. 1994;15:214–7.
78. Holländer GA, Wang B, Nichogiannopoulou A, Platenburg PP, Van Ewijk W, Burakoff SJ, et al. Developmental control point in induction of thymic cortex regulated by a subpopulation of prothymocytes. Nature. 1995;373(6512):350–3.
79. Blackburn CC, Manley NR. Developing a new paradigm for thymus organogenesis. Nat Rev Immunol. 2004;4(4):278–89.
80. Manley NR, Capecchi MR. The role of Hoxa-3 in mouse thymus and thyroid development. Development. 1995;121(7):1989–2003.
81. Wallin J, Eibel H, Neubüser A, Wilting J, Koseki H, Balling R. Pax1 is expressed during development of the thymus epithelium and is required for normal T-cell maturation. Development. 1996;122(1):23–30.
82. Peters H, Neubüser A, Kratochwil K, Balling R. Pax9-deficient mice lack pharyngeal pouch derivatives and teeth and exhibit craniofacial and limb abnormalities. Genes Dev. 1998;12(17):2735–47.
83. Zou D, Silvius D, Davenport J, Grifone R, Maire P, Xu PX. Patterning of the third pharyngeal pouch into thymus/parathyroid by Six and Eya1. Dev Biol. 2006;293(2):499–512.
84. Jerome LA, Papaioannou VE. DiGeorge syndrome phenotype in mice mutant for the T-box gene, Tbx1. Nat Genet. 2001;27(3):286–91.
85. Blackburn CC, Augustine CL, Li R, Harvey RP, Malin MA, Boyd RL, et al. The nu gene acts cell-autonomously and is required for differentiation of thymic epithelial progenitors. Proc Natl Acad Sci U S A. 1996;93(12):5742–6.
86. Liu Z, Yu S, Manley NR. Gcm2 is required for the differentiation and survival of parathyroid precursor cells in the parathyroid/thymus primordia. Dev Biol. 2007;305(1):333–46.

87. Zamisch M, Moore-Scott B, Su D, Lucas PJ, Manley N, Richie ER. Ontogeny and Regulation of IL-7-Expressing Thymic Epithelial Cells. J Immunol. 2005;174(1):60–7.
88. Bleul CC, Boehm T. BMP Signaling Is Required for Normal Thymus Development. J Immunol. 2005;175(8):5213–21.
89. Gordon J, Patel SR, Mishina Y, Manley NR. Evidence for an early role for BMP4 signaling in thymus and parathyroid morphogenesis. Dev Biol. 2010;339(1):141–54.
90. Balciunaite G, Keller MP, Balciunaite E, Piali L, Zuklys S, Mathieu YD, et al. Wnt glycoproteins regulate the expression of FoxNI, the genes defective in nude mice. Nat Immunol. 2002;3(11):1102–8.
91. Heinonen KM, Vanegas JR, Brochu S, Shan J, Vainio SJ, Perreault C. Wnt4 regulates thymic cellularity through the expansion of thymic epithelial cells and early thymic progenitors. Blood. 2011;118(19):5163–73.
92. Saldaña JI, Solanki A, Lau CI, Sahni H, Ross S, Furmanski AL, et al. Sonic Hedgehog regulates thymic epithelial cell differentiation. J Autoimmun. 2016;68:86–97.
93. Jenkinson WE, Jenkinson EJ, Anderson G. Differential requirement for mesenchyme in the proliferation and maturation of thymic epithelial progenitors. J Exp Med. 2003;198(2):325–32.
94. Alves NL, Takahama Y, Ohigashi I, Ribeiro AR, Baik S, Anderson G, et al. Serial progression of cortical and medullary thymic epithelial microenvironments. Eur J Immunol. 2014;44(1):16–22.
95. Bennett AR, Farley A, Blair NF, Gordon J, Sharp L, Blackburn CC. Identification and characterization of thymic epithelial progenitor cells. Immunity. 2002;16(6):803–14.
96. Rossi SW, Jenkinson WE, Anderson G, Jenkinson EJ. Clonal analysis reveals a common progenitor for thymic cortical and medullary epithelium. Nature. 2006;441(7096):988–91.
97. Mayer CE, Žuklys S, Zhanybekova S, Ohigashi I, Teh HY, Sansom SN, et al. Dynamic spatio-temporal contribution of single β5t+ cortical epithelial precursors to the thymus medulla. Eur J Immunol. 2016;46(4):846–56.
98. Ohigashi I, Zuklys S, Sakata M, Mayer CE, Zhanybekova S, Murata S, et al. Aire-expressing thymic medullary epithelial cells originate from β5t-expressing progenitor cells. Proc Natl Acad Sci U S A. 2013;110(24):9885–90.
99. Akiyama N, Takizawa N, Miyauchi M, Yanai H, Tateishi R, Shinzawa M, et al. Identification of embryonic precursor cells that differentiate into thymic epithelial cells expressing autoimmune regulator. J Exp Med. 2016;213(8):1441–58.
100. Ohigashi I, Zuklys S, Sakata M, Mayer CE, Hamazaki Y, Minato N, et al. Adult Thymic Medullary Epithelium Is Maintained and Regenerated by Lineage-Restricted Cells Rather Than Bipotent Progenitors. Cell Rep. 2015;13(7):1432–43.
101. Ribeiro AR, Rodrigues PM, Meireles C, Di Santo JP, Alves NL. Thymocyte Selection Regulates the Homeostasis of IL-7–Expressing Thymic Cortical Epithelial Cells In Vivo. J Immunol. 2013;191(3):1200–9.
102. Baik S, Jenkinson EJ, Lane PJL, Anderson G, Jenkinson WE. Generation of both cortical and Aire+ medullary thymic epithelial compartments from CD205+

progenitors. Eur J Immunol. 2013;43(3):589–94.
103. Bleul CC, Corbeaux T, Reuter A, Fisch P, Mönting JS, Boehm T. Formation of a functional thymus initiated by a postnatal epithelial progenitor cell. Nature. 2006;441(7096):992–6.
104. Rossi SW, Kim MY, Leibbrandt A, Parnell SM, Jenkinson WE, Glanville SH, et al. RANK signals from CD4+3- inducer cells regulate development of Aire-expressing epithelial cells in the thymic medulla. J Exp Med. 2007;204(6):1267–72.
105. Hikosaka Y, Nitta T, Ohigashi I, Yano K, Ishimaru N, Hayashi Y, et al. The Cytokine RANKL Produced by Positively Selected Thymocytes Fosters Medullary Thymic Epithelial Cells that Express Autoimmune Regulator. Immunity. 2008;29(3):438–50.
106. Boehm T, Scheu S, Pfeffer K, Bleul CC. Thymic medullary epithelial cell differentiation, thymocyte emigration, and the control of autoimmunity require lympho-epithelial cross talk via LTβR. J Exp Med. 2003;198(5):757–69.
107. Gray D, Abramson J, Benoist C, Mathis D. Proliferative arrest and rapid turnover of thymic epithelial cells expressing Aire. J Exp Med. 2007;204(11):2521–8.
108. Goldfarb Y, Kadouri N, Levi B, Sela A, Herzig Y, Cohen RN, et al. HDAC3 Is a Master Regulator of mTEC Development. Cell Rep. 2016;15(3):651–65.
109. Sansom SN, Shikama-Dorn N, Zhanybekova S, Nusspaumer G, Macaulay IC, Deadman ME, et al. Population and single-cell genomics reveal the Aire dependency, relief from Polycomb silencing, and distribution of self-antigen expression in thymic epithelia. Genome Res. 2014;24(12):1918–31.
110. Danan-Gotthold M, Guyon C, Giraud M, Levanon EY, Abramson J. Extensive RNA editing and splicing increase immune self-representation diversity in medullary thymic epithelial cells. Genome Biol. 2016;17(1):219.
111. Chakravarty S, Zeng L, Zhou MM. Structure and Site-Specific Recognition of Histone H3 by the PHD Finger of Human Autoimmune Regulator. Structure. 2009;17(5):670–9.
112. Org T, Rebane A, Kisand K, Laan M, Haljasorg U, Andreson R, et al. AIRE activated tissue specific genes have histone modifications associated with inactive chromatin. Hum Mol Genet. 2009;18(24):4699–710.
113. Greer EL, Shi Y. Histone methylation: A dynamic mark in health, disease and inheritance. Nat Rev Genet. 2012;13(5):343–57.
114. Penit C, Vasseur F. Sequential events in thymocyte differentiation and thymus regeneration revealed by a combination of bromodeoxyuridine DNA labeling and antimitotic drug treatment. J Immunol. 1988;140(10):3315–23.
115. Godfrey DI, Kennedy J, Suda T, Zlotnik A. A developmental pathway involving four phenotypically and functionally distinct subsets of CD3-CD4-CD8- triple-negative adult mouse thymocytes defined by CD44 and CD25 expression. J Immunol. 1993;150(10):4244–52.
116. Robey E, Fowlkes BJ. Selective Events in T Cell Development. Annu Rev Immunol. 1994;12(1):675–705.
117. Mombaerts P, Iacomini J, Johnson RS, Herrup K, Tonegawa S, Papaioannou VE. RAG-1-deficient mice have no mature B and T lymphocytes. Cell. 1992;68(5):869–77.
118. Shinkai Y, Koyasu S, Nakayama K, Murphy K, Loh D, Reinherz E, et al. Restoration of T cell development in RAG-2-deficient mice by functional TCR

transgenes. Science (80-). 1993;259(5096):822–5.
119. Negishi I, Motoyama N, Nakayama KI, Nakayama K, Senju S, Hatakeyama S, et al. Essential role for ZAP-70 in both positive and negative selection of thymocytes. Nature. 1995;376(6539):435–8.
120. Van Oers NSC, Lowin-Kropf B, Finlay D, Connolly K, Weiss A. αβ T cell development is abolished in mice lacking both Lck and Fyn protein tyrosine kinases. Immunity. 1996;5(5):429–36.
121. Clements JL, Yang B, Ross-Barta SE, Eliason SL, Hrstka RF, Williamson RA, et al. Requirement for the leukocyte-specific adapter protein SLP-76 for normal T cell development. Science (80-). 1998;281(5375):416–9.
122. von Boehmer H, Teh HS, Kisielow P. The thymus selects the useful, neglects the useless and destroys the harmful. Immunol Today. 1989;10(2):57–61.
123. Germain RN. T-cell development and the CD4-CD8 lineage decision. Nat Rev Immunol. 2002;2(5):309–22.
124. Egerton M, Scollay R, Shortman K. Kinetics of mature T-cell development in the thymus. Proc Natl Acad Sci U S A. 1990;87(7):2579–82.
125. Goldrath AW, Bevan MJ. Selecting and maintaining a diverse T-cell repertoire. Nature. 1999;402(S6763):6–13.
126. He X, He X, Dave VP, Zhang Y, Hua X, Nicolas E, et al. The zinc finger transcription factor Th-POK regulates CD4 versus CD8 T-cell lineage commitment. Nature. 2005;433(7028):826–33.
127. Seo W, Tanaka H, Miyamoto C, Levanon D, Groner Y, Taniuchi I. Roles of VWRPY motif-mediated gene repression by Runx proteins during T-cell development. Immunol Cell Biol. 2012;90(8):827–30.
128. Taniuchi I. CD4 Helper and CD8 Cytotoxic T Cell Differentiation. Annu Rev Immunol. 2018;36(1):579–601.
129. Reichert RA, Weissman IL, Butcher EC. Phenotypic analysis of thymocytes that express homing receptors for peripheral lymph nodes. J Immunol. 1986;136(10):3521–8.
130. Bendelac A, Matzinger P, Seder RA, Paul WE, Schwartz RH. Activation events during thymic selection. J Exp Med. 1992;175(3):731–42.
131. Ramsdell F, Jenkins M, Dinh Q, Fowlkes BJ. The majority of CD4+8- thymocytes are functionally immature. J Immunol. 1991;147(6):1779–85.
132. Chaffin KE, Perlmutter RM. A pertussis toxin-sensitive process controls thymocyte emigration. Eur J Immunol. 1991;21(10):2565–73.
133. Matloubian M, Lo CG, Cinamon G, Lesneski MJ, Xu Y, Brinkmann V, et al. Lymphocyte egress from thymus and peripheral lymphoid organs is dependent on S1P receptor 1. Nature. 2004;427(6972):355–60.
134. Allende ML, Dreier JL, Mandala S, Proia RL. Expression of the Sphingosine 1-Phosphate Receptor, S1P1, on T-cells Controls Thymic Emigration. J Biol Chem. 2004;279(15):15396–401.
135. Edsall LC, Spiegel S. Enzymatic measurement of sphingosine 1-phosphate. Anal Biochem. 1999;272(1):80–6.
136. Ueno T, Hara K, Willis MS, Malin MA, Höpken UE, Gray DHD, et al. Role for CCR7 ligands in the emigration of newly generated T lymphocytes from the neonatal thymus. Immunity. 2002;16(2):205–18.
137. Lind EF, Prockop SE, Porritt HE, Petrie HT. Mapping precursor movement through the postnatal thymus reveals specific microenvironments supporting

defined stages of early lymphoid development. J Exp Med. 2001;194(2):127–34.
138. Abramson J, Anderson G. Thymic Epithelial Cells. Annu Rev Immunol. 2017;35(1):85–118.
139. Ueno T, Saito F, Gray DHD, Kuse S, Hieshima K, Nakano H, et al. CCR7 signals are essential for cortex-medulla migration of developing thymocytes. J Exp Med. 2004;200(4):493–505.
140. Hu D, Shilatifard A. Epigenetics of hematopoiesis and hematological malignancies. Vol. 30, Genes and Development. 2016. p. 2021–41.
141. Bosselut R. Control of intra-thymic αβ T cell selection and maturation by H3K27 methylation and demethylation. Vol. 10, Frontiers in Immunology. 2019.
142. McGinnis W, Krumlauf R. Homeobox genes and axial patterning. Cell. 1992;68(2):283–302.
143. Qian S, Capovilla M, Pirrotta V. The bx region enhancer, a distant cis-control element of the Drosophila Ubx gene and its regulation by hunchback and other segmentation genes. EMBO J. 1991;10(6):1415–25.
144. Zhang CC, Muller J, Hoch M, Jackle H, Bienz M. Target sequences for hunchback in a control region conferring Ultrabithorax expression boundaries. Development. 1991;113(4):1171–9.
145. Lewis EB. A gene complex controlling segmentation in Drosophila. Nature. 1978;276(5688):565–70.
146. Struhl G. A gene product required for correct initiation of segmental determination in Drosophila. Nature. 1981;293(5827):36–41.
147. Jürgens G. A group of genes controlling the spatial expression of the bithorax complex in Drosophila. Nature. 1985;316(6024):153–5.
148. Orlando V, Jane EP, Chinwalla V, Harte PJ, Paro R. Binding of Trithorax and Polycomb proteins to the bithorax complex: Dynamic changes during early Drosophila embryogenesis. EMBO J. 1998;17(17):5141–50.
149. Strutt H, Paro R. The polycomb group protein complex of Drosophila melanogaster has different compositions at different target genes. Mol Cell Biol. 1997;17(12):6773–83.
150. Mendenhall EM, Koche RP, Truong T, Zhou VW, Issac B, Chi AS, et al. GC-rich sequence elements recruit PRC2 in mammalian ES cells. PLoS Genet. 2010;6(12):1–10.
151. Chittock EC, Latwiel S, Miller TCR, Müller CW. Molecular architecture of polycomb repressive complexes. Biochem Soc Trans. 2017;45(1):193–205.
152. Cao R, Wang L, Wang H, Xia L, Erdjument-Bromage H, Tempst P, et al. Role of histone H3 lysine 27 methylation in polycomb-group silencing. Science (80-). 2002;298(5595):1039–43.
153. Cooper S, Dienstbier M, Hassan R, Schermelleh L, Sharif J, Blackledge NP, et al. Targeting Polycomb to Pericentric Heterochromatin in Embryonic Stem Cells Reveals a Role for H2AK119u1 in PRC2 Recruitment. Cell Rep. 2014;7(5):1456–70.
154. Kalb R, Latwiel S, Baymaz HI, Jansen PWTC, Müller CW, Vermeulen M, et al. Histone H2A monoubiquitination promotes histone H3 methylation in Polycomb repression. Nat Struct Mol Biol. 2014;21(6):569–71.
155. Cui K, Zang C, Roh TY, Schones DE, Childs RW, Peng W, et al. Chromatin Signatures in Multipotent Human Hematopoietic Stem Cells Indicate the Fate of Bivalent Genes during Differentiation. Cell Stem Cell. 2009;4(1):80–93.

156. Schoeftner S, Sengupta AK, Kubicek S, Mechtler K, Spahn L, Koseki H, et al. Recruitment of PRC1 function at the initiation of X inactivation independent of PRC2 and silencing. EMBO J. 2006;25(13):3110–22.
157. Pasini D, Bracken AP, Hansen JB, Capillo M, Helin K. The Polycomb Group Protein Suz12 Is Required for Embryonic Stem Cell Differentiation. Mol Cell Biol. 2007;27(10):3769–79.
158. Peters AHFM, Kubicek S, Mechtler K, O'Sullivan RJ, Derijck AAHA, Perez-Burgos L, et al. Partitioning and Plasticity of Repressive Histone Methylation States in Mammalian Chromatin. Mol Cell. 2003;12(6):1577–89.
159. Raphael Margueron DR. The Polycomb complex PRC2 and its mark in life. Nature. 2011;469:343 349.
160. Bernstein BE, Mikkelsen TS, Xie X, Kamal M, Huebert DJ, Cuff J, et al. A Bivalent Chromatin Structure Marks Key Developmental Genes in Embryonic Stem Cells. Cell. 2006;125(2):315–26.
161. Vastenhouw NL, Schier AF. Bivalent histone modifications in early embryogenesis. Curr Opin Cell Biol. 2012;24(3):374–86.
162. Margueron R, Li G, Sarma K, Blais A, Zavadil J, Woodcock CL, et al. Ezh1 and Ezh2 Maintain Repressive Chromatin through Different Mechanisms. Mol Cell. 2008;32(4):503–18.
163. Antonysamy S, Condon B, Druzina Z, Bonanno JB, Gheyi T, Zhang F, et al. Structural context of disease-associated mutations and putative mechanism of autoinhibition revealed by X-Ray crystallographic analysis of the EZH2-SET domain. PLoS One. 2013;8(12):e84147.
164. Margueron R, Justin N, Ohno K, Sharpe ML, Son J, Drury WJ, et al. Role of the polycomb protein EED in the propagation of repressive histone marks. Nature. 2009;461(7265):762–7.
165. Birve A, Sengupta AK, Beuchle D, Larsson J, Kennison JA, Rasmuson-Lestander Å, et al. Su(z)12, a novel Drosophila Polycomb group gene that is conserved in vertebrates and plants. Development. 2001;128(17):3371–9.
166. Schmitges FW, Prusty AB, Faty M, Stützer A, Lingaraju GM, Aiwazian J, et al. Histone Methylation by PRC2 Is Inhibited by Active Chromatin Marks. Mol Cell. 2011;42(3):330–41.
167. Ciferri C, Lander GC, Maiolica A, Herzog F, Aebersold R, Nogales E. Molecular architecture of human polycomb repressive complex 2. Elife. 2012;2012(1):e00005.
168. Kim H, Kang K, Kim J. AEBP2 as a potential targeting protein for Polycomb Repression Complex PRC2. Nucleic Acids Res. 2009;37(9):2940–50.
169. Grijzenhout A, Godwin J, Koseki H, Gdula MR, Szumska D, McGouran JF, et al. Functional analysis of AEBP2, a PRC2 polycomb protein, reveals a trithorax phenotype in embryonic development and in ESCs. Dev. 2016;143(15):2716–23.
170. Son J, Shen SS, Margueron R, Reinberg D. Nucleosome-binding activities within JARID2 and EZH1 regulate the function of PRC2 on chromatin. Genes Dev. 2013;27(24):2663–77.
171. He GP, Kim S, Ro HS. Cloning and characterization of a novel zinc finger transcriptional repressor. A direct role of the zinc finger motif in repression. J Biol Chem. 1999;274(21):14678–84.
172. Liu Y, Montell DJ. Jing: A downstream target of slbo required for developmental control of border cell migration. Development. 2001;128(3):321–30.

173. Sedaghat Y, Miranda WF, Sonnenfeld MJ. The jing Zn-finger transcription factor is a mediator of celllular differentiation in the Drosophila CNS midline and trachea. Development. 2002;129(11):2591–606.
174. Chen S, Jiao L, Shubbar M, Yang X, Liu X. Unique Structural Platforms of Suz12 Dictate Distinct Classes of PRC2 for Chromatin Binding. Mol Cell. 2018;69(5):840-852.e5.
175. Kasinath V, Faini M, Poepsel S, Reif D, Feng XA, Stjepanovic G, et al. Structures of human PRC2 with its cofactors AEBP2 and JARID2. Science (80-). 2018;359(6378):940–4.
176. Lee CH, Holder M, Grau D, Saldaña-Meyer R, Yu JR, Ganai RA, et al. Distinct Stimulatory Mechanisms Regulate the Catalytic Activity of Polycomb Repressive Complex 2. Mol Cell. 2018;70(3):435-448.e5.
177. Boyer LA, Plath K, Zeitlinger J, Brambrink T, Medeiros LA, Lee TI, et al. Polycomb complexes repress developmental regulators in murine embryonic stem cells. Nature. 2006;441(7091):349–53.
178. Carpenter AC, Bosselut R. Decision checkpoints in the thymus. Nat Immunol. 2010;11(8):666–73.
179. Su IH, Dobenecker MW, Dickinson E, Oser M, Basavaraj A, Marqueron R, et al. Polycomb group protein Ezh2 controls actin polymerization and cell signaling. Cell. 2005;121(3):425–36.
180. Miyazaki M, Miyazaki K, Itoi M, Katoh Y, Guo Y, Kanno R, et al. Thymocyte Proliferation Induced by Pre-T Cell Receptor Signaling Is Maintained through Polycomb Gene Product Bmi-1-Mediated Cdkn2a Repression. Immunity. 2008;28(2):231–45.
181. Tumes DJ, Onodera A, Suzuki A, Shinoda K, Endo Y, Iwamura C, et al. The Polycomb protein Ezh2 regulates differentiation and plasticity of CD4+ T helper Type 1 and type 2 cells. Immunity. 2013;39(5):819–32.
182. Zhang Y, Kinkel S, Maksimovic J, Bandala-Sanchez E, Tanzer MC, Naselli G, et al. The polycomb repressive complex 2 governs life and death of peripheral T cells. Blood. 2014;124(5):737–49.
183. Dobenecker MW, Kim JK, Marcello J, Fang TC, Prinjha R, Bosselut R, et al. Coupling of T cell receptor specificity to natural killer T cell development by bivalent histone H3 methylation. J Exp Med. 2015;212(3):297–306.
184. Cao R, Zhang Y. SUZ12 is required for both the histone methyltransferase activity and the silencing function of the EED-EZH2 complex. Mol Cell. 2004;15(1):57–67.
185. Kim H, Ekram MB, Bakshi A, Kim J. AEBP2 as a transcriptional activator and its role in cell migration. Genomics. 2015;105(2):108–15.
186. Bodega B, Marasca F, Ranzani V, Cherubini A, Della Valle F, Neguembor MV, et al. A cytosolic Ezh1 isoform modulates a PRC2-Ezh1 epigenetic adaptive response in postmitotic cells. Nat Struct Mol Biol. 2017;24(5):444–52.
187. Kosugi S, Hasebe M, Tomita M, Yanagawa H. Systematic identification of cell cycle-dependent yeast nucleocytoplasmic shuttling proteins by prediction of composite motifs. Proc Natl Acad Sci U S A. 2009;106(25):10171–6.
188. Kim H, Kang K, Ekram MB, Roh TY, Kim J. Aebp2 as an epigenetic regulator for neural crest cells. PLoS One. 2011;6(9):e25174.
189. Di Carlo V, Mocavini I, Di Croce L. Polycomb complexes in normal and malignant hematopoiesis. Vol. 218, Journal of Cell Biology. 2019. p. 55–69.

190. Yamashita I, Nagata T, Tada T, Nakayama T. CD69 cell surface expression identifies developing thymocytes which audition for T cell antigen receptor-mediated positive selection. Int Immunol. 1993;5(9):1139–50.
191. Tarakhovsky A, Kanner SB, Hombach J, Ledbetter JA, Müller W, Killeen N, et al. A role for CD5 in TCR-mediated signal transduction and thymocyte selection. Science (80-). 1995;269(5223):535–7.
192. Kwan J, Killeen N. CCR7 Directs the Migration of Thymocytes into the Thymic Medulla. J Immunol. 2004;172(7):3999–4007.
193. McCaughtry TM, Baldwin TA, Wilken MS, Hogquist KA. Clonal deletion of thymocytes can occur in the cortex with no involvement of the medulla. J Exp Med. 2008;205(11):2575–84.
194. Ross EM, Bourges D, Hogan T V., Gleeson PA, van Driel IR. Helios defines T cells being driven to tolerance in the periphery and thymus. Eur J Immunol. 2014;44(7):2048–58.
195. Daley SR, Hu DY, Goodnow CC. Helios marks strongly autoreactive CD4+ T cells in two major waves of thymic deletion distinguished by induction of PD-1 or NF-κB. J Exp Med. 2013;210(2):269–85.
196. Handel AE, Shikama-Dorn N, Zhanybekova S, Maio S, Graedel AN, Zuklys S, et al. Comprehensively Profiling the Chromatin Architecture of Tissue Restricted Antigen Expression in Thymic Epithelial Cells Over Development. Front Immunol. 2018;9:2120.
197. Bansal K, Yoshida H, Benoist C, Mathis D. The transcriptional regulator Aire binds to and activates super-enhancers. Nat Immunol. 2017;18(3):263–73.
198. Ripen AM, Nitta T, Murata S, Tanaka K, Takahama Y. Ontogeny of thymic cortical epithelial cells expressing the thymoproteasome subunit β5t. Eur J Immunol. 2011;41(5):1278–87.
199. Kondo M, Weissman IL, Akashi K. Identification of clonogenic common lymphoid progenitors in mouse bone marrow. Cell. 1997;91(5):661–72.
200. Shortman K, Wu L. Early T Lymphocyte Progenitors. Annu Rev Immunol. 1996;14(1):29–47.
201. Allman D, Sambandam A, Kim S, Miller JP, Pagan A, Well D, et al. Thymopoiesis independent of common lymphoid progenitors. Nat Immunol. 2003;4(2):168–74.
202. Hogquist KA, Xing Y, Hsu F-C, Shapiro VS. T Cell Adolescence: Maturation Events Beyond Positive Selection. J Immunol. 2015;195(4):1351–7.
203. Foulds KE, Zenewicz LA, Shedlock DJ, Jiang J, Troy AE, Shen H. Cutting Edge: CD4 and CD8 T Cells Are Intrinsically Different in Their Proliferative Responses. J Immunol. 2002;168(4):1528–32.
204. Bettelli E, Carrier Y, Gao W, Korn T, Strom TB, Oukka M, et al. Reciprocal developmental pathways for the generation of pathogenic effector TH17 and regulatory T cells. Nature. 2006;441(7090):235–8.
205. Barthlott T, Bosch AJT, Berkemeier C, Nogales-Cadenas R, Jeker LT, Keller MP, et al. A subpopulation of CD103posICOSpos Treg cells occurs at high frequency in lymphopenic mice and represents a lymph node specific differentiation stage. Eur J Immunol. 2015;45(6):1760–71.
206. Kiel MJ, Yilmaz ÖH, Iwashita T, Yilmaz OH, Terhorst C, Morrison SJ. SLAM family receptors distinguish hematopoietic stem and progenitor cells and reveal endothelial niches for stem cells. Cell. 2005;121(7):1109–21.

207. Akashi K, Traver D, Miyamoto T, Weissman IL. A clonogenic common myeloid progenitor that gives rise to all myeloid lineages. Nature. 2000;404(6774):193–7.
208. Pronk CJH, Rossi DJ, Månsson R, Attema JL, Norddahl GL, Chan CKF, et al. Elucidation of the Phenotypic, Functional, and Molecular Topography of a Myeloerythroid Progenitor Cell Hierarchy. Cell Stem Cell. 2007;1(4):428–42.
209. Davenport JW, Fernandes ER, Harris LD, Neale GAM, Goorha R. The mouse mitotic checkpoint gene Bub1b, a novel Bub1 family member, is expressed in a cell cycle-dependent manner. Genomics. 1999;55(1):113–7.
210. Bilir Ş, Kojidani T, Mori C, Osakada H, Kobayashi S, Koujin T, et al. Roles of Nup133, Nup153 and membrane fenestrations in assembly of the nuclear pore complex at the end of mitosis. Genes to Cells. 2019;24(5):338–53.
211. Schneider MA, Christopoulos P, Muley T, Warth A, Klingmueller U, Thomas M, et al. AURKA, DLGAP5, TPX2, KIF11 and CKAP5: Five specific mitosis-associated genes correlate with poor prognosis for non-small cell lung cancer patients. Int J Oncol. 2017;50(2):365–72.
212. Yang XP, Jiang K, Hirahara K, Vahedi G, Afzali B, Sciume G, et al. EZH2 is crucial for both differentiation of regulatory T cells and T effector cell expansion. Sci Rep. 2015;5.
213. Pereira RM, Martinez GJ, Engel I, Cruz-Guilloty F, Barboza BA, Tsagaratou A, et al. Jarid2 is induced by TCR signalling and controls iNKT cell maturation. Nat Commun. 2014;5.
214. He A, Shen X, Ma Q, Cao J, von Gise A, Zhou P, et al. PRC2 directly methylates GATA4 and represses its transcriptional activity. Genes Dev. 2012;26(1):37–42.
215. Lee JM, Lee JS, Kim H, Kim K, Park H, Kim JY, et al. EZH2 Generates a Methyl Degron that Is Recognized by the DCAF1/DDB1/CUL4 E3 Ubiquitin Ligase Complex. Mol Cell. 2012;48(4):572–86.
216. Kim E, Kim M, Woo DH, Shin Y, Shin J, Chang N, et al. Phosphorylation of EZH2 Activates STAT3 Signaling via STAT3 Methylation and Promotes Tumorigenicity of Glioblastoma Stem-like Cells. Cancer Cell. 2013;23(6):839–52.
217. Gunawan M, Venkatesan N, Loh JT, Wong JF, Berger H, Neo WH, et al. The methyltransferase Ezh2 controls cell adhesion and migration through direct methylation of the extranuclear regulatory protein talin. Nat Immunol. 2015;16(5):505–16.
218. Jung J, Kim TG, Lyons GE, Kim HRC, Lee Y. Jumonji regulates cardiomyocyte proliferation via interaction with retinoblastoma protein. J Biol Chem. 2005;280(35):30916–23.
219. Shirato H, Ogawa S, Nakajima K, Inagawa M, Kojima M, Tachibana M, et al. A jumonji (Jarid2) protein complex represses cyclin D1 expression by methylation of histone H3-K9. J Biol Chem. 2009;284(2):733–9.
220. Sanulli S, Justin N, Teissandier A, Ancelin K, Portoso M, Caron M, et al. Jarid2 Methylation via the PRC2 Complex Regulates H3K27me3 Deposition during Cell Differentiation. Mol Cell. 2015;57(5):769–83.
221. Xie H, Xu J, Hsu JH, Nguyen M, Fujiwara Y, Peng C, et al. Polycomb repressive complex 2 regulates normal hematopoietic stem cell function in a developmental-stage-specific manner. Cell Stem Cell. 2014;14(1):68–80.
222. Lee ST, Li Z, Wu Z, Aau M, Guan P, Karuturi RKM, et al. Context-Specific Regulation of NF-κB Target Gene Expression by EZH2 in Breast Cancers. Mol

Cell. 2011;43(5):798–810.
223. Xu K, Wu ZJ, Groner AC, He HH, Cai C, Lis RT, et al. EZH2 Oncogenic Activity in Castration-Resistant Prostate Cancer Cells Is Polycomb-Independent. Science (80-). 2012;338(6113):1465–9.
224. Goldenson B, Crispino JD. The aurora kinases in cell cycle and leukemia. Oncogene. 2015;34(5):537–45.
225. Goldenson B, Kirsammer G, Stankiewicz MJ, Wen QJ, Crispino JD. Aurora kinase a is required for hematopoiesis but is dispensable for murine megakaryocyte endomitosis and differentiation. Blood. 2015;125(13):2141–50.
226. Zhou H, Kuang J, Zhong L, Kuo WL, Gray JW, Sahin A, et al. Tumour amplified kinase STK15/BTAK induces centrosome amplification, aneuploidy and transformation. Nat Genet. 1998;20(2):189–93.
227. Bischoff JR, Anderson L, Zhu Y, Mossie K, Ng L, Souza B, et al. A homologue of Drosophila aurora kinase is oncogenic and amplified in human colorectal cancers. EMBO J. 1998;17(11):3052–65.
228. Sen S, Zhou H, White RA. A putative serine/threonine kinase encoding gene BTAK on chromosome 20q13 is amplified and overexpressed in human breast cancer cell lines. Oncogene. 1997;14(18):2195–200.
229. Littlepage LE, Wu H, Andresson T, Deanehan JK, Amundadottir LT, Ruderman J V. Identification of phosphorylated residues that affect the activity of the mitotic kinase Aurora-A. Proc Natl Acad Sci U S A. 2002;99(24):15440–5.
230. Furukawa T, Kanai N, Shiwaku HO, Soga N, Uehara A, Horii A. AURKA is one of the downstream targets of MAPK1/ERK2 in pancreatic cancer. Oncogene. 2006;25(35):4831–9.
231. Jacobsen A, Bosch LJW, Martens-De Kemp SR, Carvalho B, Sillars-Hardebol AH, Dobson RJ, et al. Aurora kinase A (AURKA) interaction with Wnt and Ras-MAPK signalling pathways in colorectal cancer. Sci Rep. 2018;8(1).
232. Ku WL, Nakamura K, Gao W, Cui K, Hu G, Tang Q, et al. Single-cell chromatin immunocleavage sequencing (scChIC-seq) to profile histone modification. Nat Methods. 2019;16(4):323–5.

Appendix

Supplement Figure 1: CD4 vs CD8 gating

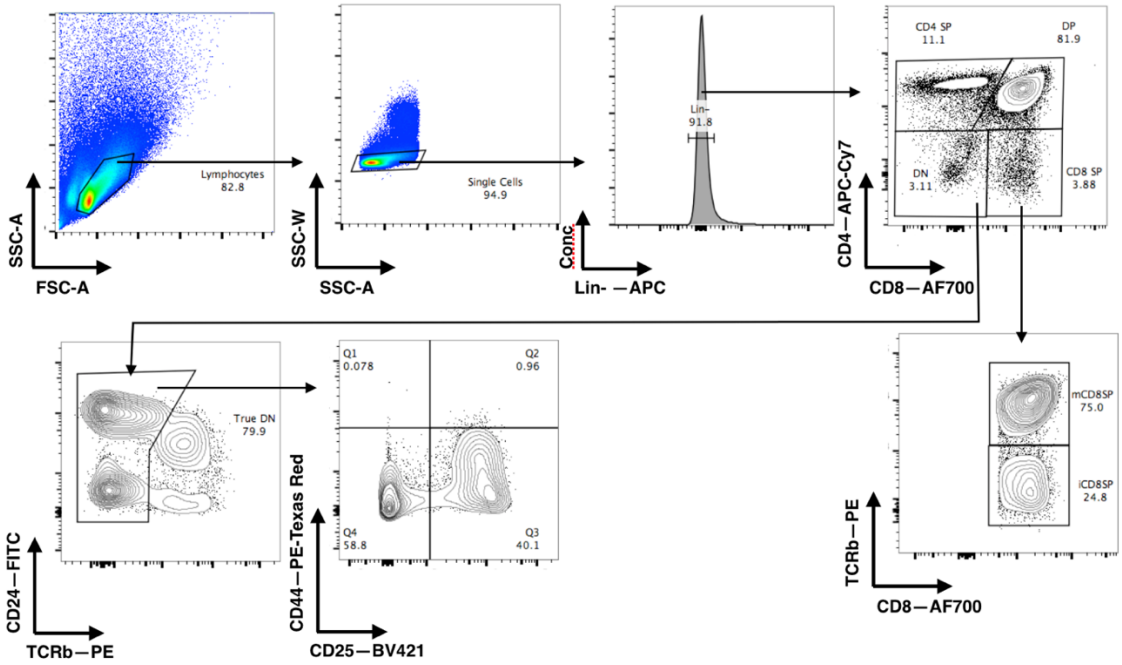

Supplement Figure 2: CD4 maturation

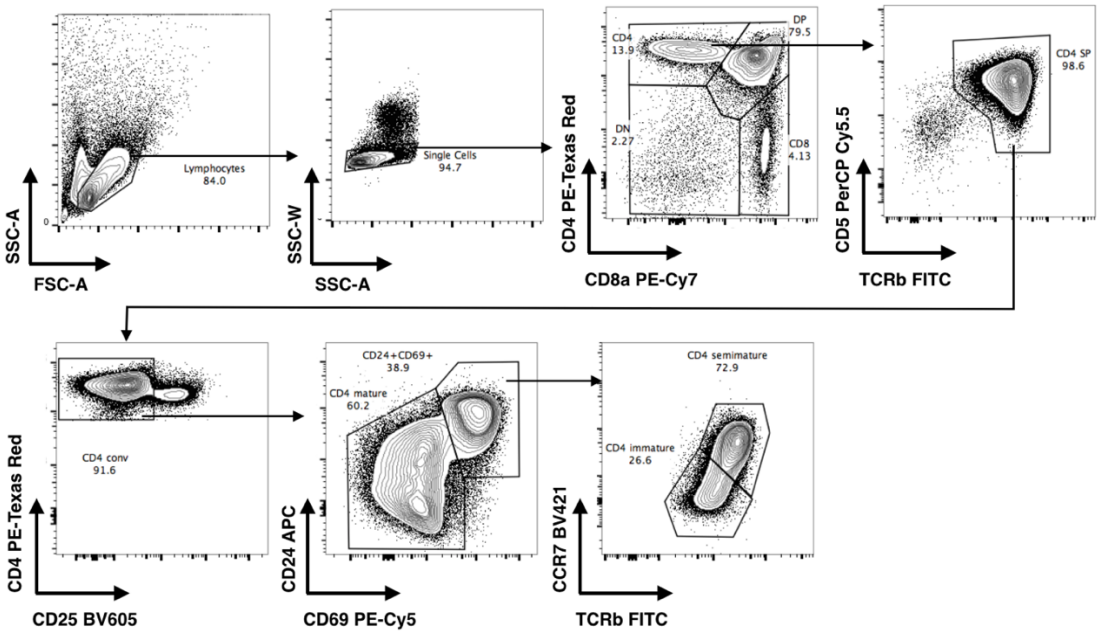

Supplement Figure 3: CD8 maturation

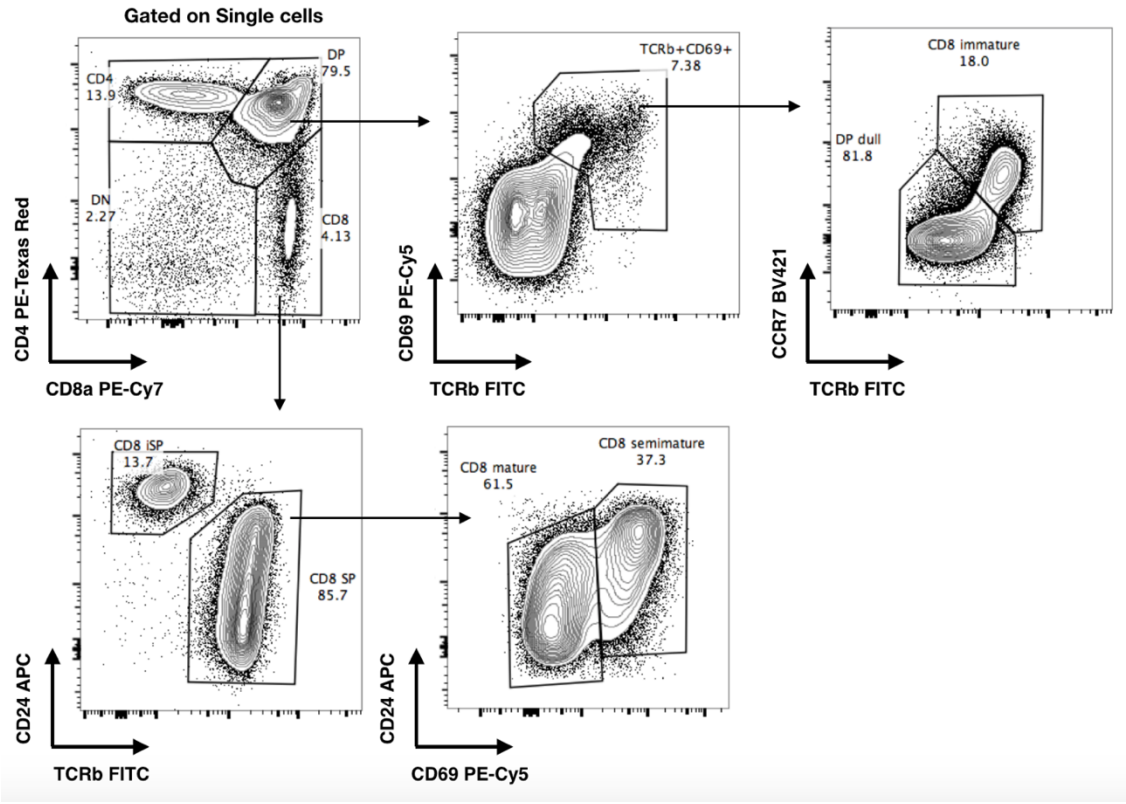

Supplement Figure 4: Negative selection of CD4 lineage

